



저작자표시-변경금지 2.0 대한민국

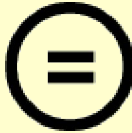
이용자는 아래의 조건을 따르는 경우에 한하여 자유롭게

- 이 저작물을 복제, 배포, 전송, 전시, 공연 및 방송할 수 있습니다.
- 이 저작물을 영리 목적으로 이용할 수 있습니다.

다음과 같은 조건을 따라야 합니다:



저작자표시. 귀하는 원저작자를 표시하여야 합니다.



변경금지. 귀하는 이 저작물을 개작, 변형 또는 가공할 수 없습니다.

- 귀하는, 이 저작물의 재이용이나 배포의 경우, 이 저작물에 적용된 이용허락조건을 명확하게 나타내어야 합니다.
- 저작권자로부터 별도의 허가를 받으면 이러한 조건들은 적용되지 않습니다.

저작권법에 따른 이용자의 권리는 위의 내용에 의하여 영향을 받지 않습니다.

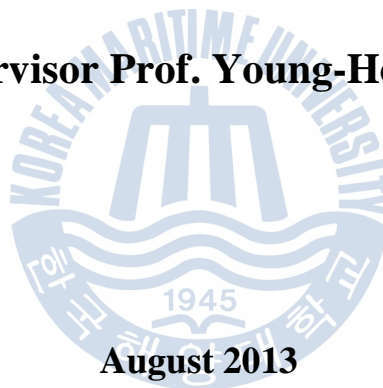
이것은 [이용허락규약\(Legal Code\)](#)을 이해하기 쉽게 요약한 것입니다.

[Disclaimer](#)

Master's Thesis

**A CFD Study on Vortex Control
Techniques in Micro-class Francis Hydro
Turbine**

Supervisor Prof. Young-Ho LEE



August 2013

**Graduate School of Korea Maritime University
Department of Mechanical Engineering**

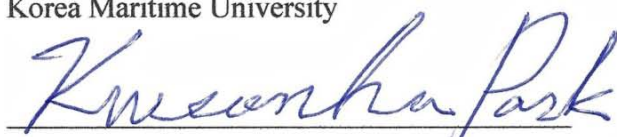
Anup KC

We certify that we have read this thesis and that, in our opinion, it is satisfactory in scope and quality as a thesis for the degree of Master of Mechanical Engineering, submitted by **Anup KC**.

THESIS COMMITTEE

Chairperson: Prof. Kweon-Ha PARK, Ph.D

Division of Mechanical and Energy System Engineering,
Korea Maritime University



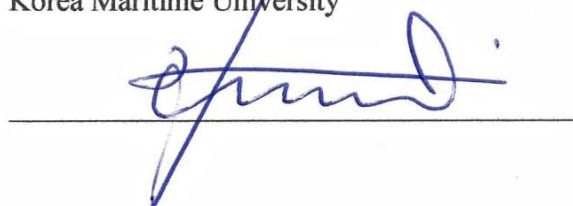
Co- Chairperson: Prof. Hyung-Ho JUNG, Ph.D

Division of Mechanical and Energy System Engineering,
Korea Maritime University



Supervisor: Prof. Young-Ho LEE, Ph.D

Division of Mechanical and Energy System Engineering,
Korea Maritime University



26 July 2013

Department of Mechanical Engineering
Graduate School of Korea Maritime University

본論文을 아늑케이시의 工學碩士學位論文으로
認准함

위원장: 공학박사 박권하



위원: 공학박사 정형호



위원: 공학박사 이영호



2013 년 07 월 26 일

한국해양대학교 대학원

기계공학과

Table of Contents

Table of Contents	i
List of Tables	iii
List of Figures	iv
Abstract	vii
Nomenclature	ix
Chapter 1 Introduction	1
1.1 Prelude	1
1.2 Small hydro powers and hydro turbines.....	3
1.3 Energy conversion in hydro turbine	9
1.4 Components of Francis hydro turbine.....	12
1.4.1 Runner.....	12
1.4.2 Casing, guide vanes and draft tube	16
1.5. Cavitation in Francis turbine.....	18
Chapter 2 Design and performance analysis of 70kW runner	20
2.1 Design	20
2.2 Numerical analysis.....	28
2.3 Results and dissusions.....	30
Chapter 3 Partial load performance of Francis turbine	38
3.1 Flow theory	38
3.2 Flow analysis.....	42
Chapter 4 Vortex shedding in draft tube	55
4.1 Vortex rope in part flow	55
4.2 Remedial attempts.....	64

Chapter 5 Evaluation of vortex control techniques	66
5.1 Influence of runner hub profile	66
5.2 Influence of misaligned guide vanes (MGVs)	72
5.3 Application of J-grooves in the draft tube.....	78
Chapter 6 Conclusion	87
Acknowledgement	89
References	90



List of Tables

Table 1.1 Classification of hydropower plant (HPP) by size	4
Table 1.2 General classification of turbine types	5
Table 1.3 Types of turbines by specific speed, N_s	6



List of Figures

Fig. 1.1	Velocity diagram of a reaction turbine	13
Fig. 1.2	A 70kW x-blade Francis runner, Shin Han Precision Co., Korea	15
Fig. 2.1	Velocity diagram of flow at runner outlet	22
Fig. 2.2	Velocity diagram of flow at runner inlet	23
Fig. 2.3	Screenshot of Excel worksheet to generate design dimensions	25
Fig. 2.4	Improved dimension of the runner as modeled in Unigraphics NX6	26
Fig. 2.5	Spiral case with wicket gates and stay vanes for 70kW Francis runner	27
Fig. 2.6	Tetrahedral mesh of spiral case, runner and draft tube with prism layers	28
Fig. 2.7	Computational domain of 70kW Francis turbine	29
Fig. 2.8	Performance characteristics at different flow rates	30
Fig. 2.9	Head loss at different mass flow rates	31
Fig. 2.10	Pressure distribution in spiral casing by flow rates	32
Fig. 2.11	Velocity distribution in the spiral case by flow rates	32
Fig. 2.12	Flow streamlines in runner	33
Fig. 2.13	Pressure and surface velocity distribution on runner blade at full load	34
Fig. 2.14	Pressure distribution in runner by flow rates	35
Fig. 2.15	Cp graph at 50% of runner blade for 4 flow rates	35
Fig. 2.16	Velocity streamlines and vector contour and vector plots at $0.5\text{m}^3/\text{s}$	36
Fig. 2.17	Velocity streamlines in mid section of draft tube by flow rates	36
Fig. 3.1	Flow features in the mid span of casing	42
Fig. 3.2	Pressure contour and velocity distribution in the tandem cascade	43
Fig. 3.3	Surface streamlines on mid span of casing and guide vanes, 100% load	44
Fig. 3.4	Pressure distribution in the runner blade, pressure side and suction side	45
Fig. 3.5	Velocity streamlines on runner blade at full load	46
Fig. 3.6	Velocity distribution in casing, runner and draft tube at full load	47
Fig. 3.7	Velocity profiles in the draft tube	48
Fig. 3.8	Torque fluctuation and average torque distribution in runner blade	49

Fig. 3.9 Average pressure distribution in runner blades	50
Fig. 3.10 Average pressure distribution in spiral case	50
Fig. 3.11 Pressure fluctuation in draft tube for 3 runner rotation	51
Fig. 3.12 Pressure recording locations in casing, runner blade and draft tube	51
Fig. 3.13 Fourier transformed pressure signal in casing (c1).....	52
Fig. 3.14 Fourier transformed pressure signal in draft tube (dt3).....	52
Fig. 3.15 Vibration spectra in draft tube and casing.....	53
Fig. 4.1 Effect of turbulence model on shape of vortex rope	57
Fig. 4.2 Velocity vector of flow in draft tube	59
Fig. 4.3 Shape of vortex rope at part load.....	59
Fig. 4.4 Low pressure region in mid section of draft tube	60
Fig. 4.5 Amplitude spectra at draft tube and casing	62
Fig. 4.6 Amplitude spectra in runner blade	63
Fig. 5.1 Profiles of modified hub.....	66
Fig. 5.2 Vortex rope due to hub case1 and case2 at 0.481s.....	67
Fig. 5.3 Comparative circumferential velocity in draft tube with new hub.....	68
Fig. 5.4 Pressure maps at 4 layers of draft tube cones.....	70
Fig. 5.5 Cp graph for blade pressure distribution with hub-case2.....	71
Fig. 5.6 Position of misaligned guide vanes	73
Fig. 5.7 Performance evaluation with modified hub and MGV	74
Fig. 5.8 Shape of vortex rope with MGV at 0.555s.....	75
Fig. 5.9 Pressure distribution at central plane of draft tube with MGV.....	75
Fig. 5.10 Average circumferential velocity in draft tube with MGV	76
Fig. 5.11 Comparison of Cp with base model and MGVs.....	77
Fig. 5.12 Performance of turbine with different J-grooves.....	79
Fig. 5.13 Pressure map in central plane of draft tube	80
Fig. 5.14 Velocity distribution in base model and J-grooved draft tube.....	81
Fig. 5.15 Average circumferential velocity with J-groove 13G-10mm.....	82
Fig. 5.16 Average axial velocity with J-groove.....	83
Fig. 5.17 Vorticity curves of base model draft tube with J-groove cases.....	84

Fig. 5.18 Turbulence kinetic energy with J-groove, 2 cases..... 85
Fig. 5.19 Shape of vortex rope with J-groove..... 86



A CFD Study on Vortex Control Techniques in Micro-class Francis Hydro Turbine

Anup KC

Department of Mechanical Engineering
Graduate School of Korea Maritime University

Abstract

Micro-hydropower stands out as one of the most cost-effective energy technologies for hydroelectricity by tapping local water resources and catering to green energy generation. Francis Turbines are emerging as efficient and better-performing turbines for Micro Hydro Power (MHP) generation schemes. With robust computer technologies and design developments, a Computational Fluid Dynamics (CFD) based study on design, performance evaluation, flow analyses and vortex control techniques are carried out in this research work. A preliminary mathematics to design a 70kW Francis hydro turbine for small scale hydropower plant has been dealt with out of available hydrodynamic parameters of head, discharge and rotational speed of the turbine. The adopted direct method of design procedure is based on the basic principal of fluid dynamics of turbo machineries, turbine design theory and rule of thumb which was later fine-tuned in solid modeling tools. The so designed turbine was numerically analyzed to evaluate its Best Efficiency Point (BEP) and its performance in part-load operating regimes.

A time dependent numerical simulation was then carried out at its full load to study the interaction between rotating and stationary components, and at its partial load to study draft tube surge and flow instability brought about by vortex shedding. Pressure fluctuation, torque variation and level of vibration were the parameters of interest in this analysis. A periodical behavior was observed for pressure distribution and torque variation in runner blades at full load while a distinct vortex rope was observed in draft tube at part load operation as the flow became unstable due to swirl component of the velocity attached with

the exiting flow downstream the runner. The swirling flow at the runner outlet generated a corkscrew-shaped vortex resulting in pressure pulsation, fluctuation in torque, axial and radial forces and structure vibration causing the turbine to suffer loss in its performance.

In order to minimize the vortex shedding and the flow instability, three different vortex control techniques viz. Misaligned Guide Vanes (MGVs), hub modification of runner and J-grooves in draft tube have been proposed and evaluated numerically.

Two axisymmetrically located misaligned guide vanes (MGV) in casing did not contribute in controlling the vortex breakdown. The unstable flow was further aggravated by the use of MGVs. As for runner hub modification, two different profiles of runner hub were analyzed and their effects on the flow in the draft tube were examined. The modified hub did alter the flow instability in the draft tube, relatively minimizing the swirl velocity and intensity of the vortex rope however at the expense of some efficiency. This opened an avenue for the design optimization of the modified hub for better flow control and for suppressing the vortex breakdown. Likewise, the use of J-grooves in draft tube turned out to be an effective technique to minimize the swirling flow and recover energy loss in the draft tube. Five different cases of J-grooves, by varying its number and depth, were numerically analyzed. It was inferred that all the cases altered the flow configuration of the draft tube without significant loss in the efficiency at given operating point. However, the level of surge control changed with different number of grooves and their depths. For the given level of swirl and vortex breakdown with base model draft tube, a draft tube with best number of grooves and depth was figured out that helped minimize vortex at larger extent.

Swirling flow in draft tube at off design operating regimes of Francis hydro turbine is a major operation challenge and the aforementioned techniques can be optimized and applied to mitigate the flow instability.

KEY WORDS: Micro-hydro, Francis turbine, vortex rope, misaligned guide vanes, J-grooves, hub modification

Nomenclature

B	Height of guide vane	[m]
C	Absolute component of velocity	[m/s]
C_m	Meridional component of velocity	[m/s]
\underline{C}_{m1}	Reduced meridional velocity at inlet	[-]
\underline{C}_{m2}	Reduced meridional velocity at outlet	[-]
C_u	Swirl/whirl component of velocity	[m/s]
C_p	Coefficient of pressure	[-]
\underline{C}_{u1}	Reduced whirl velocity	[-]
D	Diameter of runner	[m]
E	Kinetic energy	[Joules]
f_d	Dominating frequency	[Hz]
f_n	Rotational frequency	[Hz]
g	Acceleration due to gravity	[m/s ²]
H_a	Atmospheric pressure head	[m]
H_n	Net hydraulic head	[m]
H_s	Suction pressure head	[m]
h_s	Submergence	[m]
H_v	Vapor pressure head	[m]
k	Turbulence kinetic energy	[m ² /s ²]
LE	Leading edge	[-]
L_g	Length of guide vanes	[m]
n	Rotational speed of the turbine	[rpm]
n_s	Specific speed of the turbine (in SI)	[-]
P	Pressure	[Pa]
P_a	Shaft power output	[kW]
P_r	Power transferred from fluid to turbine	[kW]
P_t	Theoretical power output	[kW]
Q	Flow rate	[m ³ /s]
\underline{Q}	Reduced discharge	[-]
R	Mean radius of runner	[m]
R_r	Reaction ratio	[-]

t_g	Centre to centre distance between successive guide vanes	[m]
u	Instantaneous (laminar) velocity	[m/s]
u_i	Fluctuating velocity in x_i -direction	[m/s]
U	Peripheral velocity	[m/s]
V_r	Relative component of velocity	[m/s]
\underline{x}	Reduced parameter	[-]
x^*	Value at Best Efficiency Point (BEP)	[-]
x_0	Parameter at guide vane outlet	[-]
x_1	Parameter at inlet of runner	[-]
x_2	Parameter at outlet of runner	[-]
x_{max}	Maximum allowable value for given parameter	[-]
TE	Trailing edge	[-]
α	Guide vane outlet angle	[°]
β	Runner blade angle	[°]
η_h	Hydraulic efficiency of turbine	[%]
κ	Capacity ratio	[-]
ρ	Density of fluid	[m ³ /kg]
σ	Thoma's cavitation factor	[-]
σ_c	Critical value of cavitation	[-]
T	Torque generated by runner	[Nm]
ϕ	Discharge coefficient	[-]
ψ	Energy coefficient	[-]
ω	Angular velocity	[s ⁻¹]
ν	Dynamic viscosity	[Ns/m ²]
ν_T	Kinetic turbulent viscosity	[m ² /s]
$\underline{\omega}$	Reduced angular velocity	[-]
Ω	Speed number	[-]

Chapter 1 Introduction

1.1 Prelude

Naturally available water and air have been utilized to produce useful work ever since ancient time. Water wheels and windmills, the ancient version of modern turbines, are apparently the best examples that reflect innovation to harness nature's energy and put it into useful work. The Romans and the Greeks were traced to be using waterwheels for grinding purpose in around 70 B.C. while Persians used windmills in around 700 A. D.

The use of hydro turbine to convert water power into mechanical work can be traced in the form of a very simple and rudimentary water wheel that utilized the weight of the water primarily for grinding and pumping purpose. Howsoever, it took a long leap for the water wheels to emerge as a modern hydro turbine. Ancient engineers scrutinized the performance and operational characteristics of the waterwheels; they realized that more mechanical work can be achieved by properly guiding water in some encasement and directing maximum amount of water to strike the paddle or blade. Although it was realized that only a less amount of water striking the blades was converted into useful work and majority of energy contained in out-rushing water went underutilized, lack of theoretical understanding of fluid dynamics and precision machine tools hindered the evolution of modern hydro turbine. These problems were addressed to some extent in 1750 by a German mathematician and naturalist Johann Andres von Segner (1704-1777) when he built a water wheel system in which water was directed in a cylindrical box containing shaft of rotating wheels. The inclined vanes of the rotor were acted upon by the weight of the water and water flowed out in the tangential opening, it thus being the earliest reaction turbine system and precursor of modern hydraulic turbine system. [1].

A French engineer, Claude Bourdin coined the term Turbine in 1828 A.D. The word turbine is derived from Latin word Turbo which means whirling or a vortex. This term segregated the classical turbine from the ancient waterwheels that would signify a new turbine which featured a swirling motion of water passing the energy to the rotor. Other distinguishing features of new water turbines were that they were smaller in size for same energy conversion, were capable of processing more water by spinning faster and could harness greater heads. Not many technical and physical alterations were observed in classical water turbines until Brnoit Fourneyron invented the first modern hydraulic turbine during late 1820s. Though his initially designed turbine was relatively of small power and had reasonable drawbacks, yet he eventually came up with a larger-sized turbine that was capable of churning higher head and could withstand higher pressure. These aside, he made a significant contribution in his invention by articulating a distributor to guide and control the flow of water to the rotor. Fourneyron's ingenious invention thus laid a foundation for the development of number of other types of hydro turbines. Pelton type turbine, already in application during this period, got revamped with curved vanes as it was realized that flat vanes were not efficient [2].

Modern Francis Turbine emerged in 1849 when James Francis, an American, built a hydraulic turbine that functioned differently than the turbines already in operation at that time. The first truly effective inward flow reaction turbine was developed and tested by Francis and his collaborators in Lowell, Massachusetts [3]. Contrast to majority of those water turbines in operation in which water entered into the rotors and flowed outward radially, he changed the shape of the rotor blades so that water flow followed radial to axial path. His design allowed the water to enter the runner from outside along the periphery and to flow inward through the radial blades. Up until now, water turbines were utilized only for mechanical works. By the late 19th century, electrical generator was developed and thus could be coupled with hydraulics to generate hydroelectricity. In modern time, hydraulic turbines are used primarily by the hydropower plants to generate electricity.

Since the advent of hydraulic turbines, the need of power generation and call for green energy has entailed considerable changes in design and application of hydro turbines. There has been significant development in the water technology and robust methodologies have emerged to achieve optimum performance of hydro machineries dealing in site-wise conditions, and boosting their performances. However, maximizing efficiency and performance improvement of turbine is a complex task as turbines are usually tailor-made with specific design of each component to suit best the hydrodynamic conditions of a given site.

1.2 Small hydro powers and hydro turbines

Hydropower plants have the highest operating efficiency of all known energy generation systems [4]. With operating cost relatively low and supplanted with automated systems, they have a key role in water resource utilization and green energy generation. A hydropower plant that can produce electricity equivalent to 100kW by utilizing the flow of water is classified as Micro Hydro type plant. These small scale power plants are effective in energy generation with locally available resources, electrifying a locality. They have proved to be boon to rural communities and isolated regions/load centers which not only provide electricity but also help improve social and economic status of the people, reducing the dependency on bio fuels and fossil fuels. Such micro hydro projects are particularly popular in developing countries where national grid has no reach and local water resource like rivers and streams are capable of generating good amount of electricity for household and community usage.

The primary purpose of the installation of micro hydro is to provide power to small and isolated communities which are accomplished by utilizing the locally available water resources and by using suitable hydro turbine. The suitable geographical areas for exploiting micro hydro powers are those where there are rivers thundering down steeply all the year round, like in hills and rivers with high volume of water flowing all the time.

The amount of water head available to produce power is calculated and a hydro scheme is developed considering the supply and demand factors. The general classification of hydropower plants according to their capacity of production is shown in Table 1.1. Head and discharge are the governing hydrodynamic parameters for the design of a turbine and choice of its type. The rotational speed of turbine is chosen accordingly to match best and avert losses with the speed of generator. Either an impulse of water flowing from an elevation can be used to drive high head turbine or a large quantity of water passing through low head can be employed to generate electricity. Various types of turbines that work according to the available hydrodynamic/site conditions are categorized in Table 1.2.

During their long history, there has been substantial development in the design of hydraulic turbines, in improving its efficiency, power output, head exploited and profile of runner blade. Francis turbines are the most widely used reaction type turbines among other hydro turbines as they have the widest range of application and ample of research and development on Francis turbines in the last decade have widened the range of new application possibilities for this type. Reaction turbines have some peculiar feature that segregates them from their impulse counterparts—the major portion of pressure drop occurring in the turbine itself, unlike in impulse turbines where a complete pressure drop occurs up to the entry point i.e. at the nozzle of the turbine. This aside, reaction turbines are completely submerged in water to maintain pressure difference.

Table 1.1 Classification of hydropower plant (HPP) by size

Large scale HPP	>100MW feeding into grid
Medium-scale HPP	15-100MW feeding into grid
Small scale HPP	1-15MW feeding into grid
Mini HPP	100kW- 1MW, either stand alone or feeding into grid
Micro HPP	5kW-100kW
Pico HPP	Up to 5kW

This classification can differ slightly according to the country standard

Table 1.2 General classification of turbine types

Turbine	High head	Medium head	Low head
Impulse	- Pelton with single or multiple jets - Turgo	- Cross flow - Turgo - Multi jet Pelton	- Cross flow
Reaction		- Francis	- Propeller - Kaplan

Francis type water turbine is an inward flow reaction turbine that combines radial and axial flow concepts of the working fluid (water). Water is contained in a spiral-shaped casement that shrouds the turbine runner. Modern Francis turbine utilizes purely radial inlet flow through stationary guide vanes but the runners are mixed flow devices with a component of the flow in the axial direction. After energy transfer, the water comes out from a conical diffuser called draft tube. The trend from purely radial inflow through mixed flow to near axial flow increase as the specific speed of the turbine is increased.

Specific speed is the primary numerical classification of a turbine. It signifies the speed of the turbine working at its maximum efficiency with respect to the rated power and flow rate. Specific speed is expressed as an independent quantity for a turbine size. With the available mass flow rate and the power output desired, the specific speed of a turbine can be calculated and appropriate design of turbine can be selected for given hydrodynamic parameters. Table 1.3 categorizes turbines according to their specific speed and indicates the shape of turbine with respect to its specific speed.

Table 1.3 Types of turbines by specific speed, N_s

Type of Turbine	Dimensionless N_s	British unit	SI unit
	$N_s = \frac{n\sqrt{P_a/\rho}}{(gH)^{5/4}}$ <p>where n=rps P=Watts g=m/s² H=meters</p>	$N_s = \frac{n\sqrt{P_a}}{H^{5/4}}$ <p>where n=rpm, P=H.P. H=feet</p>	$N_s = \frac{n\sqrt{P_a}}{H^{5/4}}$ <p>where n=rpm P=kW H=meters</p>
Pelton (single jet)	0.015-0.024	4-6.5	15.66-25.0
Pelton (Two jet)	0.022-0.033	6-9	23.0-34.4
Pelton (Multi jet)	to 0.055	up to 15	up to 57
Francis (for head below 370m)	0.055-0.37	15-100	57-385
Francis (for head below 60m)	0.29-0.73	80-200	300-760
	0.055	15	57
	0.110	30	115
	0.201	55	210
	0.403	110	420
	0.769	210	800
(figures not to scale)		[X 3.66x10 ⁻³]*	[X.960x10 ⁻³]*

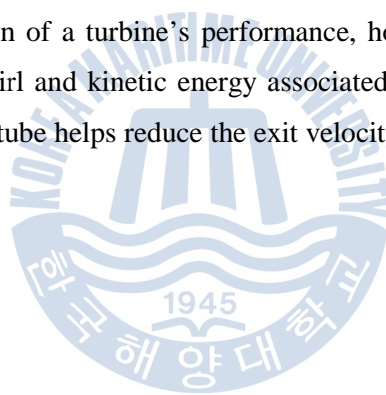
*Multiply to N_s to obtain the dimensionless units

Increase in specific speed signifies increase in flow rate and relative decrease in the head. As specific speed of turbine increases, the radius at inlet decreases accordingly shifting inward towards the centre. This relates to the wider runner vane giving increased inlet space for increasing flow rate. After a certain value of specific speed, the inlet radius converges to the centre transforming itself into a new type of turbine called Kaplan Turbine. For an instance, pelton type hydro turbine has lowest value of specific speed while the value of N_s goes on increasing with high head Francis turbine, medium head Francis, low head Francis and eventually propeller turbines have the highest value. Francis turbines make an appropriate usage in the locations with medium head and comparatively large flow rates, large enough to impart sufficient pressure difference for an optimum output and efficiency of the unit.

In reaction turbines, two effects trigger the energy transfer from the flow to mechanical energy on the turbine shaft. First is the reaction part of the energy conversion in which drop in the pressure from inlet to outlet is followed which is obtained from the completely submerged runner. Second is the change in the direction of the velocity vectors of the flow through the runner blades transferring the impulse force. The spiral case of Francis turbine distributes the velocity uniformly at inlet to stay vanes in circumferential direction such that the incident angle over the height of the stay vanes varies as less as possible. Stay vanes carry the pressure loads in the spiral case and runner to the head cover [5]. Stay vane too serves to direct the flow towards the adjustable guide vanes (or wicket gates) with an optimal incident angle. It is only the guide vanes (g.v.) that are can be adjusted to control flow and eventually power output of the Francis turbine.

Water particle starting off at the inlet of the guide vane enters the turbine through the outer periphery of the runner in the radial direction and leaves in the axial direction. The tangential component of the velocity produced by the water flowing radially, causes runner to spin. The guide vanes are so designed and arranged that the movement of the water changes from radial direction at inlet to leave the outer edge of vane cascade spaces with rather larger velocity component

in the peripheral direction when striking the blades of the runner at optimum angle. The adjustable guide vanes arranged along the periphery of the casing direct the water tangentially to the runner. Thus, with the high flow, pressure head decreases as the water flows over the runner blades. With the static pressure at the runner exit being less than the atmospheric pressure, water fills up all the passages of the runner blades. As water glides along the blades of the turbine runner, it produces a pressure difference between the inlet and the outlet thereby imparting a rotational motion to the turbine. Besides, as the water passes along the runner, pressure and angular momentum reduce. This reduction imparts reaction on the runner causing it to rotate. The decreasing angular momentum also results in decreasing swirling radius of fluid and the water exits the runner with no swirl component and very less energy. This is an ideal condition of a turbine's performance, howsoever in real practice, there is always some swirl and kinetic energy associated with the exiting water at runner outlet and a draft tube helps reduce the exit velocity and recover the required pressure.



1.3 Energy conversion in hydro turbine

The hydraulic turbines convert potential energy of water directed on to it to mechanical energy. Energy is transferred from flowing water to turbine as the water with potential energy passes through the runner causing it to spin about its axis. The ideal power that can be extracted from this flowing water is expressed as:

$$P_t = \rho Q g H_n \quad (1.1)$$

where H_n is the net head defined at the inlet of the turbine to the level of the tailwater level for a reaction turbine .

Also, Power transferred from fluid to turbine is

$$P_r = \rho Q (U_1 C_{u1} - U_2 C_{u2}) \quad (1.2)$$

The hydraulic efficiency of the turbine is expressed as,

$$\eta_h = \frac{P_r}{P_t} \quad (1.3)$$

$$\text{Or, } \eta_h = \frac{(U_1 C_{u1} - U_2 C_{u2})}{g H_n} \quad (1.4)$$

where 'u' is the peripheral velocity of the runner blades and 'c_u' is the component of absolute velocity in the direction of 'u', also referred to as whirl velocity.

In terms of the reduced parameters of head and velocity components,

$$\eta_h = 2(u_1 c_{u1} - u_2 c_{u2}) \quad (1.5)$$

Principally, turbine is designed according to the available discharge (Q), net head (H_n), and chosen rotational speed (n). These parameters, however, differ over wide ranges from site to site. For this variability, it is useful to have relations to compare the values with some ratio parameters [6]. These ratio parameters are designated as reduced quantities transferred from the corresponding dimensional quantities.

$$\underline{c} = \frac{c}{\sqrt{2gH_n}} \text{ as reduced absolute velocity} \quad (1.6)$$

$$\underline{u} = \frac{u}{\sqrt{2gH_n}} \text{ as reduced peripheral velocity} \quad (1.7)$$

$$\underline{v} = \frac{v}{\sqrt{2gH_n}} \text{ as reduced relative velocity} \quad (1.8)$$

$$\underline{h} = \frac{h_p}{H_n} \text{ is reduced piezometric head} \quad (1.9)$$

$$\underline{Q} = \frac{Q}{\sqrt{2gH_n}} \text{ is reduced discharge.} \quad 1.10)$$

At BEP, $\underline{Q} = *Q$ is called the turbine capacity

$$\underline{\omega} = \frac{\omega}{\sqrt{2gH_n}} \text{ is reduced angular velocity} \quad (1.11)$$

To designate the best efficiency points, the capacities of the turbine annotated as $*Q$, $*\omega$, $*c$, and so on. The capacity of the turbine is limited only to the measure of the size of the turbine. Speed number is a parameter for the classification of turbine that groups different types of turbines in certain band of speed numbers. Speed number is dimensionless and all geometrically similar turbines have the same speed number.

$*\Omega = *\underline{\omega}\sqrt{*Q}$ where *(asterisk) signifies the condition at the Best Efficiency Point (BEP).

Alternatively, speed number, Ω , can be expressed in terms of Q , H_n and n ,

$$\Omega = \frac{\pi.n\sqrt{Q}}{30(2gH_n)^{3/4}} \quad (1.12)$$

Sometimes the turbines need to operate beyond the designed discharge. So a quantitative comparison of the part-loading or over-loading condition is done with the designed load indicated by admission or the capacity ratio of the turbine, κ , where,

$$\kappa = \frac{Q}{*Q} \quad (1.13)$$

is a dimensionless quantity proportional to the guide vane opening. At BEP when $Q=*Q$ (and consequently $\omega=* \omega$), $\kappa=1.0$. The value of ' κ ' below '0' signifies part load while that greater than '0' signifies the turbine operating in over-load condition. There are other two expressions for specific speed which are not dimensionless.

$$n_q = \frac{n\sqrt{Q}}{H_n^{3/4}} \quad \text{and} \quad n_s = \frac{n\sqrt{*P_r}}{H_n^{5/4}} \quad (1.14)$$

where, 'n' is the synchronous rotational speed, 'Q' is the discharge, 'H_n' is the net head and '*P_r' is the maximum power of the turbine.

$n_q = 89.\Omega$ and $n_s = 379\sqrt{* \eta * \kappa * \Omega}$ where '* η ' is the efficiency at maximum turbine power and '* κ ' is the admission at maximum turbine power

The speed number can also be expressed as the function of reduced circumferential speed at the blade outlet and the blade outlet angle.

$$* \Omega = \sqrt{\pi} \cdot \underline{u}_2^{3/2} \sqrt{\tan(\pi - \beta_2)} \quad (1.15)$$

where, $\underline{u}_2 = \frac{u_2}{\sqrt{2gH_n}}$ is a dimensionless blade outlet velocity and $(\pi - \beta_2)$ or β_2

is the blade outlet angle in the flow direction.

Solving the above equation,

$$\underline{u}_2 = \frac{* \Omega^{2/3}}{(\pi \tan(\pi - \beta_2))^{1/3}} \quad (1.16)$$

From this equation, we can deduce that within the same specific speed number, increase in diameter and circumferential speed can be compensated by decreasing outlet blade angle within the limited range of angles [7].

1.4 Components of Francis hydro turbine

1.4.1 Runner

Runner of a Francis turbine consists of series of curved, three dimensional sculpted vanes or blades that are arranged evenly around the circumference in the angular space between hub and band. The shape of runner and angle of vanes are so arranged that water enters the runner in radial direction at its outer periphery and changes to axial direction as it passes over blades, thereby changing the angular momentum of the fluid and producing torque that rotates the runner. Labyrinth seal is provided at the crown and band to reduce the leakage flow between the runner and the casing. The runner is keyed to the turbine shaft.

As for the purely radial- flow turbine as developed by James B. Francis, it had in-flow in the tangential to radial direction and entirely radial at the outlet with almost no tangential component. This entailed the water to make a 90° turn to pass into draft tube which was constrained by the smaller flow area, perpendicular to the radial direction, of the runner to maintain low velocity at exit. Contrary to this, a mixed flow type of runner turns water from radial to axial direction within the rotor giving axial flow at outlet with negligible radial/tangential component. This allows larger flow area, perpendicular to the axial direction, to pass the large amount of water maintaining low outlet velocity at runner exit. For optimum performance, the blades of the runner are so shaped that there remains no whirl or tangential component of the velocity at outlet, i.e., $v_{w2}=0$. This corresponds to the maximum kinetic energy (KE) maintained at the runner outlet.

From equation (1.2)

$$E = \Gamma \omega = \rho Q (U_1 C_{u1} - U_2 C_{u2}) \quad (1.17)$$

Considering no swirl at outlet, $v_{w2}=0$,

$$E = \rho Q U_1 C_{u1} \quad (1.18)$$

Energy transfer to rotor per unit mass of the fluid,

$$\frac{E}{m} = e = U_1 C_{u1} \quad (1.19)$$

At inlet of the runner,

$$\tan \alpha_1 = \frac{C_{m1}}{C_{u1}} \quad (1.20)$$

$$\text{or, } C_{u1} = C_{m1} \cdot \cot \alpha_1$$

$$\text{and, } U_1 = C_{m1} (\cot \alpha_1 + \cot \beta_1)$$

$$\text{so, } e = C_{m1} (\cot \alpha_1 + \cot \beta_1) \cdot C_{m1} \cdot \cot \alpha_1$$

$$\text{or, } e = C_{m1}^2 \cdot \cot \alpha_1 (\cot \alpha_1 + \cot \beta_1)$$

The velocity diagram of a typical reaction type hydro turbine is shown in Fig. 1.1.

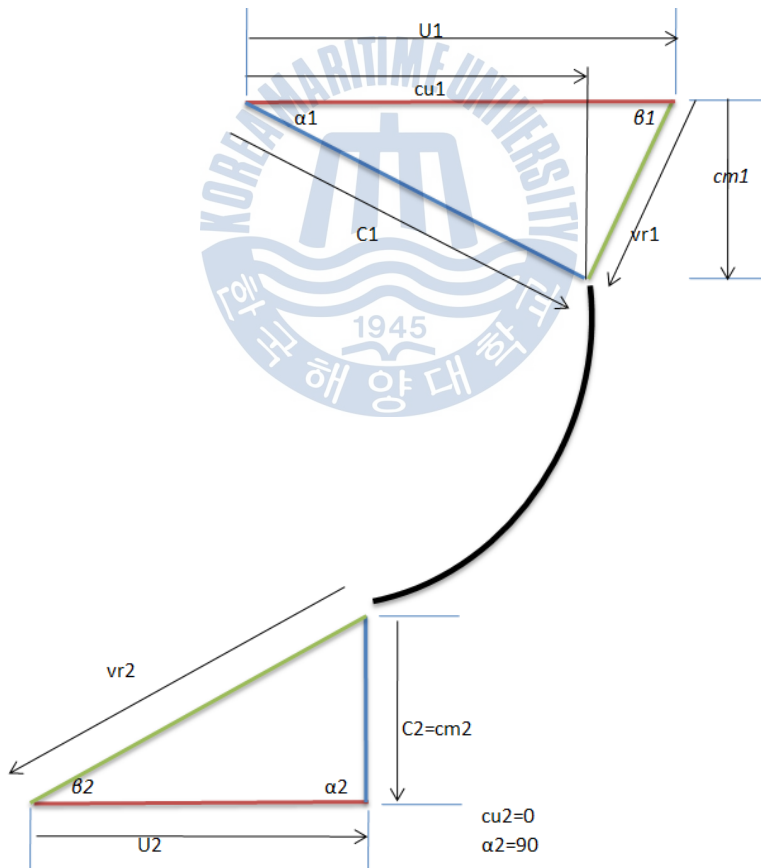


Fig. 1.1 Velocity diagram of a reaction turbine

Loss of KE/unit mass, $e' = \frac{C_{m2}^2}{2}$

So, blade efficiency, $\eta_b = \frac{e}{e' + e} = 2C_{m1}^2 \frac{\cot \alpha_1 (\cot \alpha_1 + \cot \beta_1)}{e' + e}$

$$\text{or, } \eta_b = \frac{2C_{m1}^2 \cot \alpha_1 (\cot \alpha_1 + \cot \beta_1)}{C_{m2}^2 + 2C_{m1}^2 \cot \alpha_1 (\cot \alpha_1 + \cot \beta_1)} \quad (1.21)$$

We have, $C_{m1} = C_{m2}$ for constant flow velocity throughout.

$$\therefore \eta_b = 1 - \frac{1}{1 + 2 \cot \alpha_1 (\cot \alpha_1 + \cot \beta_1)}$$

Calculating change in pressure energy of the fluid in the rotor, degree of reaction is expressed as,

$$R_r = \frac{e - \frac{1}{2}(C_1^2 - C_{m2}^2)}{e}$$

$$\because C_1^2 - C_{m2}^2 = C_1^2 - C_{m1}^2 = C_{m1}^2 \cot^2 \alpha_1$$

$$\therefore R_r = 1 - \frac{\frac{1}{2} C_{m1}^2 \cot^2 \alpha_1}{e}$$

$$\text{i.e. } R_r = 1 - \frac{\cot \alpha_1}{2(\cot \alpha_1 + \cot \beta_1)} \quad (1.22)$$

Usually, β_1 ranges from 45° to 120° and α_1 lies between 10° to 40° . The ration of blade width to diameter of runner, B/D at inlet depends on specific speed and varies from 1/20 to 2/3. The Specific speed of the runner is closely associated with the shape of the runner.

$n_s = \frac{n\sqrt{P_r}}{H_n^{5/4}}$ signifies that higher will be the N_s value for lower value of H_n , which

means a comparatively large amount of discharge is necessary at lower head to maintain given power output. Also, the velocity of the discharge at the runner outlet should be small enough to avert the occurrence of cavitation.

With the constant research and design modification observed in the Francis Runners to upgrade and enhance its performance, a new type of x-blade runner has come up which is considered as a major breakthrough in the Francis runner design, for medium and low head machines [8]. Compared to its traditional counterpart, the x-blade provides better stability over large flow and head ranges, has good cavitation resistance, and has low pressure pulsation levels and higher efficiency. Based on the years of experience supplemented by extensive model testing and CFD analyses, x-blade was developed by GE Energy. Initially owned by Kvaerner, the patent of x-blade was acquired by GE when Kvaerner was sold to GE. These hydraulic advantages of x-blade design were confirmed by GE and it was first implemented during the early stages of China's Three Gorges Project. X-blade runner maintains its maximum efficiency comparatively higher than that of runners based on conventional geometry. So much so, x-blade runner exhibits higher efficiency at off-design operating conditions which is noteworthy for the runner that is to operate through a large range of net heads. An x-blade runner of 70kW Francis turbine from Sin Han Precision Co. is shown in Fig. 1.2.

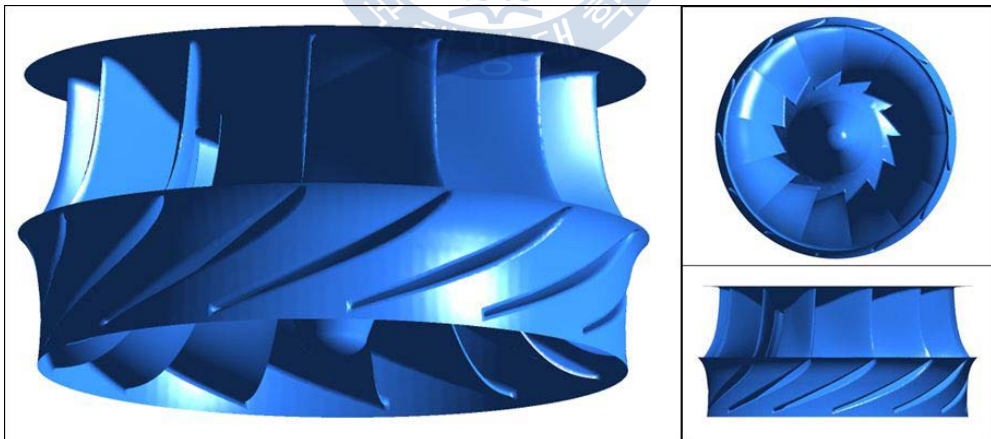


Fig. 1.2 A 70kW x-blade Francis runner, Shin Han Precision Co., Korea

The primary attribute of the x-blade designs relates to the uniform flow distribution in the runner [9]. As Francis blades face high velocity along the band, they are prone to create low pressure zones that lead to the occurrence of cavitation and secondary flow problems in runner. This leads to genesis of inlet cavitation erosion on the suction side along the vicinity of band, decreased efficiency and hydraulic instability. These design drawbacks are well addressed by x-blade geometry which otherwise would not be totally avoided by conventional designs of runner. With the enhancement in performance, x-blade provides higher efficiency, greater range of stable operation and reduced maintenance costs for the hydro plant [9].

1.4.2 Casing, guide vanes and draft tube

Spiral case or casing shrouds the turbine runner. With its decreasing cross section area, it maintains a uniform flow velocity around the stay vanes and wicket gates. Stay vanes are affixed along the outlet. They align the flow from the spiral case that moves forth to wicket gates or guide vanes. Guide vanes are required in Francis turbine to regulate the quantity of water reaching the runner and to adjust the direction of flow so that water enters the runner blades with as minimum shock as possible [10]. The position of the wicket gate blades can be adjusted with the aid of a ring driven by servomotors. They rotate around their axis and alter the net inflow area of the water. By changing the position of the blades, the value of the water flow passing through the turbine is modified. This regulation also permits the appropriate inflow angle to the runner in varying discharge conditions. The guide vanes speed up the water current gliding along its blade surface to produce optimum angle acting on the runner blades. They are designed to change the movement of water particle from radial at inlet to leave the outer edge of guide vane opening with rather a large velocity component in peripheral direction. The direction of absolute velocity of the fluid is supposed to coincide with the direction of the vanes at outlet of the guide vane cascade.

Once water releases its energy in runner, it leaves the runner at minimum pressure through draft tube. The draft tube acts as a conduit that articulates runner outlet with the tailrace where water is finally discharged. The main purpose of draft tube is to convert dynamic pressure into static pressure and hereby it increases the efficiency of the turbine which is done by gradually increasing the cross section area and consequently decelerating the fluid flow motion [11]. It acts as a diffuser and reduces the exit velocity of the flow to minimize the loss of kinetic energy or to recover maximum energy at the outlet. This allows the turbine to be installed above the tailrace level giving that extra head below the centerline of turbine.



1.5. Cavitation in Francis turbine

Cavitation is a hydrodynamic phenomenon typically faced by reaction turbines. One of the reasons for the declined performance of turbine, erosive wear and damage of the turbine parts is due to cavitation phenomenon. Francis turbines operating at off-design conditions suffer two major problems viz. component damage due to cavitation in runner blades and vortex rope formation in draft tube.

Cavitation is a dynamic process of the formation, growth and collapse of cavities in the fluid. It occurs when the static pressure of liquid falls below its vapor pressure. The pressure will fall in the regions where the velocity of the flow increases according to Bernoulli's equation. For a high fluid flow region, the local static pressure drops so much that when it surpasses a critical value corresponding to vapor pressure of the liquid, phase changes from liquid to vapor occur at constant temperature. A large number of vapor bubbles are formed and are carried to higher pressure zones by the fluid stream where the vapor condenses and the bubbles collapse resulting to the formation of cavity. The surrounding fluid is sucked in to the cavity to fill it raising the local pressure as high as 7000 atm [12]. These collapsing bubbles produce a strong characteristic noise and when they collapse near the turbine surfaces repeatedly, they erode the runner surfaces causing cavitation erosion. Because of sudden implosive collapse of the bubbles, high pressure is produced on the surface causing high local stress. The material then fails by fatigue, added by corrosion [13].

Prof. Thoma suggested a dimensionless number called Thoma's cavitation factor ' σ ' that can be used to determine the regions where cavitation is occurring in the reaction turbines.

$$\text{Mathematically, } \sigma = \frac{H_a - H_v - H_s}{H_n} \quad (1.23)$$

For a particular type of turbine, the value of ' σ ' is calculated and is compared with the critical cavitation factor σ_c for that type of turbine. For cavitation not to occur, the value of σ should be greater than σ_c for a given turbine. The value of σ depends

on the specific speed of the turbine, n_s . For a turbine with a particular n_s , σ can be reduced up to a value where efficiency remains constant. Further decrease of σ beyond the critical value called σ_c causes efficiency to drop.

Mathematically, $\sigma > T_c$ where $T_c = 431 \times 10^{-8} \cdot n_s^2$ for Francis turbines.

Liquid entering the hydro turbines at high pressure has static and dynamic components of pressure energy- dynamic pressure due to the flow velocity and static pressure which is the actual fluid pressure. It is the static pressure component that governs the process of formation of vapor bubbles. The type of cavity developing in runner of a Francis turbine for a designed operating range is closely driven by specific energy coefficient ψ , the flow coefficient φ influencing only the cavity whirl. High and low values of ψ correspond to a cavity onset at the leading edge suction and pressure side of the blades respectively [14]. The angular velocity ω and the reference radius R of the runner define the reference area πR^2 and the reference kinetic energy $\frac{1}{2} \omega^2 R^2$, which in turn provide the definition of ψ and φ the dimensionless discharge coefficient and energy coefficient.

$$\varphi = \frac{Q}{\pi \omega R^3} \text{ and } \psi = \frac{2E}{\omega^2 R^3} \quad (1.24)$$

Cavitation can occur in the hydraulic turbines under different forms depending on its hydraulic design and operating conditions. Francis turbine mainly suffer leading edge cavitation, travelling bubble cavitation, Von Karman vortex cavitation and draft tube swirl when operated at off-design regimes of operation. Cavitation has various aspects of impact on hydro turbines, depending on its location and intensity, damaging blades, inducing vibration, deteriorating the performance and changing the discharge through the flow domain significantly. For a Francis runner, none or slightest amount of cavitation is acceptable during the normal operation, contrary to the idea of Kaplan runner where admissible amount of cavitation is obvious and acceptable [15].

Chapter 2 Design and performance analysis of 70kW runner

2.1 Design

A direct method to calculate the general dimension and flow parameters for the runner is presented in this study and CFD tool is utilized to enhance the design and evaluate the performance of the turbine. In the design of a Francis runner, the preliminary parameters considered are the net head (H_n) and Discharge (Q). The hydraulic parameters for the turbine are $H_n=18\text{m}$ and $Q=0.5\text{m}^3/\text{s}$. So the theoretical power of the turbine is

$$P_t = \rho Q g H_n = 88 \quad (2.1)$$

Considering 80% efficiency of the turbine,

$$P_r = \eta \rho Q g H_n = 70 \quad (2.2)$$

In order to first determine the type of the runner and figure out its shape and size, a dimensionless parameter called specific speed is invoked. The maximum allowable value of specific speed for a turbine for given head is calculated as,

$$n_{s-\max} \leq \frac{20,000}{H + 20} + 30 \quad (2.3)$$

$n_{s-\max} \leq 556.3$ indicates suitability of Kaplan type hydro turbine for the given head. Since we don't want to drift to Kaplan, we will choose a suitable rotational speed of the turbine that embraces value of specific speed within the regime of Francis turbine.

The maximum Specific speed allowed for $n_{s-\max}$,

$$n_s = \frac{\sqrt{P_a}}{H_n^{\frac{5}{4}}} \cdot n \quad (2.4)$$

The speed number of Francis turbines has a wide range of $0.2 < \Omega < 1.5$. This wide range imply that the hydraulic design of the runner in these turbines differ rather much from the lowest to the highest speed numbers [16]. The speed number

is a dimensionless quantity and all geometrically similar turbines have the same speed number. At best efficiency point (indicated by *), the speed number of the turbine is expressed in terms of reduced angular velocity and reduced discharge.

$$*\underline{\Omega} = \underline{\omega} \sqrt{\underline{Q}} = \frac{\pi \cdot n \cdot \sqrt{Q^*}}{30 \cdot \sqrt[4]{(2gH_n)^3}} \times 0.819 \quad (2.5)$$

* $\Omega=0.189$ indicates the regime of Francis, we stick on to Francis type hydro turbine and choose $n=900\text{rpm}$. The corresponding specific speed $N_s=203.09$ indicates a Francis turbine with (relatively) large discharge and small head. Francis runners are prone to cavitation damage particularly at their outlet during off-design operating conditions and runners are designed to avert cavitation as much as possible.

Starting off with an empirical relation for the outlet angle of the runner blade [6], $13^\circ < \beta_2 < 22^\circ$.

A smaller value of β_2 is less preferred due to welding constrains. For maximum efficiency, a free vortex performance is applied at the runner outlet with no swirl for the best performance, i.e. the swirl component of the velocity at outlet is zero.

Taking $\beta=16^\circ$, Diameter at outlet,

$$D_2 = \sqrt[3]{\frac{240 \cdot Q^*}{\pi^2 \cdot n \cdot \tan \beta_2}} = 0.350 \quad (2.6)$$

where Q^* indicates best efficiency point at $\kappa=Q/Q^*$ (the capacity ratio ' κ ' taken as 1.1).

The peripheral velocity of the turbine, U_1 , will be proportional to D_2 and speed of the turbine.

$$U_2 = \frac{\pi \cdot n \cdot D_2}{60} = 16.48 \quad (2.7)$$

Also, the meridional velocity at runner outlet can be computed as,

$$C_{m2} = \frac{4Q^*}{\pi D_2^2} = 4.73 \quad (2.8)$$

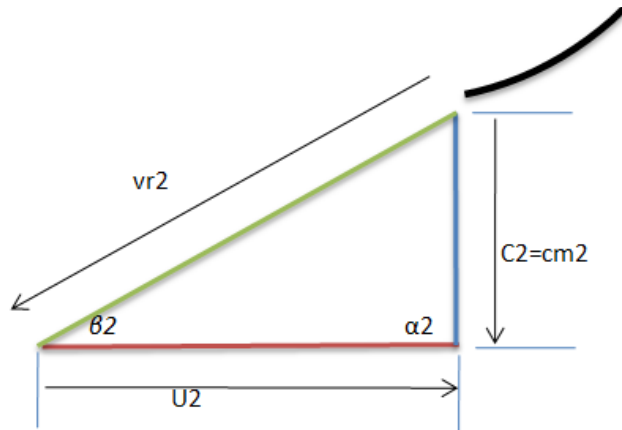


Fig. 2.1 Velocity diagram of flow at runner outlet

For no swirl condition ($C_{u2} = 0$), absolute component of the velocity at outlet, $C_2 = C_{m2} = 4.72$ as in Fig. 2.1.

Now, the values of parameters at inlet can be computed by using Euler's turbine equation. The hydraulic efficiency of the turbine is expressed as,

$$\eta_h = \frac{P_r}{P_t} \quad (2.9)$$

$$\text{Or, } \eta_h = \frac{(U_1 C_{u1} - U_2 C_{u2})}{gH_n} \quad (2.10)$$

where 'U' is the peripheral velocity of the runner blades and 'C_u' is the component of absolute velocity in the direction of U, also referred to as whirl velocity.

In terms of the reduced parameters of head and velocity components,

$$\eta_h = 2(u_1 c_{u1} - u_2 c_{u2}) \quad (2.11)$$

Since, the design is done for no whirl condition,

$$\eta_h = 2(u_1 c_{u1}) \quad (2.12)$$

At 80% efficiency of the turbine,

$$\underline{u_1 c_{u1}} = 0.4 \quad (2.13)$$

Using the empirical relation to compute the reduced peripheral velocity of the blade at inlet,

$$0.7 < \underline{u}_1 < 0.8 \quad (2.14)$$

From calculation iteration and experience, taking $\underline{u}_1 = 0.8$

$$\underline{c}_{u1} = \frac{0.4}{0.8} = 0.5 \quad (2.15)$$

Thus,

$$U_1 = \underline{u}_1 \sqrt{2gH} = 15.03 \quad (2.16)$$

$$\text{And, } C_{u1} = \underline{c}_{u1} \sqrt{2gH} = 9.4 \quad (2.17)$$

Now, the diameter of the runner at inlet is,

$$U_1 = \frac{\pi \cdot n \cdot D_1}{60} \quad (2.18)$$

$$D_1 = 0.319$$

The meridional velocity at the inlet is taken at least equal to or at most 10% of the meridional velocity at outlet of the runner to prevent the backflow and accelerate the meridional flow, as per the rule of thumb [17]. Adopting this value differs from different manufacturer and design philosophy of the runner.

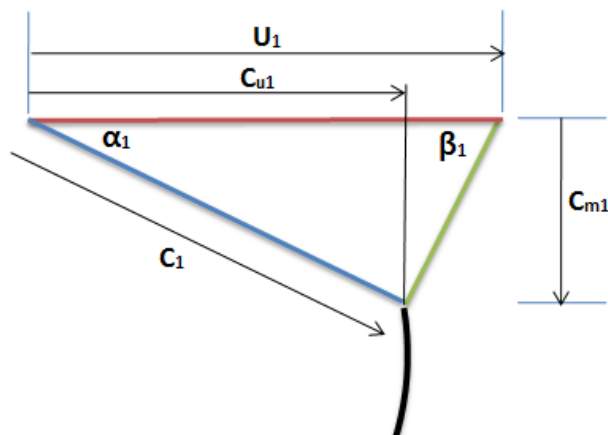


Fig. 2.2 Velocity diagram of flow at runner inlet

Taking C_{m2} 2% larger than C_{m1} ,

$$C_{m1} = 0.98 * C_{m2} = 4.63 \quad (2.19)$$

The inlet blade angle can be determined by solving the velocity triangle as in Fig. 2.2.

$$\tan \beta_1 = \frac{C_{m1}}{U_1 - C_{u1}} \Rightarrow \beta_1 = 39.42 \quad (2.20)$$

And the height of the runner blade equivalent to the width of the guide vanes is determined by solving the continuity equation.

$$B_1 = \frac{Q^*}{\pi D_1 C_{m1}} = 0.98 \quad (2.21)$$

The design equation solver was prepared in MS Excel v.2007 to calculate the above equations and generate the design dimensions of the runner and guide vanes along with the corresponding velocity diagrams at inlet and outlet (Fig. 2.3). The runner is modeled in Unigraphics NX6 using the afore-calculated parameters with legitimate improvement in dimension taking into account the thickness of the blades (Fig. 2.4). An x-blade design is adopted for the profile of the runner blades.

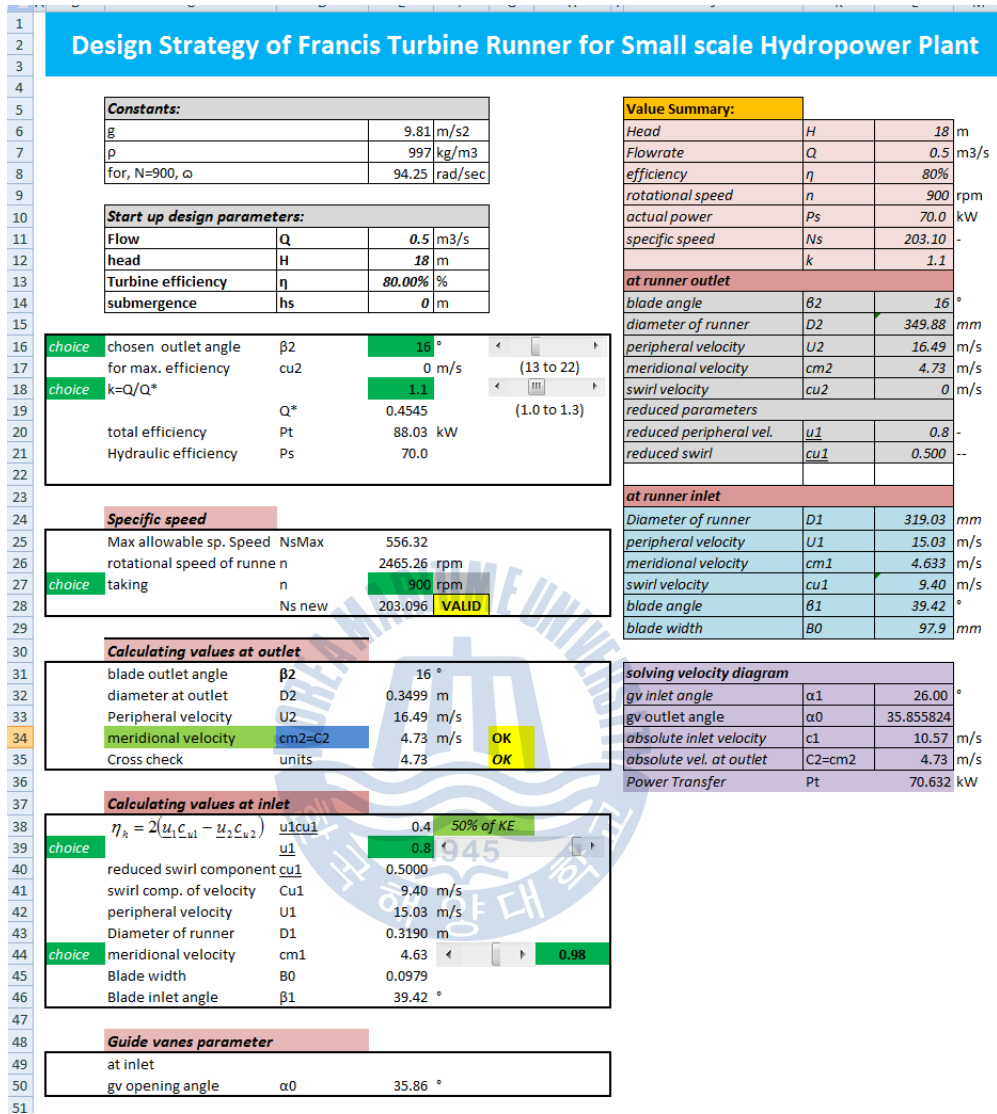


Fig. 2.3 Screenshot of Excel worksheet to generate design dimensions

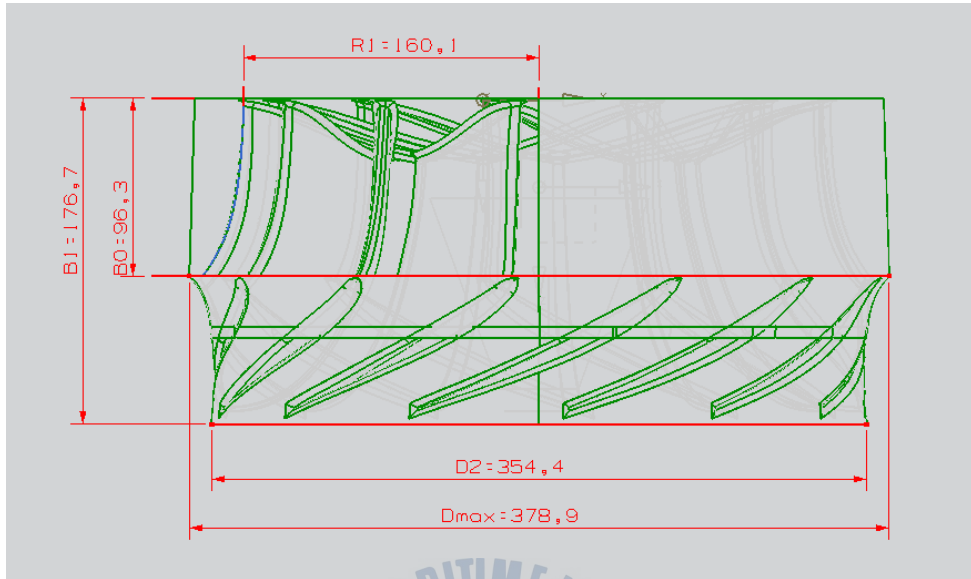


Fig. 2.4 Improved dimension of the runner as modeled in Unigraphics NX6

The relation between the diameter of the runner and the diameter of circle passing through guide vanes centre, D_g , is expressed as:

$$\frac{D_g}{D_R} = (0.29\Omega + 1.07) \quad (2.22)$$

Taking $D_R=0.378\text{m}$, $D_g=0.494\text{m}$.

Length of the guide vanes or guide vane camber length for 6% overlap (Fig. 2.5) can be calculated [18] as,

$$L_g = \frac{\pi D_g}{Z_{gv}} \cdot \frac{1}{0.94} \quad (2.23)$$

The vertical distance between successive guide vanes can be computed as,

$$t_g \approx \frac{\pi D_g}{Z_{gv}} = 0.0971 \quad (2.24)$$

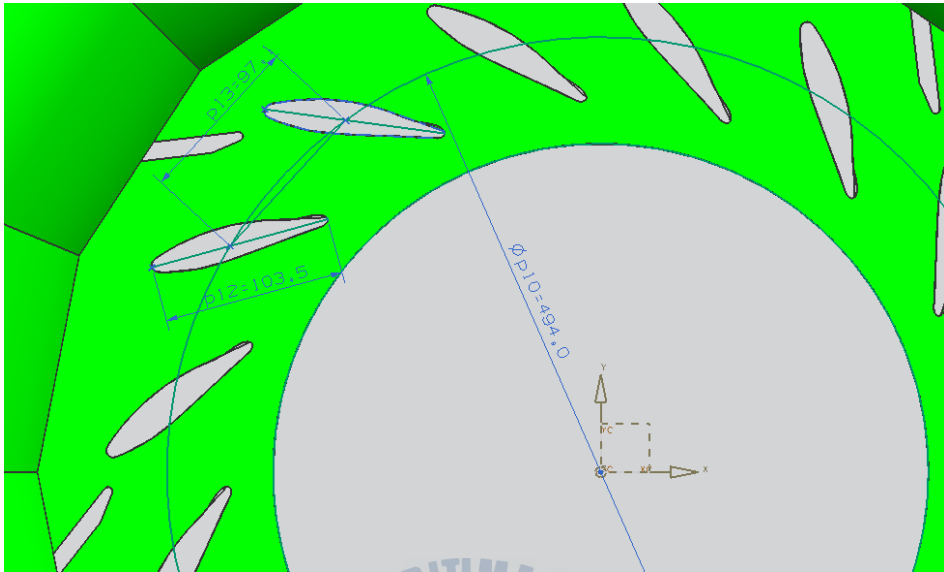


Fig. 2.5 Spiral case with wicket gates and stay vanes for 70kW Francis runner

A complete closure of the guide vanes is necessary and therefore the length of the guide vanes is always slightly larger than the pitch distance i.e.

$$\frac{L_g}{t_g} = 1.06 \text{ (indicating 6\% overlap)} \quad (2.25)$$

The maximum opening of the guide vane angle (α_0) at full load of $0.5\text{m}^3/\text{s}$ is calculated using the following relation,

$$\alpha_0 = (-4.\Omega^2 + 13.\Omega + 1) = 35.86 \quad (2.26)$$

An elbow shaped single channel draft tube is used in this Francis turbine setting.

2.2 Numerical analysis

For the calculation, the computation domain was segregated into 4 components- an inlet pipe, a spiral casing with 16 guide vanes and 8 stay vanes, a runner having 13 blades with crown and band and a draft tube. The domain of runner, spiral casing and draft tube were drafted in Unigraphics NX v.6 and ANSYS ICEM was used for numerical discretization of these domains. The discretization of the fluid domain of the turbine components in 3D CFD are based on tetrahedral volumes (Fig. 2.6). The unstructured tetrahedral cells near the boundary are irregular and require special treatment as tetrahedral cells are not desirable near the walls. A layer of regular prisms is added at the solid boundary to capture boundary layer separation. This approach enhances the grid near the walls and results to accurate solution and better convergence of the numerical solution methods.

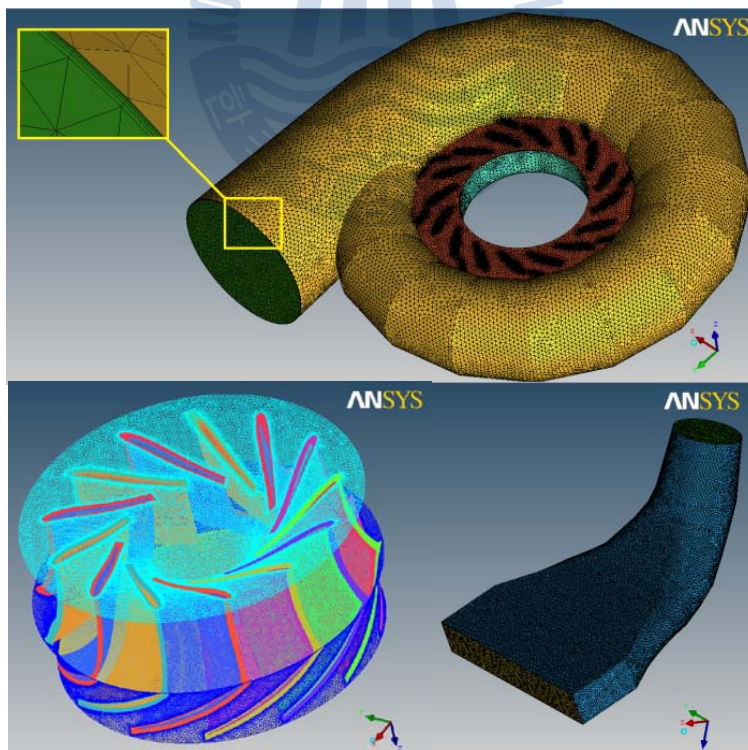


Fig. 2.6 Tetrahedral mesh of spiral case, runner and draft tube with prism layers

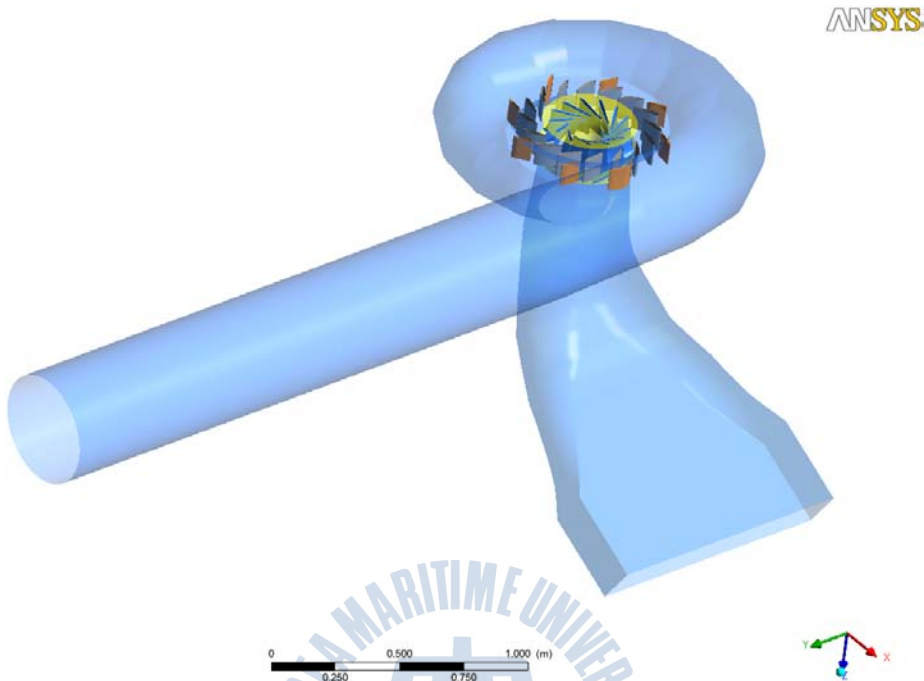


Fig. 2.7 Computational domain of 70kW Francis turbine

The commercial 3D Navier-Stokes CFD-solver ANSYS-CFX has been used to analyze the performance of the turbine. Considering a steady state incompressible uniform flow of fluid in the circumferential direction of the turbine, a steady state single phase (water only) analysis of the full turbine model was performed at full load of and part load conditions maintaining head and rpm (Fig. 2.7). Effective head in terms of pressure is mentioned at the inlet of spiral case and mass flow rate is specified at the outlet of the draft tube as boundary conditions. The inlet boundary condition is comprised of radial velocity or transport velocity and whirl component of the velocity for a given operating condition. The Spiral case and draft tube are stationary components while runner is a rotating component. The entire model of the turbine is formed by combining the components with a frozen rotor interface, each, between casing and runner and runner and draft tube using General Grid Interface (GGI) method for mesh connection. Shear Stress Transport (SST) model is used for turbulence treatment with a high resolution advection scheme. Performance

analysis was done at 0.5m³/s full load discharge and part load discharge of 0.43 m³/s, 0.35 m³/s and 0.29 m³/s at a constant guide vane opening angle of 35° and rotational speed of 900rpm. A correlation between discharge, efficiency and power output was inferred. All simulations were performed using ANSYS CFX v.13 in parallel network workstation.

2.3 Results and dissusions

The performance evaluation of the complete francis turbine was accomplished for the operating regime of 58% to 100% discharge at 4 different flow rates keeping RPM, head and guidevane opening constant.

The efficiency and power output graph in Fig. 2.8 infers that the turbine has a maximum efficiency of 88% generating 70kW of shaft power and both the characteristics decrease towards part flow regime due to increase in head loss.

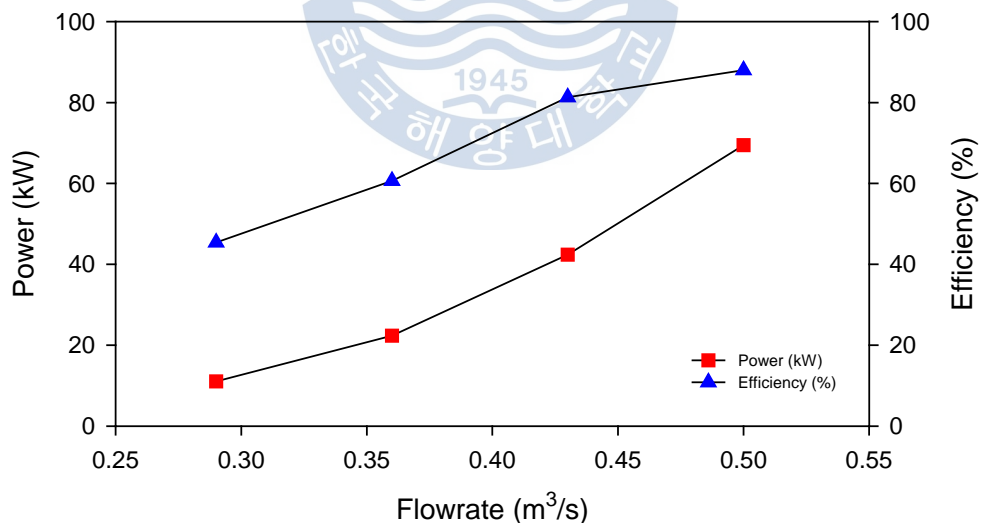


Fig. 2.8 Performance characteristics at different flow rates

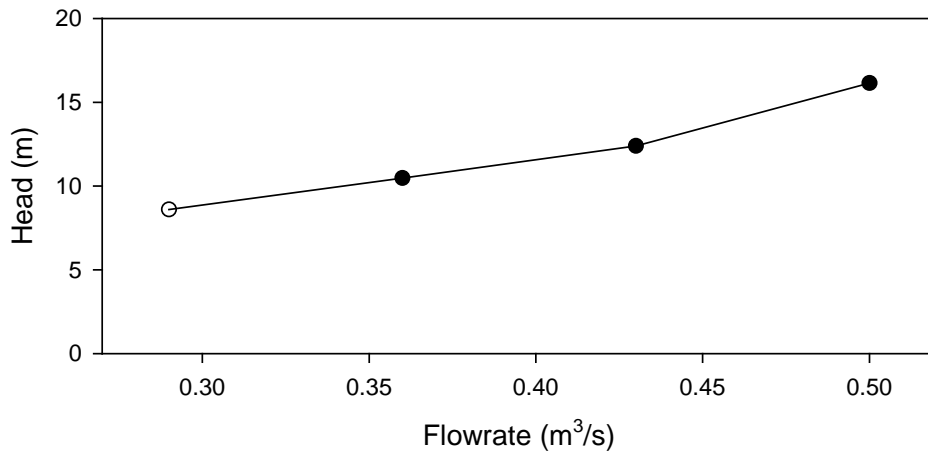


Fig. 2.9 Head loss at different mass flow rates

Head loss in guide vane is higher at part load due to shock and frictional loss and it reduces as load increases. Head loss in draft tube is higher at part load as well as at over load, only near to BEP region it is maximum. Head loss in runner is also higher at part load as well as at overload, only near to BEP region it is minimum [19]. Head loss results of flow separation at part load and hampers the performance of the turbine. The head loss in these components decreases as flow rate moves towards BEP improving the performance of the machine (Fig. 2.9).

Pressure distribution in the central plane of the casing at 4 different operating conditions is shown Fig. 2.10. High pressure zones could be observed at the stay vane regions while magnitude of pressure decreased towards the inner radius as flow moved inward towards the runner.

The corresponding velocity profiles in Fig. 2.11 at the respective flow rates correlate the pressure distribution with high velocity of flow towards the inner radius signifying the change in the flow from circumferential direction to axial direction. The symmetrical distribution of pressure in stay vane region near BEP indicated uniform flow distribution in the casing. As flow rate decreased, pressure distribution was less uniform due to non- uniform flow distribution.

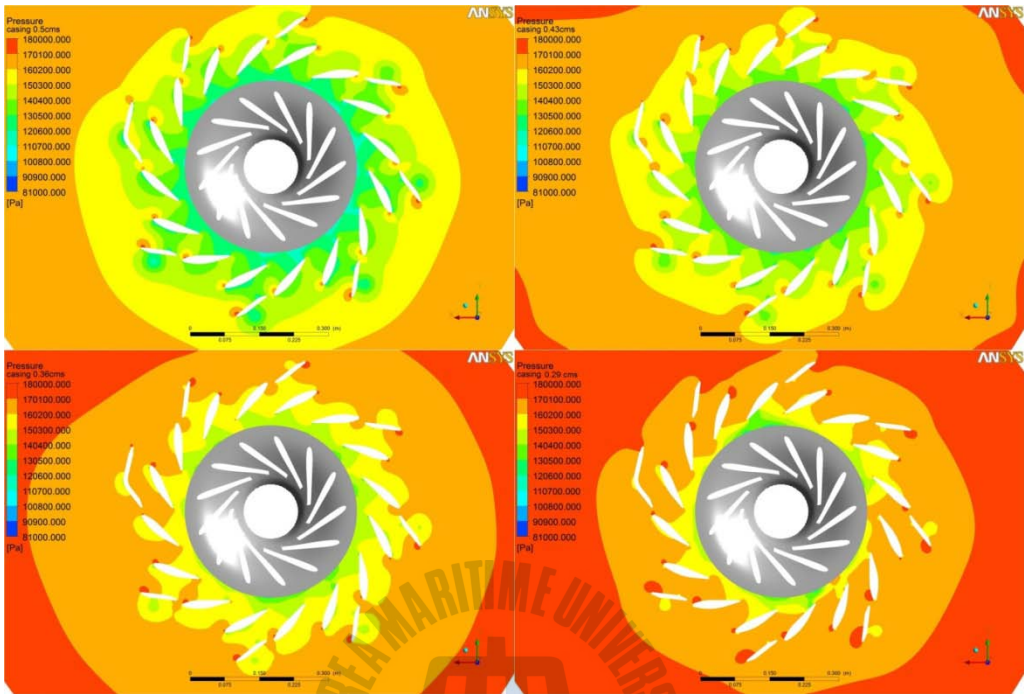


Fig. 2.10 Pressure distribution in spiral casing by flow rates

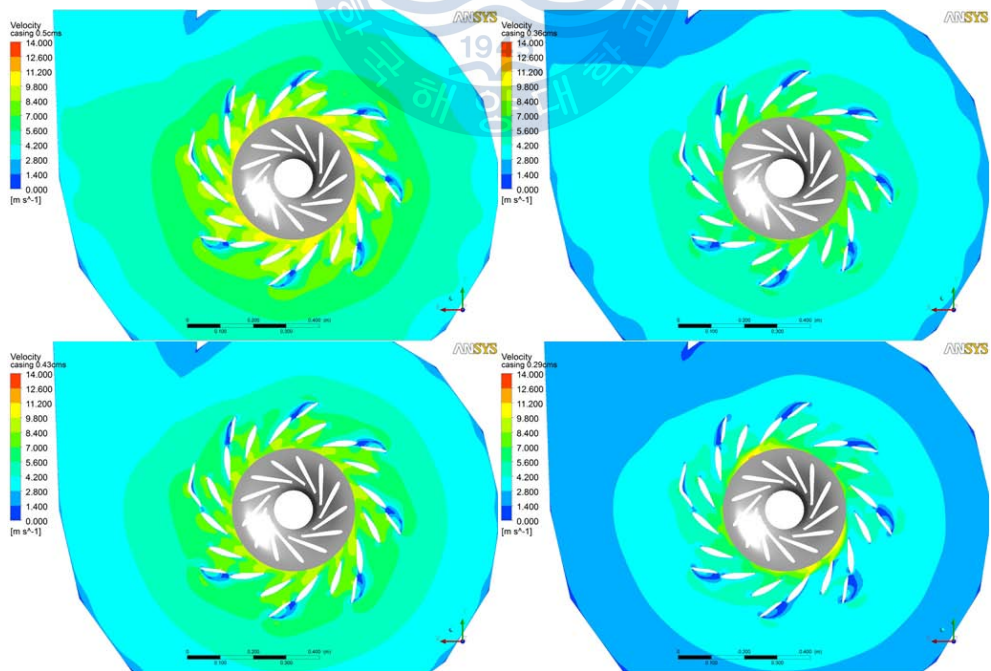


Fig. 2.11 Velocity distribution in the spiral case by flow rates

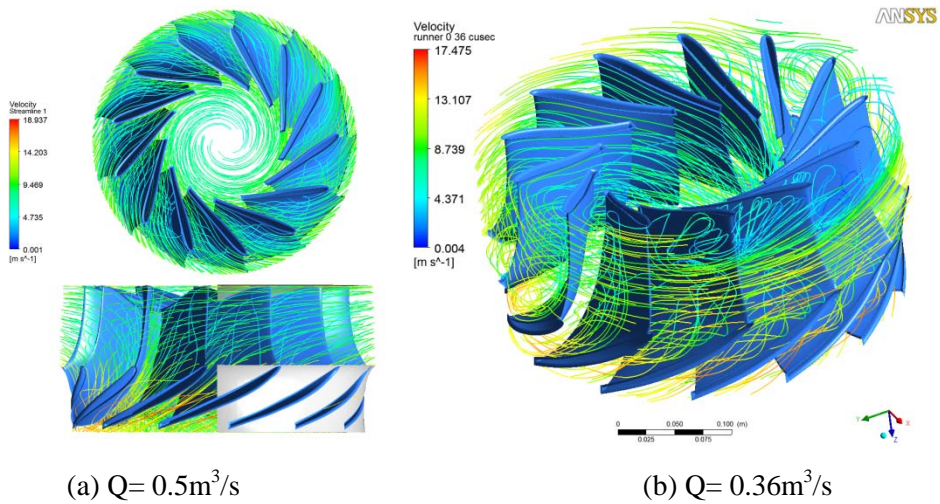


Fig. 2.12 Flow streamlines in runner

A symmetrical inflow in the runner at full load operating point could be observed in Fig. 2.12 which came from the uniform distribution of flow in the casing. The streamlines glided along the crown, making radial entry and axial flow at the centre downstream the runner. However, upon reducing the flow rate, the flow streamlines were disturbed due to the unsymmetrical flow distribution in the spiral case.

The pressure distribution in pressure side and suction side of a runner blade at full load in Fig. 2.13 (a) illustrates uniform distribution of pressure in the runner vanes. The pressure contour revealed a gradual decrease in pressure from inlet to outlet region on both pressure side and suction side. With the magnitude of pressure in pressure side being more than that on suction side, it was this difference in pressure that imparted rotational motion to the runner to produce necessary torque in all operating regimes. The higher the operating load, the more will the blade loading, i.e. more pressure difference between pressure side and suction side and hence more output power. The stagnation region so formed at the leading edge of pressure side was caused by the acceleration of flow when it changed its direction from radial to axial.

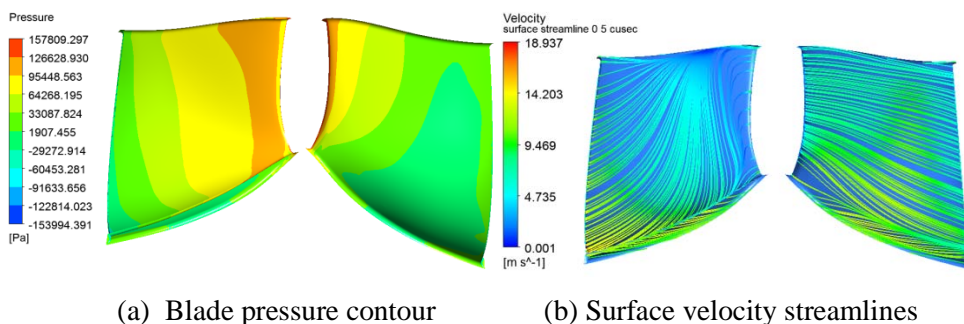


Fig. 2.13 Pressure and surface velocity distribution on runner blade at full load

Likewise, from the velocity streamlines in Fig. 2.13 (b) on the runner blade surface, the velocity in the hub region was small and increased as flow advanced towards the band. This aside, the velocity of flow in pressure side is smaller as compared to that in suction side near the trailing edge, evident to pressure distribution in runner blades. For a given operating regime, Francis turbine is subject to two types of static loads viz. the centrifugal force induced by rotation and the load due to water pressure. The stress caused by the centrifugal force is small as compared to the stress caused by water pressure and is thus not considered. The flow analysis takes into account only the pressure variation caused by the load of water particles.

The pressure distribution in the runner depends on the inflowing water as water imparts different pressure at different operating regimes. The pressure distribution from the crown to hub is shown in Fig. 2.14 where the pressure difference between the regions decreased as the flow rate decreased resulting to lower value of blade loading and generation of smaller torque. The decreasing difference in pressure at suction side and pressure side was also depicted by C_p graph at corresponding flow rates. The C_p graph in Fig. 2.15 is plotted for a single runner blade for the 4 cases of flow rates. As flow rate decreased, the pressure in the blade surface at pressure side also decreased especially in the leading edge (LE). The trend of blade surface

pressure distribution changed drastically for part load conditions drastically relative to that at full load.

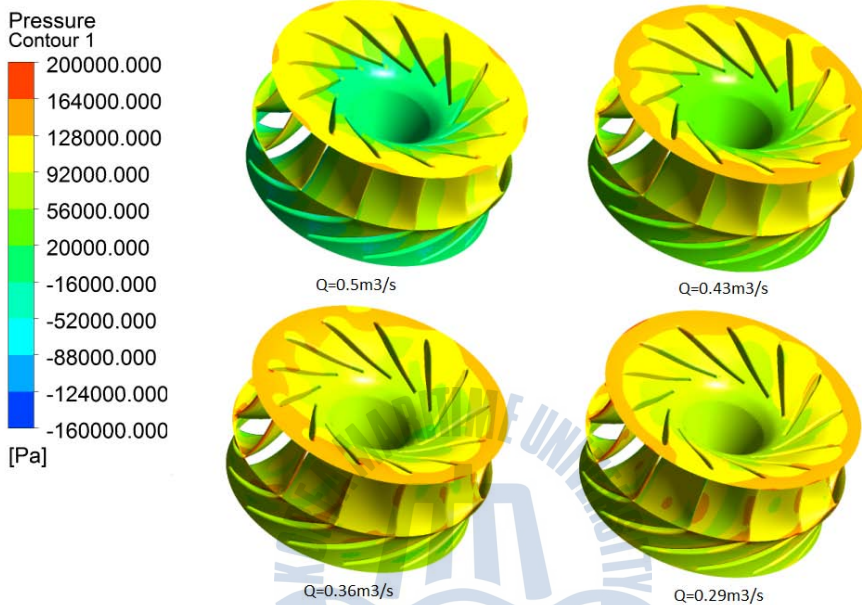


Fig. 2.14 Pressure distribution in runner by flow rates

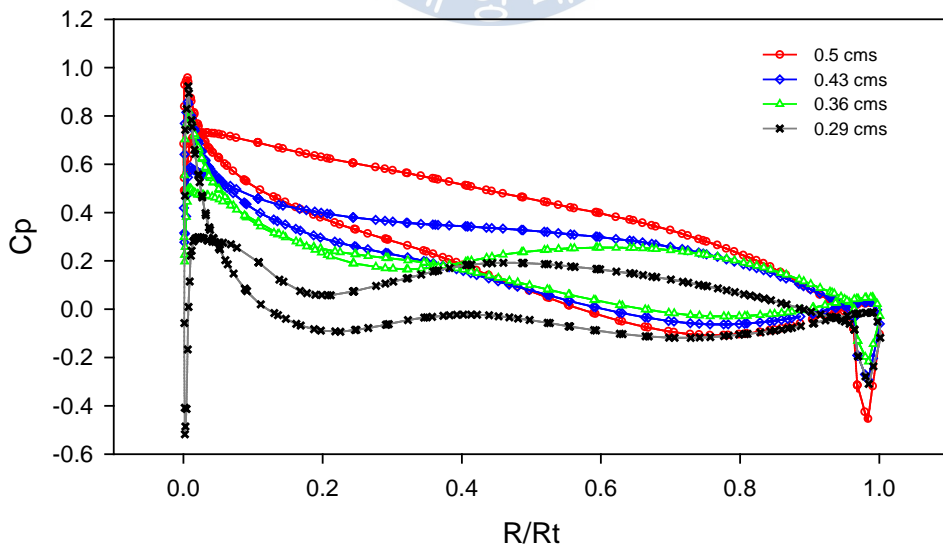


Fig. 2.15 Cp graph at 50% of runner blade for 4 flow rates

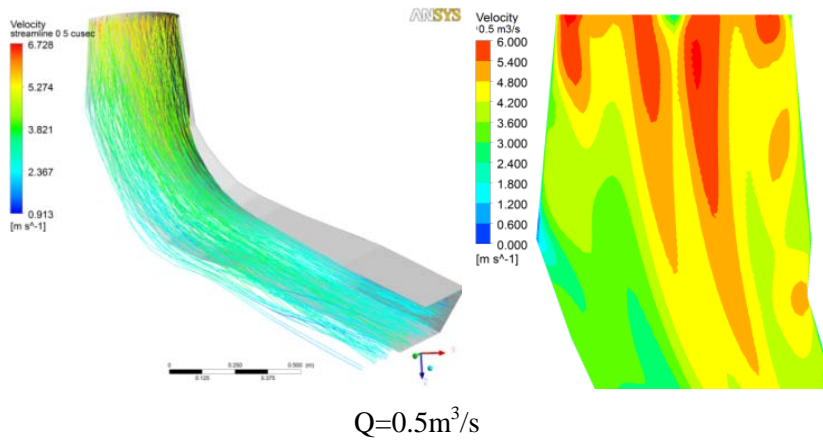


Fig. 2.16 Velocity streamlines and vector contour and vector plots at 0.5m³/s

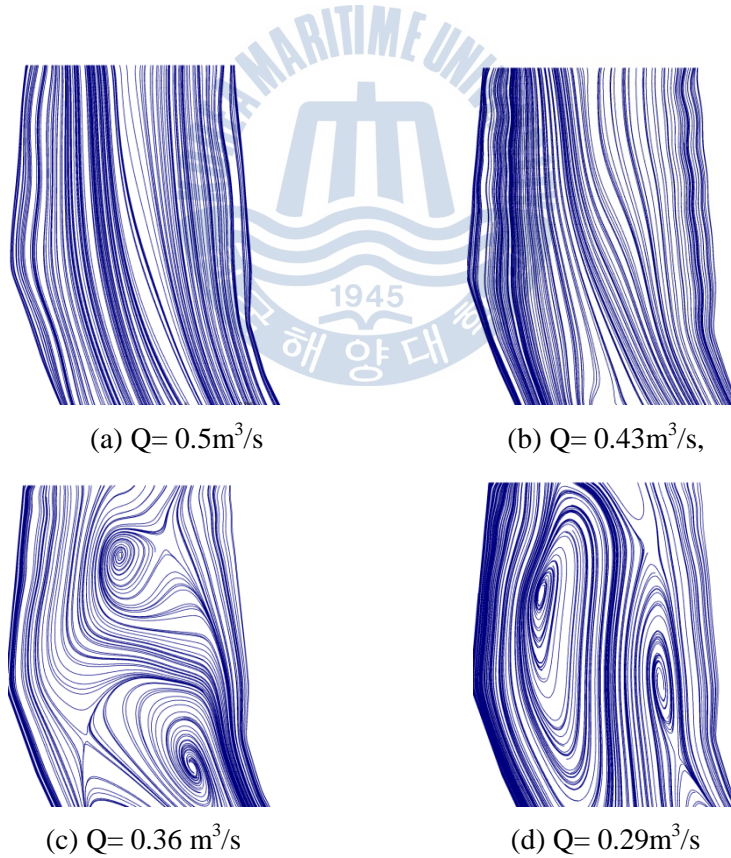


Fig. 2.17 Velocity streamlines in mid section of draft tube by flow rates

An elbow type draft tube having a single channel outlet is incorporated for the so designed runner. The velocity distributions in the draft tube at full load and part load (Fig. 2.16, 2.17) operating points are depicted with flow streamlines and velocity contour velocity vector plot at the central plane of the draft tube. At full load, the velocity in the draft tube was streamlined without presence of any swirl at runner outlet and recirculation in draft tube wall.

The gradual increase in pressure (and corresponding decrease in velocity) from runner downstream towards the outlet of draft tube signified good energy recovery and homogeneous distribution of static pressure. The flow pattern in the draft tube changed drastically upon changing the flow rate. When turbine operated in partial loads, swirl appears at the outlet of the runner with more of the streamline being concentrated at the wall of the draft tube flow domain and stagnation regions appear in the inner fluid zone of draft tube. The swirling flow in draft tube is often related to appearance of vortex rope and pressure fluctuation. Such secondary flows and cross flows appearing in runner outlet at part load operations trigger vortex breakdown in draft tube. The additional inertial force produced by the flow moving past draft tube elbow makes the flow in the diffuser unbalanced. A time-dependent transient flow analysis with an appropriate turbulence model along with reasonable timestep is required to analyze transient particularities.

Chapter 3 Partial load performance of Francis turbine

3.1 Flow theory

In hydro machineries, a small improvement in the geometry of rotating components can have a large positive effect from the point of operation and maintenance cost. To identify such room for improvement, it is a good idea to consider the interaction between the components of the turbine. The components of Francis turbine experience strong three-dimensional rotational flow due to the change in the flow configuration from radial to axial direction. At part-load operation of the turbine, swirling flow appears downstream the runner which produces vortex rope. The consequences of vortex developed are pressure pulsation, axial and radial forces, torque fluctuation, structure vibration- the unpleasant features exhibited by Francis type hydro turbine that occur with unsteady flow [20].

The flow in the different components of turbine are interrelated and react mutually; especially the components like guide vanes, runner and draft tube have strong influence on one another due to the dynamic forces and resulting vibration. While a steady-state simulation can predict turbine performance parameters like efficiency, cavitation and hydraulic losses, the analysis of dynamic forces demands calculation of unsteady flow with advanced turbulence model to achieve accurate results. Shear Stress Model (SST) [21], Realizable $k-\epsilon$ [22], standard $k-\epsilon$ including hybrid Kato-Launder correction[23] are of good choices for turbulence model to analyze rotor-stator interaction and pressure pulsation but more sophisticated turbulence models like Renormalization Group (RNG $k-\epsilon$) [24], [25], extended $k-\epsilon$ [26], Large Eddy Simulation (LES), Scale-Adaptive Simulation (SAS-SST), Reynolds Stress Models (RSM) [27] are opted for capturing draft tube vortex rope more accurately. These turbulence models and the numerical simulation as a whole require finer grids, extended computational effort and CPU time. In transient-state

flow analysis, the various hydrodynamic parameters are the function of the time and several unsteady phenomena transpire due to additional inertial forces.

The commercial 3D Reynolds Averaged Navier-Stokes CFD-solver Ansys-CFX v13.0 was utilized to investigate the time varying unsteady flow through a vertical shaft 70kW Francis turbine in its stationary and transient passages at 100% load ($0.5 \text{ m}^3/\text{s}$) and 72% load ($0.36 \text{ m}^3/\text{s}$) where the transient flow fields in casing, runner and draft tube were simulated. Also, for distinct vortex shedding, the guide vane angle was shifted from 35° to 37.5° . The efficiency of the turbine with 37.5° guide vane angle at $0.36 \text{ m}^3/\text{s}$ was evaluated as 58.48% from the steady state analysis.

The hydraulic parameters of the investigated turbine are discussed in Chapter 2. Owing to non-uniform inflow from the spiral case and unequal pitching of guide vanes and runner, the computational grid of the entire turbine with all channels of the runner and of the tandem cascade was considered, without applying any periodicity in any components. This arrangement represents the most general approach in predicting the rotor-stator interaction.

For transient analysis, the timestep of 2° rotation of runner was taken for 10 full rotations of the runner. So the timestep was 0.00037037s , corresponding to $1/180$ of the runner rotational period. The total computational time was 0.667s i.e. 10 rotational periods of the runner. A second order backward Euler was used as transient scheme with a high-resolution advection scheme. The maximum loop coefficient was taken as 3.

The $k-\omega$ based Shear Stress Transport (SST) model of Menter was applied for turbulence treatment [28]. The transport equations for the SST model are expressed below where the turbulent kinetic energy 'k' and turbulent frequency or dissipation per unit turbulent kinetic energy ' ω ' are computed by using the following relations:

For Turbulence Kinetic Energy,

$$\frac{\partial k}{\partial t} + \nabla \cdot (uk) = P_k - \beta^* k \omega + \nabla \cdot [(v + \sigma_k v_T) \nabla k] \quad (3.1)$$

where P_k is the production limiter.

For Specific Dissipation Rate

$$\frac{\partial \omega}{\partial t} + \nabla \cdot (u\omega) = \alpha S^2 - \beta \omega^2 + \nabla \cdot [(v + \sigma_\omega v_T) \nabla \omega] + 2(1 - F_1) \sigma_{\omega 2} \frac{1}{\omega} \nabla k \cdot \nabla \omega \quad (3.2)$$

The first blending function F_1 is calculated from

$$F_1 = \tanh \left\{ \left\{ \min \left[\max \left(\frac{\sqrt{k}}{\beta^* \omega y}, \frac{500\nu}{y^2 \omega} \right) \frac{4\rho\sigma_{\omega 2} k}{CD_{k\omega} y^2} \right] \right\}^4 \right\} \quad (3.3)$$

$$CD_{k\omega} = \max \left(2\rho\sigma_{\omega 2} \frac{1}{\omega} \nabla k \cdot \nabla \omega, 10^{-10} \right) \quad (3.4)$$

And, Kinematic eddy viscosity,

$$\nu_T = \frac{\alpha_1 k}{\max(\alpha_1 \omega, SF_2)} \quad (3.5)$$

where S is the invariant measure of the strain rate and F_2 is the second blending function expressed as

$$F_2 = \tanh \left[\left\{ \max \left(2 \frac{\sqrt{k}}{\beta^* \omega y}, \frac{500\nu}{y^2 \omega} \right) \right\}^2 \right] \quad (3.6)$$

Each of the constants is a blend of an inner (1) and outer (2) constant, blended through

$$\phi = \phi F_1 \phi_1 + (1 - F_1) \phi_2 \quad (3.7)$$

where ϕ_1 and ϕ_2 are the coefficients of the k - ω and k - ε models respectively.

The turbulence viscosity is calculated by

$$\nu_T = \min \left(\frac{\rho k}{\omega}, \frac{a_1 \rho k}{SF_2} \right) \quad (3.8)$$

where $a_1=0.31$ and blending function F_2 is obtained from eq. (3.6).

The recommended values for the constants in the above equations are:

$$\alpha_1 = 5/9, \alpha_2 = 0.44,$$

$$\beta_1 = 0.075, \beta_2 = 0.0828,$$

$$\beta' = \frac{9}{100}$$

$$\sigma_{k1} = 1.176, \sigma_{k2} = 1,$$

$$\sigma_{\omega1} = 2, \sigma_{\omega2} = 1.168$$

The governing equations are discretized by Finite Volume Method in spatial direction and by Finite Difference method in temporal direction.



3.2 Flow analysis

The overall results of the time dependent analysis are presented for full load and part load operations. Fig. 3.1 (a) depicts the velocity vector plot and pressure distribution at the mid section of the casing at 0.556sec of runner rotation for full load condition. The velocity profile at the inlet of the casing is uniform and is evenly distributed which gradually transforms into a vortex-free flow as the flow advanced inward.

The equivalent pressure contour in Fig. 3.1 (b) was in coherence with the uniform flow that was distributed evenly around the casing. From the velocity vector plot and pressure contour (Fig. 3.1 (c)), it can be inferred that there was no collision of flow at the inlet and separation of flow at the outlet of the casing. A uniform velocity flow vector of similar fashion was also observed at 72% part load which signifies that the design of the spiral case is reasonable to sustain the uniform flow even at off-design operating regimes.

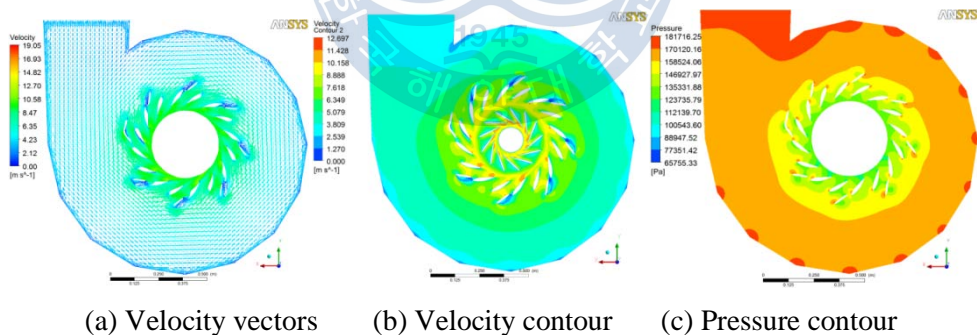
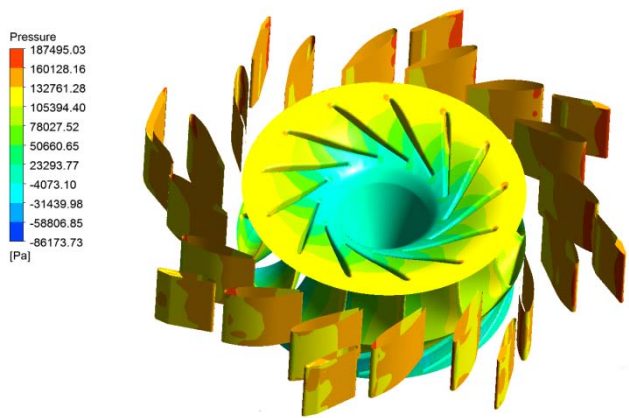
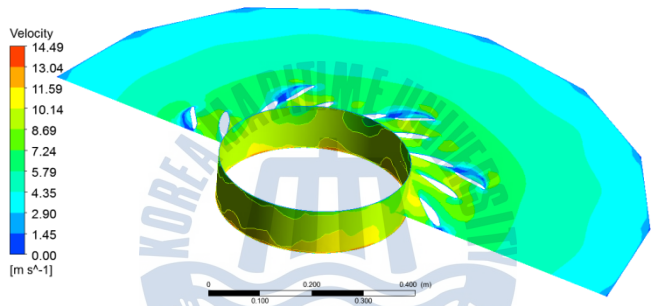


Fig. 3.1 Flow features in the mid span of casing



(a) Runner, guide vane and stay vane



(b) Mid section of casing

Fig. 3.2 Pressure contour and velocity distribution in the tandem cascade

The flow velocity increased as it moved toward the runner. As the flow advanced toward the inner radius, the corresponding pressure decreased sharply due to flow acceleration. This was confirmed by pressure distribution in runner and spiral case in Fig. 3.2 where the pressure reduced from high pressure zone in the spiral case (orange) to low pressure zone (cyan) in the runner. The pressure distribution at the stay vanes was higher whereas it was lower at the runner inlet due to the transformation of the flow from radial to axial direction. The strongly accelerated flow toward the runner indicated a relative reduction in pressure. Also observed was the wake behind the stay vanes that incited pressure fluctuation and consequently fluctuation in torque.

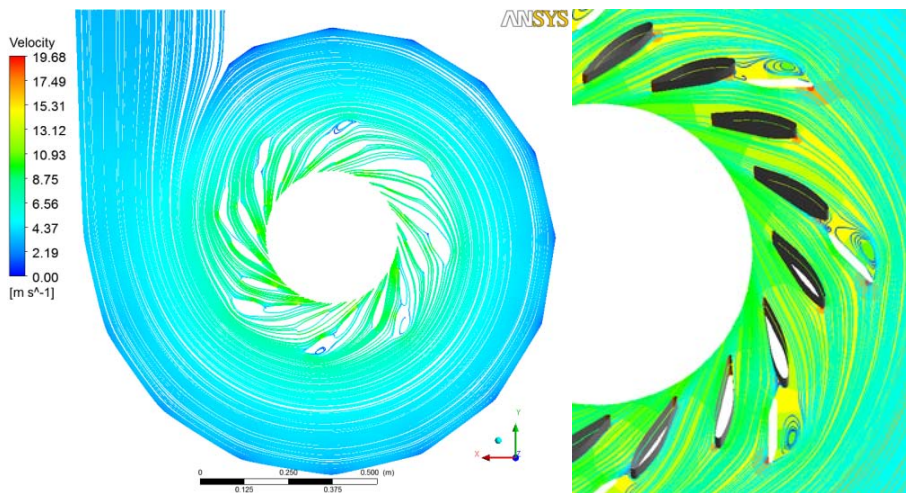
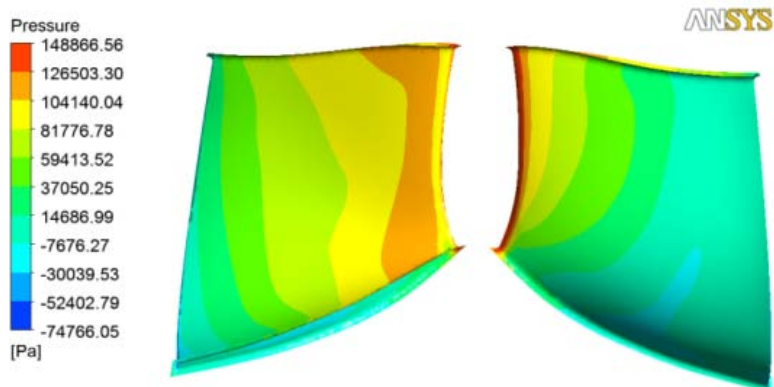
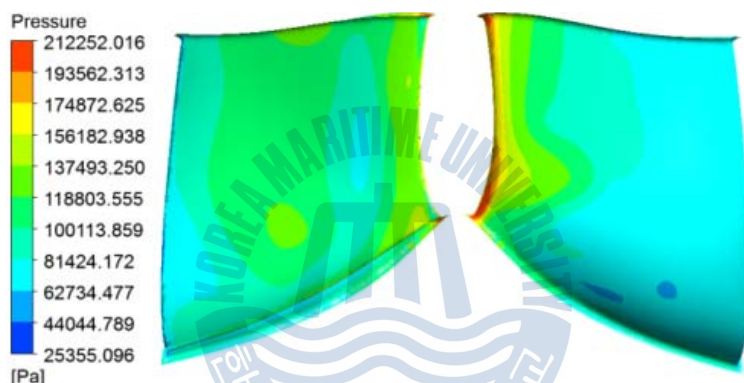


Fig. 3.3 Surface streamlines on mid span of casing and guide vanes, 100% load

The unsymmetrical pressure distribution in the circumferential direction at stay vane zones caused non-uniform flow in casing. However, the pressure distribution in the spiral case is symmetrical enough to retain uniform flow. Fig. 3.3 shows the uniform distribution of the velocity streamline in the spiral case. There was a minor collision of the flow particles at the inlet of guide vanes and no flow separation at the outlet. This was due to the fact that the guide vane angle used for this simulation was 37.5° while the design guide vane angle for optimal operating condition of this turbine is 35° . The angle of the guide vanes and their profile should be reasonably designed to achieve flow stability and maximum efficiency. With strong flow acceleration towards the runner, the accelerated flow quickly covered up the wake region near the guide vanes and minimized its effect. The effect of wake is more conspicuous in axial turbines due to the absence of strongly accelerated flow towards the runner. At the inlet of some guide vanes, the stagnation point at the leading edge was visible where the corresponding value of pressure was maximum.



(a) $Q=0.5\text{m}^3/\text{s}$ (100% load)



b) $Q=0.36\text{m}^3/\text{s}$ (72% load)

Fig. 3.4 Pressure distribution in the runner blade, pressure side and suction side

The pressure distribution in the pressure side and suction side of the runner blade was uniform. The pressure contour in Fig. 3.4 illustrates the gradual decrease in the pressure from inlet of the blade to its outlet on both pressure side and suction side, except for the region near the outlet of the runner. With the static pressure at the exit of runner being less than the atmospheric pressure, water fills up all the passages of the runner blades. As water glides along the blades of the turbine runner, it produces a pressure difference between the either sides of the blade called blade loading to produce torque and imparts a rotational motion to the turbine.

The region near the trailing edge of the runner blade on the suction side is prone to cavitation damage as the pressure in this area is lowest. Once the water gives up its energy and leaves the runner, the magnitude of pressure in the suction side and pressure side must be equal. So as to maintain the pressure value at the outlet, a small rise in pressure at the suction side becomes obvious. This explains to why the pressure gradient in the band is not gradually decreasing unlike it in the blade surface. This phenomenon facilitates to improve the performance of the turbine, wherein the runner prevents the cavitation inception and the erosion triggered by sand particles [24]. Meanwhile, the velocity of flow in the hub was smaller and it increased gradually as flow moved towards the outlet of the runner in band region, (Fig. 3.5). Likewise, the magnitude of velocity in the pressure side was small while the flow was accelerated at the suction side of the blade. The smooth distribution of velocity streamline represented uniform flow in the runner blade.

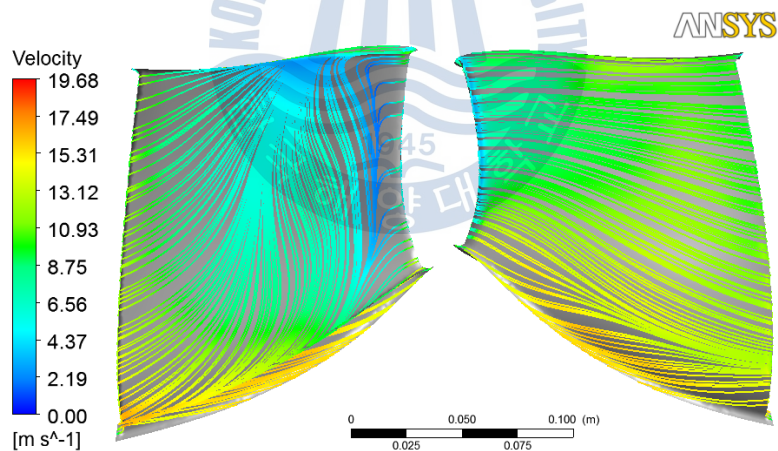
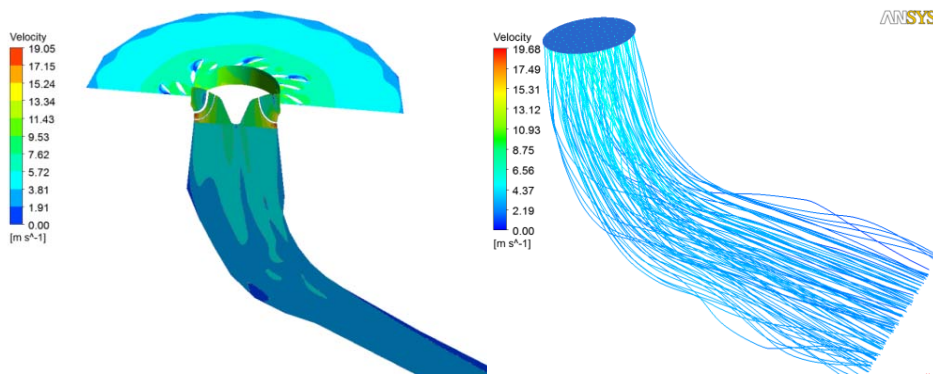


Fig. 3.5 Velocity streamlines on runner blade at full load



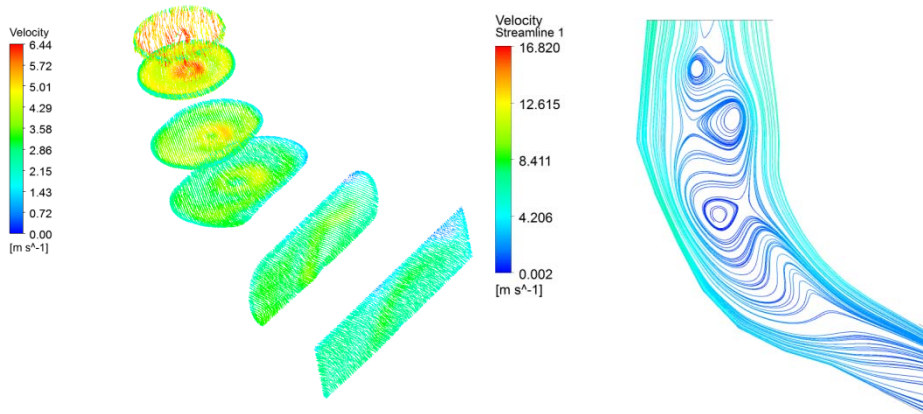
(a) Velocity contour in turbine (b) Velocity streamlines in draft tube

Fig. 3.6 Velocity distribution in casing, runner and draft tube at full load

From the flow feature in draft tube at full load operation as depicted in Fig. 3.6, the flow accelerated in the spiral case as it glided through the vanes and entered the runner. After the runner transferred the energy into torque by the pressure difference between its blades, the flow decelerated while moving toward the draft tube outlet.

Much of the turbine's performance depends on the flow behavior in the draft tube and the flow condition in draft tube depends on point of operation. The swirl rate appearing behind the runner at part-load greatly affects the flow condition in the draft tube.

Velocity gradient in the rectangular diffuser showed that most of the excess kinetic energy of outlet stream was converted into static pressure delimiting the outlet-bound velocity to minimal. Also, a symmetrical flow distribution in the entire draft tube, free of recirculation, could be observed at full load where the streamlines were well distributed. The transient velocity vector plots at different cross sections of the draft tube at full load operation complied with the uniform velocity distribution.



(a) Velocity vector in 6 sections at full load (b) Flow streamlines at 72% load

Fig. 3.7 Velocity profiles in the draft tube

Howsoever, flow distribution in the draft tube at part flow operation tells otherwise. An unsymmetrical and non uniform flow was obtained in the draft tube at 72% partial flow rate with presence of a vortex core. This decelerated flow with swirl resulted in vortex breakdown which could be considered as a reason for pressure fluctuation in the turbine. Francis turbines, with a fixed pitch runner, have a high level of residual swirl at draft tube inlet due to the mismatch between the swirl generated by the guide vanes and the angular momentum extracted by the runner [29]. In Fig. 3.7, the flow streamlines in the wall regions were streamlined and uniform but the flow field in the inner region was disturbed with a low flow velocity and occurrence of vortex core.

Operation of hydraulic turbines in some off-design conditions exhibit local pressure pulsation caused by rotor-stator interaction and draft tube vortex precession that propagate along the whole water conduit [30]. A corkscrew shaped non-cavitating positive vortex rope was obtained at the inlet of the draft tube whose magnitude and strength changed with the runner rotation. The draft tube vortex appears at partial load operating regimes usually in radial turbines and also at single regulated axial turbines [27]. The changing size of this rotating vortex rope

corresponds to the pressure surge and implies the synchronous pressure oscillation in draft tube. The synchronous pressure pulsation caused by the vortex rope can trigger pressure pulsation in the entire turbine especially when the excitation frequency is in close match with the eigenfrequency of the penstock [26]. This delimits the safe operating range of the turbine.

The rotor-stator interaction between guide vanes and runner always induces pressure fluctuations inside the runner. The measurement of pressure oscillations caused by vortex ropes is discussed in [31]. The fluctuation of pressure in the runner and eventually fluctuation in torque were caused by the wakes which appear beyond the stay vanes and expand to the runner. Fig. 3.8 shows an average torque on two of the runner blades plotted against the rotation of runner. The fluctuation of torque was about 7%. Bearing a periodic behavior, the fluctuation in the torque corresponded to the number of guide vanes. A total of 16 peaks could be counted in one rotation of runner. However, these fluctuations nullified each other as forces on all the 13 blades of the runner have different phases and consequently the forces coalesced to produce a steady effect.

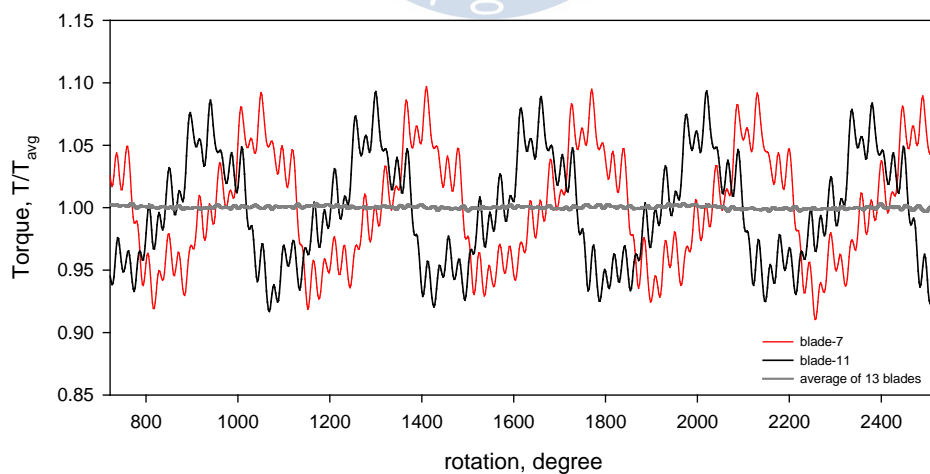


Fig. 3.8 Torque fluctuation and average torque distribution in runner blade

Similar was the trend of pressure fluctuation in the runner blade. The curves in Fig. 3.9 represent pressure fluctuation in two runner blades. With an average fluctuation of 5%, the average pressure distribution in runner blade was periodic throughout the simulation period. The pressure distribution in casing in Fig. 3.10 also demonstrated periodic behavior with uniformly fluctuating magnitude throughout the period of analysis.

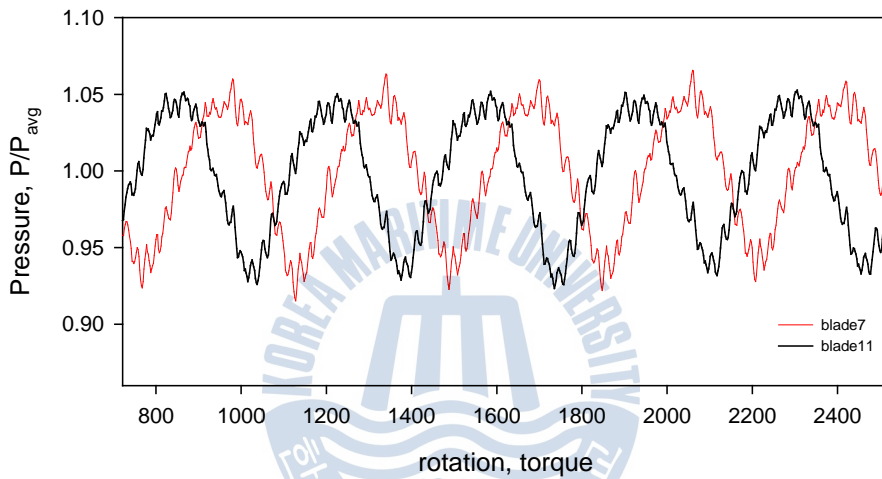


Fig. 3.9 Average pressure distribution in runner blades

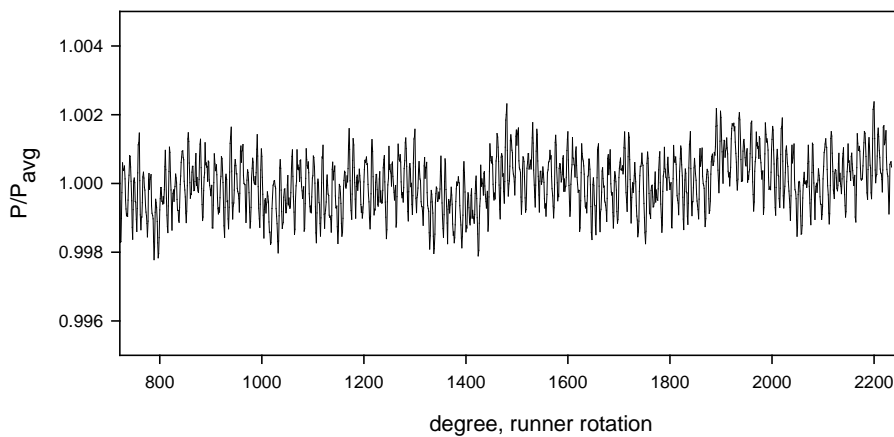


Fig. 3.10 Average pressure distribution in spiral case

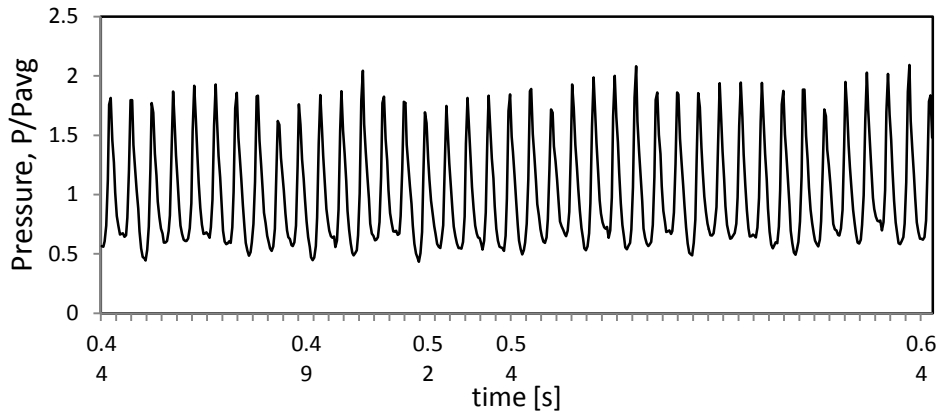


Fig. 3.11 Pressure fluctuation in draft tube for 3 runner rotation

The variation of static pressure with time under full load operation condition at dt1 of draft tube is illustrated in Fig. 3.11 for 3 rotations of runner which had a regular variation.

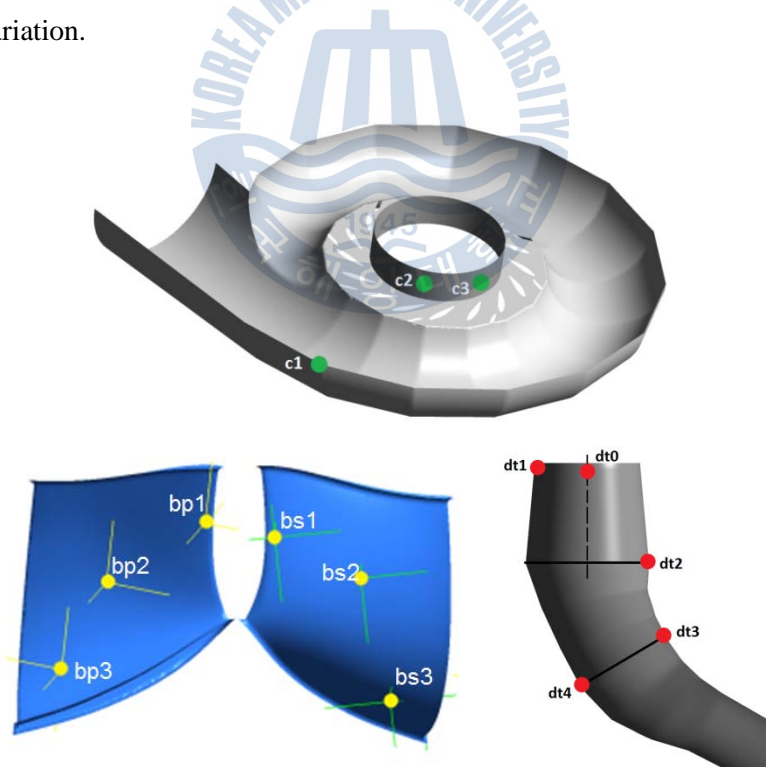


Fig. 3.12 Pressure recording locations in casing, runner blade and draft tube

For the evaluation of pressure fluctuation and vibration level in the components, 14 locations were chosen and time varying pressures were recorded in casing, runner blade and draft tube. 3 locations on spiral casing, 3 each on pressure side and suction side of the runner blade and 5 in the draft tube are designated as in the Fig. 3.12. A Fast Fourier Transformation (FFT) was carried out to gather pressure signals at the selected points of inspection.

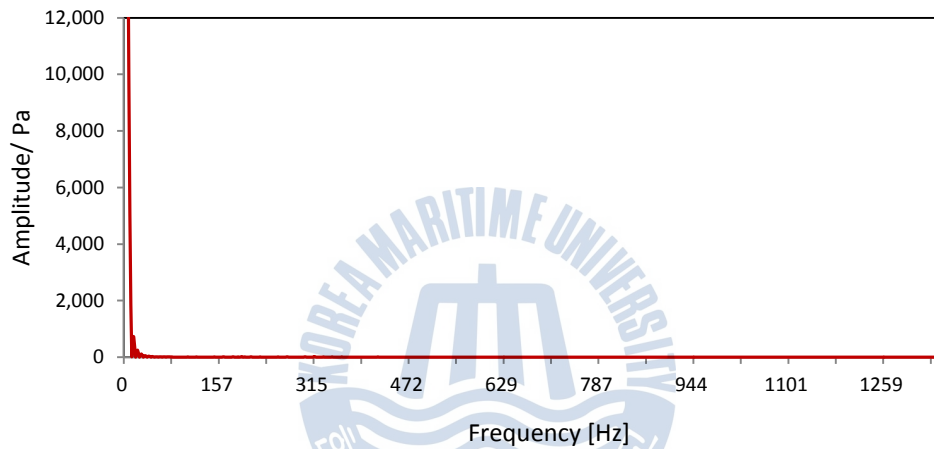


Fig. 3.13 Fourier transformed pressure signal in casing (c1)

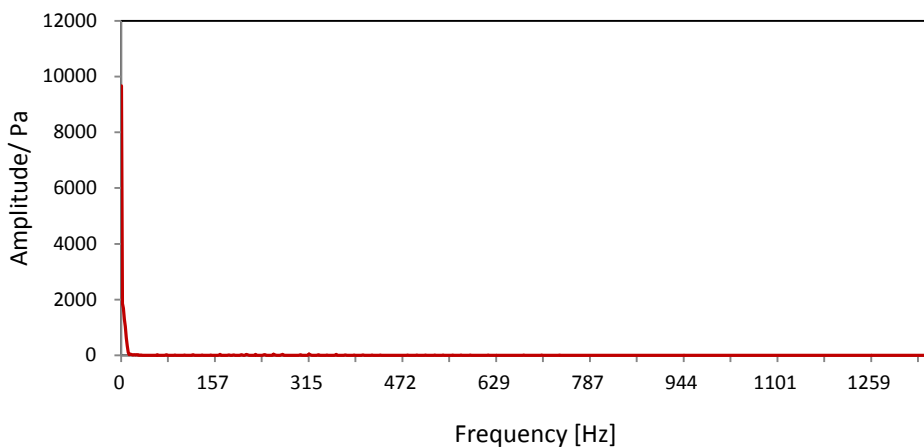


Fig. 3.14 Fourier transformed pressure signal in draft tube (dt3)

In the full load operation, the pressure variation in casing and draft tube were similar and amplitude spectra obtained at c1 (Fig. 3.13), and dt3 (Fig. 3.14) were smooth and have low frequency pressure oscillation without any dominating frequencies signifying the absence of swirl and vortex shedding. The same basic fluctuation frequencies were also traced in the locations near guide vanes and casing wall.

In part load operation where draft tube vortex rope is highly likely to occur, the pressure oscillation on the runner blade was found to be related to the precession of vortex rope that caused the pressure in the runner blades to fluctuate with a dominating frequency of $(f_n - f_d)$ where f_n is the rotational frequency of the runner and f_d is the vortex rope frequency. The detail about dominating frequency due to vortex shedding is discussed in Chapter 4.

The vibration level in draft tube and casing shown in Fig. 3.15 was found to be of similar magnitude. The waves were not in phase and thus they avoided any chance of resonance. The level of vibration in the runner blade is relatively higher than that in casing and draft tube.

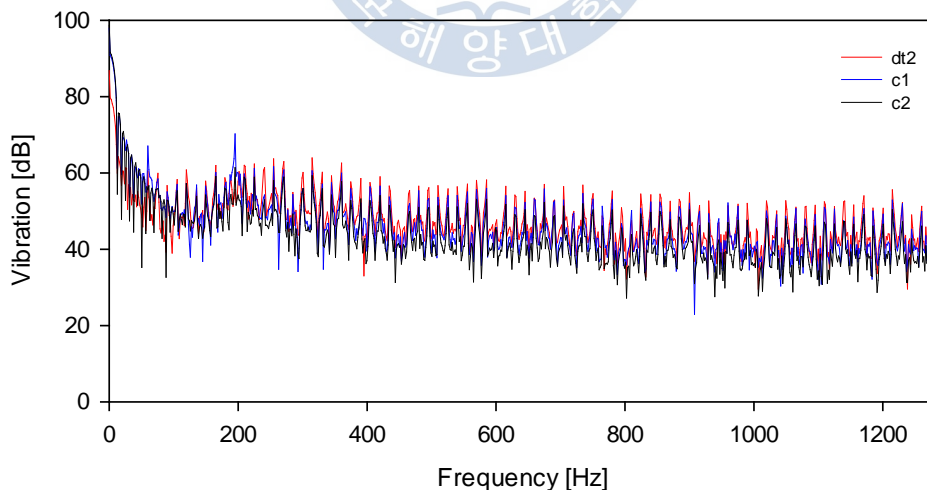


Fig. 3.15 Vibration spectra in draft tube and casing

The interaction between the rotating component and stationary components of Francis turbine is a common phenomenon during its operation but the effect is manifested more in medium to high head machines. With turbines operating at medium head and above, the velocity of the flow at the exit of the guide vanes are large with small radial gap between the blade rows which results in significant pressure fluctuation with respect to the stress levels. Since the flow field in the radial space between the guide vanes and runner is non-uniform circumferentially, the static inflow pressure, the magnitude of velocity and the flow angle passing through each runner channel also vary circumferentially, creating an unsteady load on the blade [32].



Chapter 4 Vortex shedding in draft tube

4.1 Vortex rope in part flow

Flow in draft tube of a Francis Turbine is one of the fascinating and, more often, challenging aspects of reaction type hydraulic turbine. The draft tube of a Francis Turbine acts as an important component in converting the excess kinetic energy into static pressure by decelerating the flow downstream the runner along its increasing cross section.

When energy conversion takes place in the runner, the decreasing angular momentum of the flow results in decreasing swirling radius of the fluid and the water exits the runner with no swirl component and very less energy. Under the optimal operating condition, the flow leaving the runner is essentially axial with no rotational component of the velocity and swirl. However, in part load or over load operations of the turbine, the exiting flow contains swirl component of the velocity that generates flow vortex at the center of the flow downstream the runner.

Draft tube surging refers to this unsteady flow occurring in the draft tube due to the excessive swirl in the flow that is leaving the turbine runner. The draft tube surge is characterized by the presence of a helical vortex often referred to as vortex rope. The flow associated with draft tube surge is classified as self-excited unsteadiness because the flow field within the draft tube varies with time; the discharge from the draft tube may or may not vary with time [33]. The consequences of the vortex rope in motion are pressure pulsation, fluctuation in torque, axial and radial forces. It is also the source of noise, vibration, shaft run-out and wear in the bearing [34]. Thus it becomes imperative to understand the occurrence of vortex rope and its ability to influence the hydrodynamic features of the turbine and affect civil, mechanical as well as electrical components over the turbine's range of operation and its mitigating measures. The phenomenon of draft tube vortex is limited to reaction type water turbines and is associated with the

runners having fixed blades, particularly of Francis (mixed) or single regulated Kaplan (axial) units during part load operations.

When the turbine runs in part load, the flow exiting the runner incorporates swirl. As the magnitude of the swirl increases, the axial velocity distribution in draft tube distorts and the flow is confined more in its outer wall. At a critical level of swirl, the flow in the inner wall of the draft tube reverses and forms a helical vortex in the region of reversed flow, which characterizes the genesis of the draft tube surge. The flow phenomenon associated with draft tube surging is termed as *vortex breakdown* and its motion as *precession* of the vortex.

The rope rotates in the direction of rotation of the runner when the turbine is operating for lower power output than optimum and the associated swirl is said to be positive. Usually, it rotates with a low frequency typically of about 20-30% of the runner's rotational frequency around a large recirculation zone located at the centre of the draft tube just under the runner [35] which may induce high amplitude pressure fluctuation in the draft tube exciting the components of the turbine. If this exciting frequency matches one of the eigenfrequencies of the turbine, hydro-acoustic resonance may transpire leading to component damage due to amplified unsteady fluctuations. These narrow the safe operating regime of the power plant.

The occurrence of the swirl at runner downstream and the corresponding hydrodynamic field is the direct outcome of the runner design and operating point [36]. For a given head, the twist in the vortex rope decreases as flow rate or guide vane angle decrease. The resulting hydraulic loss in the draft tube is strongly affected by the intensity of the swirl flow at the runner outlet [37]. A cavitating vortex appears when the pressure inside the draft tube is low enough and the corresponding pressure within the vortex core falls below the vapor pressure of the fluid. The cavitating volume in the rope varies with the under pressure level. The non cavitating vortex is the result of air-filled hollow vortex core in the low pressure zone at its centre.

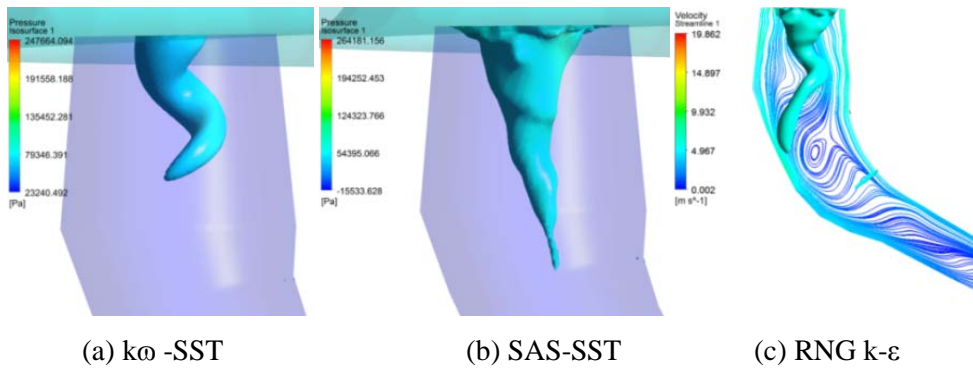


Fig. 4.1 Effect of turbulence model on shape of vortex rope

The numerically obtained shape of draft tube vortex and accuracy of its prediction largely depend on the choice of the turbulence model used for the simulation (Fig. 4.1). The vortex motion may be overly damped or may not be detected at all with inappropriate turbulence model. There are several papers, which have complimented the unsteady flow analysis numerically and experimentally, to predict the genesis of swirling flow at turbine outlet and the resulting vortex rope, its nature and effects on the fluid passage, by adopting appropriate turbulence models. The swirling intensity largely affects the size and movement of the vortex rope and entails the use of improved turbulence model to accurately capture vortex core.

Various authors have reported that standard $k-\epsilon$ is not an accurate model to predict vortex shedding while rotating vortex rope was obtained using extended $k-\epsilon$ model of Kim and Chen and realizable $k-\epsilon$ model. [23] used extended $k-\epsilon$ model and obtained draft tube rope but the result showed discrepancy with the experimental measurement due to the damping effects of the turbulence model on the swirl.

In this study, RNG $k-\epsilon$ model with second order upwind scheme was used to predict the occurrence and nature of the vortex rope which is an ensemble averaged Navier Stoke equations more responsive to streamline curvature and higher strain rates than the standard $k-\epsilon$ model. It better handles transitional flows and different turbulent length scales. The main difference of RNG $k-\epsilon$ from the standard $k-\epsilon$ model is that some coefficients that are constants in the standard model are the

functions of flow parameters in the RNG model. The effect of swirl is also accounted for in the RNG model enhancing the accuracy of swirling flows [38].

The transport equations [39] for k and ε , neglecting buoyancy, can be expressed as :

$$\frac{\partial}{\partial t}(\rho k) + \frac{\partial}{\partial x_i}(\rho k u_i) = \frac{\partial}{\partial x_j} \left[\left(\nu + \frac{\nu_T}{\sigma_k} \right) \frac{\partial k}{\partial x_j} \right] + P_k - \rho \varepsilon \quad (4.1)$$

$$\frac{\partial}{\partial t}(\rho \varepsilon) + \frac{\partial}{\partial x_i}(\rho \varepsilon u_i) = \frac{\partial}{\partial x_j} \left[\left(\nu + \frac{\nu_T}{\sigma_\varepsilon} \right) \frac{\partial \varepsilon}{\partial x_j} \right] + C_{1\varepsilon} \frac{\varepsilon}{k} P_k - C_{2\varepsilon}^* \rho \frac{\varepsilon^2}{k} \quad (4.2)$$

where $C_{2\varepsilon}^* = C_{2\varepsilon} + \frac{C_\nu \eta^3 (1 - \eta / \eta_0)}{1 + \beta \eta^3}$, $\eta = \frac{Sk}{\varepsilon}$ and $S = \sqrt{2S_{ij}S_{ij}}$

The values of the model constants are

$$C_{1\varepsilon} = 1.42, C_{2\varepsilon} = 1.68, C_\nu = 0.0845,$$

$$\sigma_k = 0.7194, \sigma_\varepsilon = 0.7194$$

$$\alpha = 1.39, \beta = 0.012 \text{ and } \eta_0 = 4.38.$$

A homogeneous multiphase model with Rayleigh Plesset cavitation model was incorporated for any presence of cavitation. As the turbine operated free of cavitation in the taken operating discharge, the vortex core so obtained was also non cavitating. The vortex rope in draft tube would expand when flow rate is reduced. Further decrease in flow rate would have distorted the vortex core and induced more instability and turbulence in the draft tube. At a smaller part loads, the vortex rope breaks and pressure field is more affected by small scale turbulence [32].

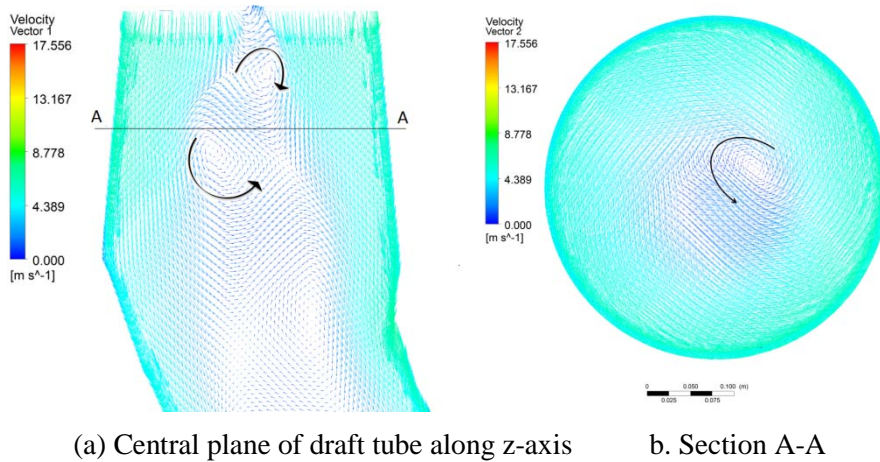


Fig. 4.2 Velocity vector of flow in draft tube

The vorticity at a given point in the vortex rope is comprised of tangential component and axial component as seen in Fig. 4.2. The profile and the angle of helical rope depend on the ratio of tangential component and axial component of the vortices. The profile of the vortex rope changes with the change in the ratio of the two components. The vortex rope will have more twist for larger flow rates and/or wider guide vane opening.

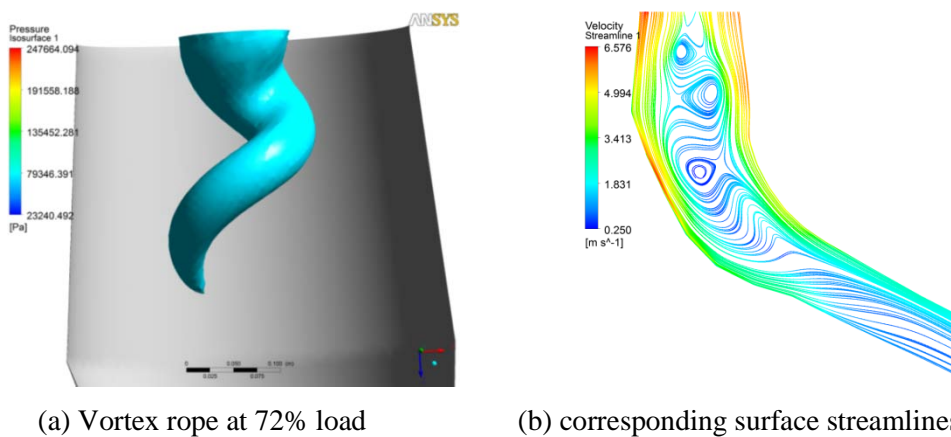


Fig. 4.3 Shape of vortex rope at part load

A mature shape of the vortex rope as obtained with taken timestep and turbulence model at 10th rotation of runner from the transient analysis is shown in Fig. 4.3 with its corresponding surface streamlines in the mid vertical plane of draft tube. A distinct vortex rope was obtained which was the obvious outcome of swirling flow in the draft tube. The distribution of pressure in mid section of the draft tube cone at different instance of runner rotation is shown in Fig. 4.4. The low pressure regions which represent the vortex centre revealed the rotation of the vortex causing pressure fluctuations. For 3 complete revolutions of the runner, the vortex rope made a single rotation.

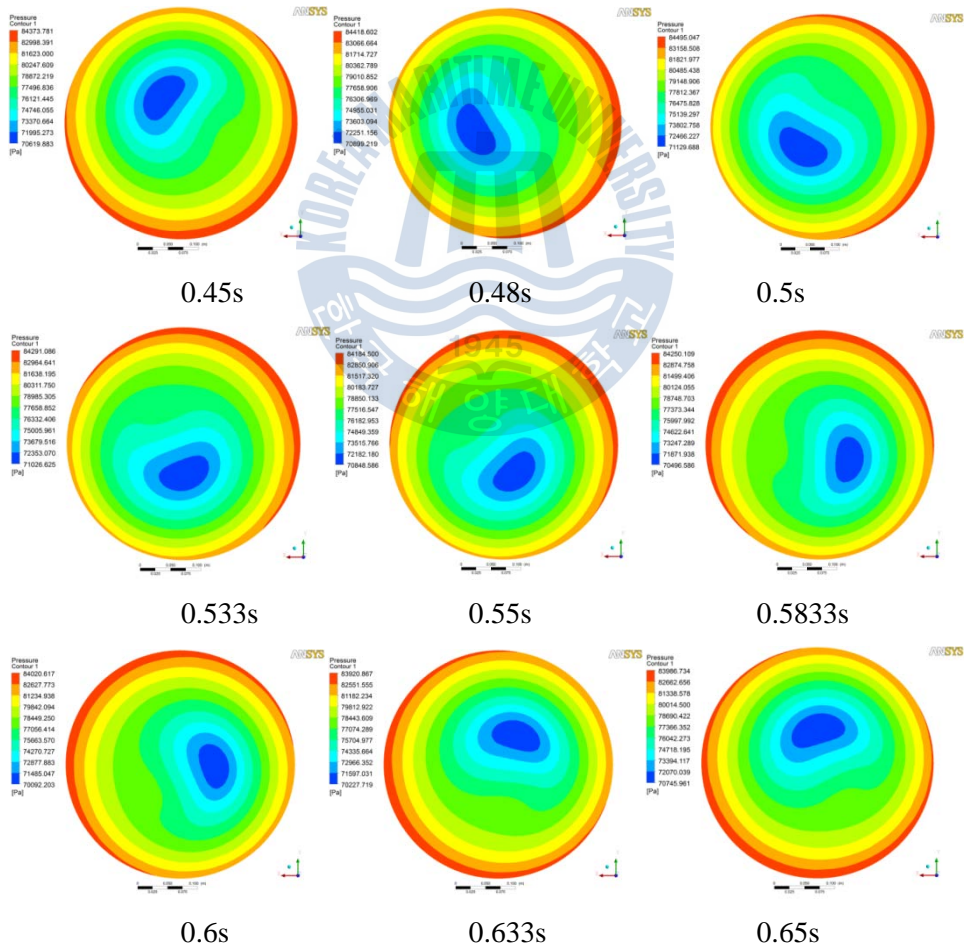
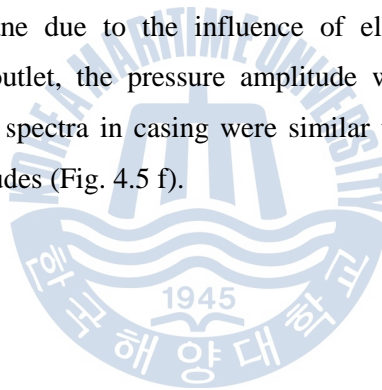


Fig. 4.4 Low pressure region in mid section of draft tube

Time varying pressures were recorded at 5 locations of the draft tube (Fig. 3.12) and casing to capture pressure pulsation. The amplitude spectra at designated location are presented in Fig. 4.5. The pressure amplitudes in the outer flow regions were found to be relatively larger than that at the centre of the flow. The pressure point dt0 (Fig. 4.5 a) being located at the centre has low influence of vortex core and thus had relatively small fluctuations while the recording points near walls and downstream the draft tube had fluctuations according to the varying strength of the vortex core. The pressure amplitudes in wall of the draft tube cone were found to be higher than that of the centre because these regions were in close influence of the vortex rope (Fig. 4.5 b, c, d).

Point dt4 near draft tube elbow had highest magnitude of fluctuation among the points lying in this plane due to the influence of elbow (Fig. 4.5 e). Going downward toward the outlet, the pressure amplitude would decrease gradually. Similarly, the amplitude spectra in casing were similar to that of draft tube, with low peak-to-peak amplitudes (Fig. 4.5 f).



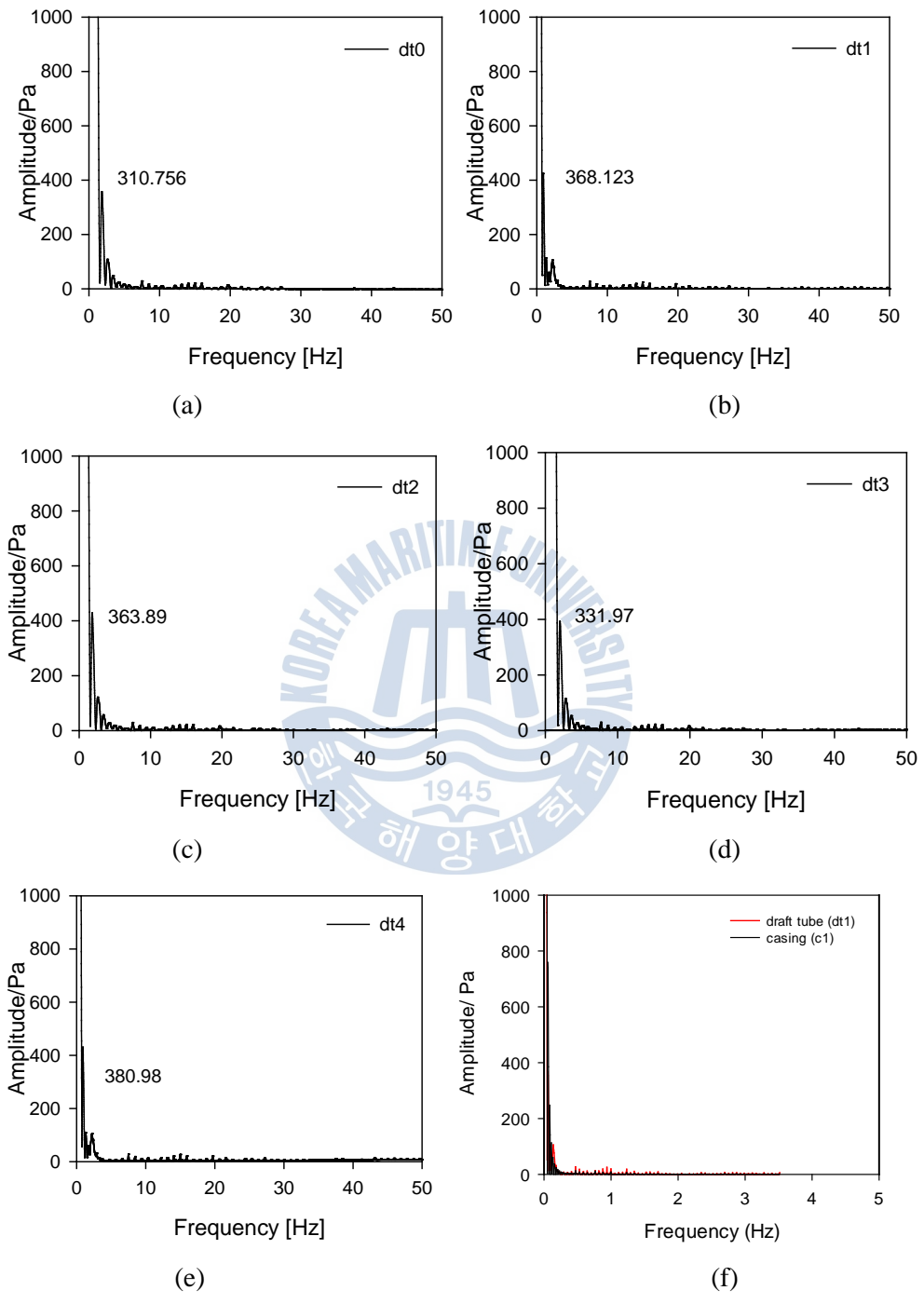
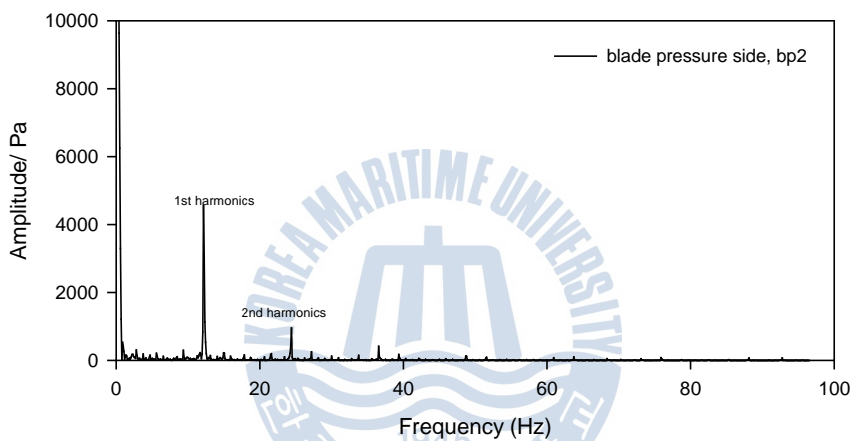
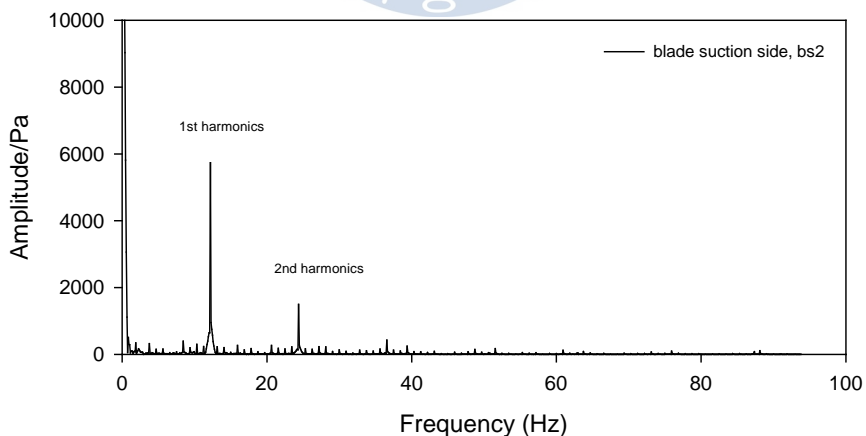


Fig. 4.5 Amplitude spectra at draft tube and casing

The amplitude spectra of pressure fluctuations at blade pressure side and suction side are presented in Fig. 4.6. The dominating frequency on the blade was 12.15Hz for the pressure side and 12.18Hz for the suction side, corresponding to $0.81f_n$ and $0.812f_n$ respectively while the rotational frequency of the vortex rope was $0.19f_n$, the sum of which was the rotational frequency of the runner, f_n . Also, the amplitudes on the suction side for both 1st and 2nd harmonics were larger than those on the pressure side.



(a) Blade pressure side (bp2)



(b) Blade suction side (bs2)

Fig. 4.6 Amplitude spectra in runner blade

4.2 Remedial attempts

The decelerating flow in the draft tube with swirling component of velocity results in the precessing vortex rope. The pressure fluctuations are caused by the transformation of an axisymmetrically swirling flow into one or more precessing helical vortices as the operating condition shifts towards part load [40]. Also, this self-induced unsteadiness from swirling flow at part load causes severe flow separation on the blade's suction side.

A pressure balanced runner with skewed outlet design also known as x-blade runner also helps to provide some improvement by reducing peak-to-peak amplitude of pressure fluctuation without actually suppressing the phenomenon of vortex shedding. However, with no freedom of adjustable blades in Francis runner, the vortex breakdown is bound to occur at partial discharge.

Air supplied just below the runner, at the draft tube inlet is a widely used and common surge suppression solution. Air is injected in the recirculation region around the vortex rope to reproduce an axially symmetric stable flow. Some units have the air admitted through the runner head cover, through the runner cone or through an extended tube attached at the runner cone. This air admission measure was also the first attempt tried out in reducing the draft tube surging problems. The air admission alters the spiral breakdown of flow into bubbles and projects the flow axially. Also, experimental results have shown a considerable reduction in the pressure fluctuations at part load and minimal effects on efficiency due to air injection. Papillon et. al. have discussed the results of three different types of runner cone for air admission and peripheral aeration by the discharge ring [41]. Literatures have it that air volume of about 3% of turbine's discharge is required to achieve significant reduction on pressure swings while larger volume of air can deter efficiency of the unit.

Couple of structural modifications of draft have also been tried and tested for suppressing vortex rope with some good results. Use of J-groove is one of the common structural modifications of draft tube. It is a flow straightener installed at

the draft tube cone that serves to break the vortex. Other typical devices are the fins attached to the draft tube wall, concentric cylinders in the draft tube that are supposed to suppress the vortex breakdown in partial discharges.

Extension of runner cone in the form of snorkel, either attached to the runner or fixed within the draft tube, sometimes in tandem with air injection, can also alter the reverse flow region to reduce flow instabilities.

A novel idea of jet control of vortex breakdown in Francis turbine is discussed in [40]. Resiga et. al. applied a highly energetic jet of water from the tip of the crown cone were able to change the precession frequency and eventually avoided the vortex rope development by eliminating the quasi-stagnant central region due to flow acceleration in the crown neighborhood due to jet injection.



Chapter 5 Evaluation of vortex control techniques

5.1 Influence of runner hub profile

Hub cut is a structural modification of runner hub of a Francis turbine attempted to minimize the vortex shedding in the draft tube. Different profiles of the runner hub were tried and tested numerically to analyze the effect of hub's shape on the flow field in draft tube. From several analyses, it was inferred that shape of the hub did influence the flow pattern in draft tube and the shape of vortex rope and pressure field in draft tube cone altered with different profiles of the hub. Flow streamlines reveal that genesis of the vortex rope in draft tube cone is related to the flow near runner hub downstream. Thus, a modification in runner hub did have influence on the flow field proceeding towards the runner.

Taking this into account, attempt was made to find out an appropriate profile of the runner hub that could render positive result in minimizing vortex shedding in terms of improving the flow in the core region of the draft tube and/or reducing the swirl velocity there on minimizing the size of the vortex.

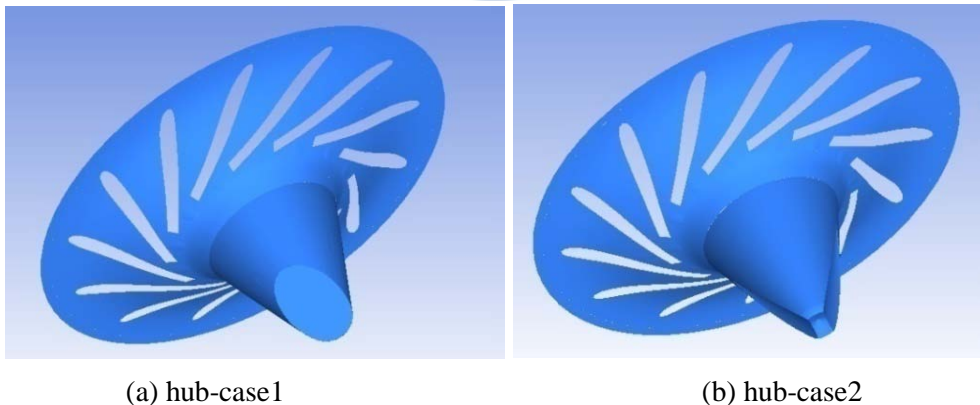


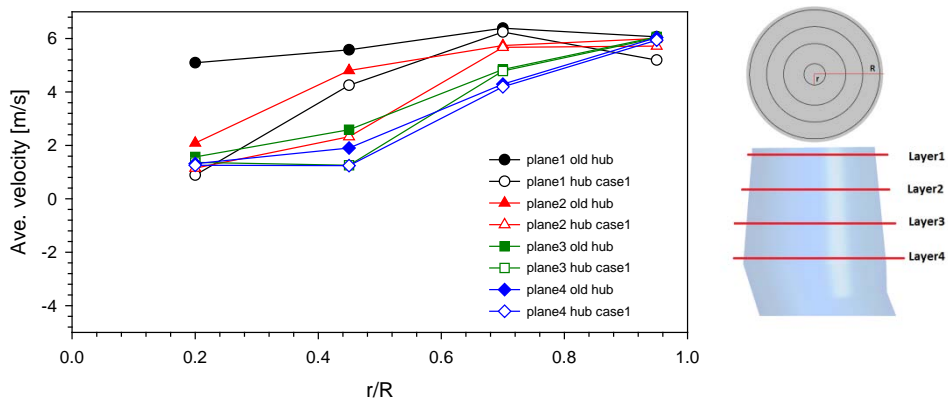
Fig. 5.1 Profiles of modified hub

Among the different profiles evaluated, two profiles, one with asymmetrically slashed hub (pertaining to frustum of a cone) and the other one with symmetrically cut hub with a central notch helped improve the flow in the draft tube and minimized the swirling rate (Fig. 5.1). In between the two cases, case2 showed better results with vortex issue however at the expense of 2.5% loss in the efficiency (Fig. 5.7).

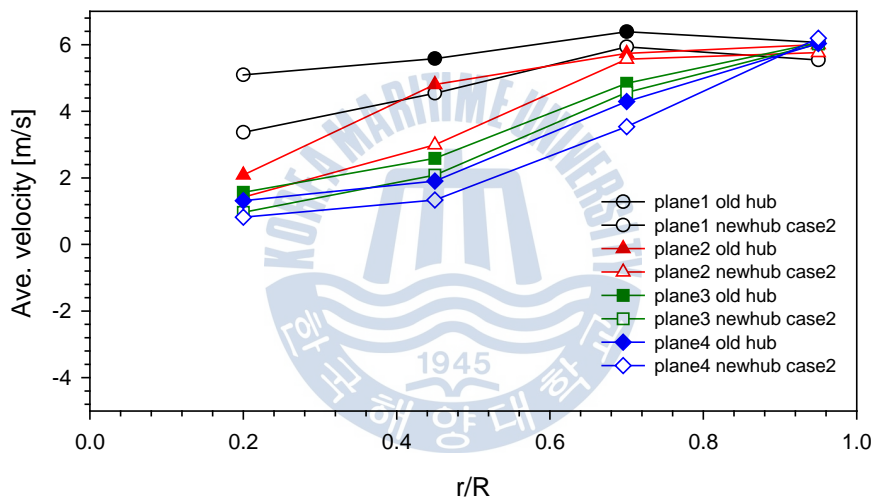
A steady state analysis was carried out to infer the flow features and performance of the turbine with modified hub followed by a transient analysis to verify the shape of the vortex and influence on flow instability. Out of the several designs of hub tried, case1 and case2 showed a relatively smaller range of low pressure zones, indicated by pressure isosurface depicting vortex rope and minimized swirl as obtained from transient analysis. Between the two profiles, case2 performed better in minimizing the size of the vortex rope and lowering the swirl intensity, as seen in Fig. 5.2.



Fig. 5.2 Vortex rope due to hub case1 and case2 at 0.481s



(a) Average circumferential velocity in 4 layers of draft tube with hub-case1



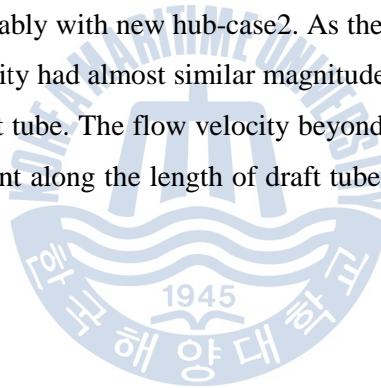
(b) Average circumferential velocity in 4 layers of draft tube with hub-case2

Fig. 5.3 Comparative circumferential velocity in draft tube with new hub

A circumferentially averaged flow field cannot precisely capture the unsteadiness of the 3D flow; however, it can be reliably invoked for stability analysis in steady state simulation. A better methodology for analyzing the swirling flows with helical vortex breakdown by using an axisymmetrically swirling flow model is discussed in [42]. From the pressure contours checked at 4 different layers of the draft tube cone, low pressure zone and intensity of swirl have relatively

reduced with new hubs as in case 1 and case 2 compared to the one with base model runner hub.

Fig. 5.4 shows the pressure distribution on 4 layers of base model draft tube cone compared with those of hub cut case1 and case2. With modified hub, the central low pressure zone is smaller for all 4 layers which indicated the diminished size of vortex rope. Also, the strength of swirl at the core of the draft tube flow was also lowered in both the cases of modified hub improving the flow in axial direction (Fig. 5.3). The curves with solid marks indicate the average circumferential velocity in the given plane while the one with hollow marks and dotted lines indicate the velocity as obtained with hub-cut. The circumferential velocity at the upper portion of the draft tube cone, along plane #1, #2 and #3 in the inner section of the flow have been reduced admirably with new hub-case2. As the flow moved past the cone region, the average velocity had almost similar magnitude as with the old hub in the lower portion of the draft tube. The flow velocity beyond $0.8 r/R$ and near the draft tube wall remains constant along the length of draft tube cone as examined in its 4 sections.



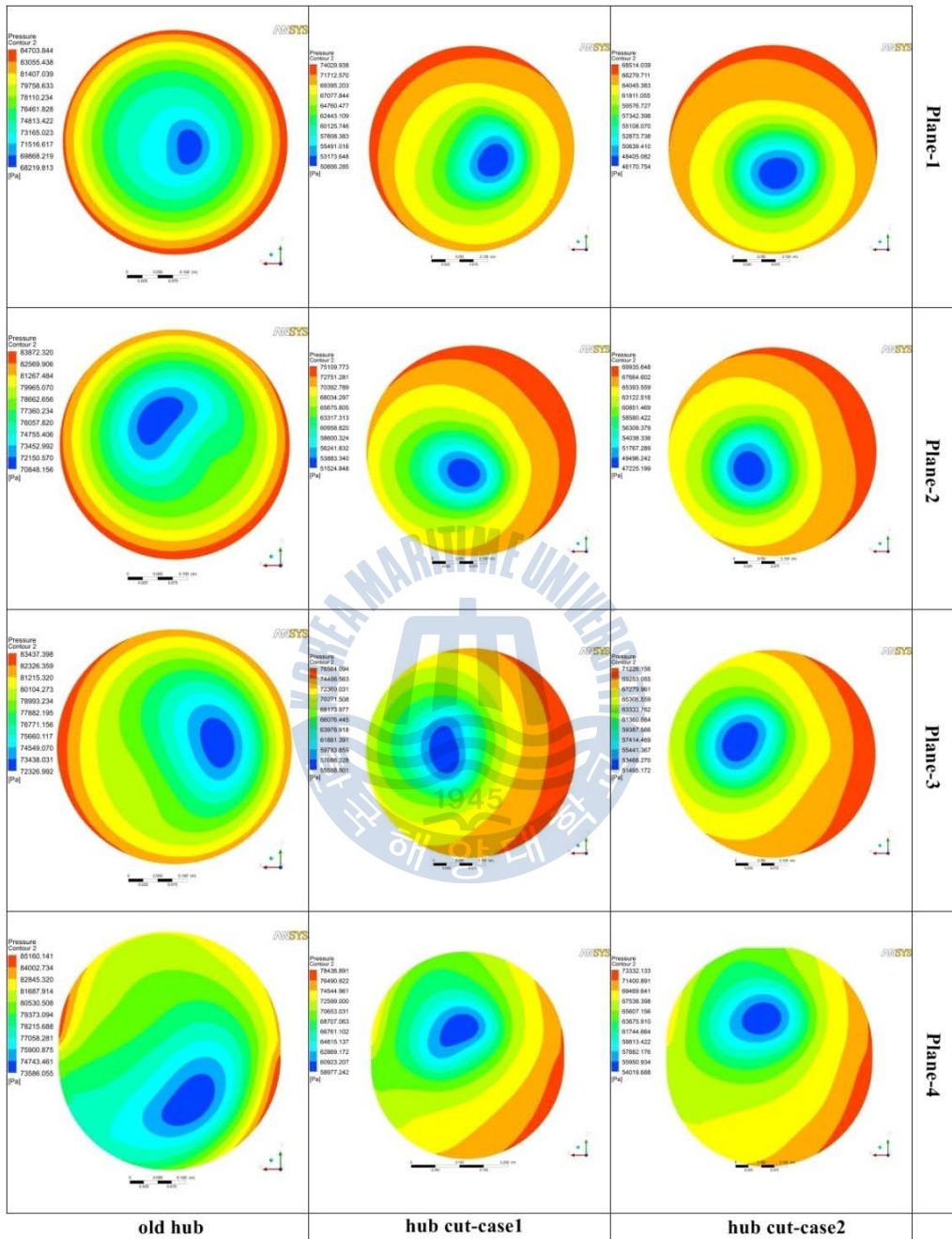


Fig. 5.4 Pressure maps at 4 layers of draft tube cones

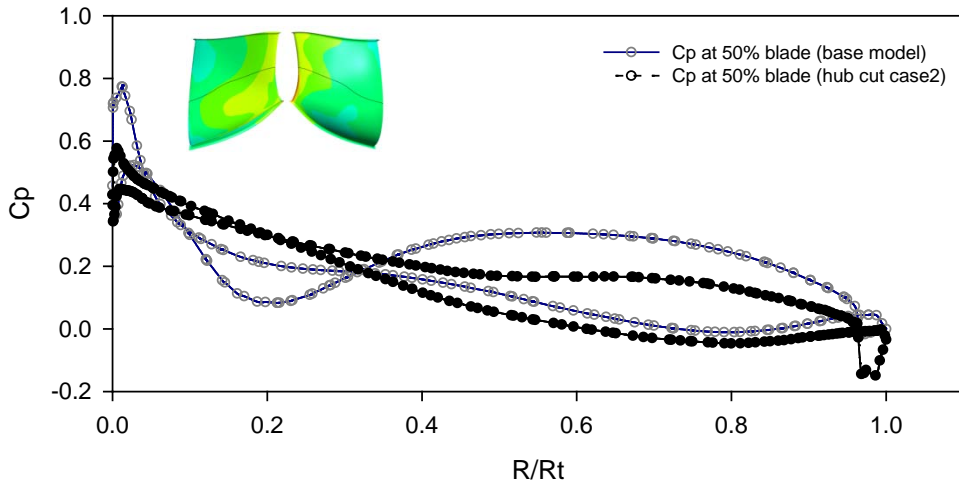


Fig. 5. 5 Cp graph for blade pressure distribution with hub-case2

Apart from altering the flow in the draft tube, the flow features in the runner too have been altered with the new hubs. Case2 hub, having better results in controlling vortex, also influenced the pressure distribution in the runner blades. The magnitude of pressure in the pressure side has been diminished and the pressure in the suction side too has been lowered toward the leading edge, improving the pressure distribution on both the side of runner blades, as depicted by the Cp graph in Fig. 5.5 taken at 50% of blade. The smaller pressure difference between the pressure side and the suction side renders smaller torque and is thus related to the efficiency loss.

With case2 hub performing relatively better against the vortex shedding, the hub profile can be optimized to retain the efficiency and incite more stability to the flow in draft tube.

5.2 Influence of misaligned guide vanes (MGVs)

Where casing provides even distribution of water around the circumference of the runner and maintains constant velocity, the flow is controlled by the inlet guide vanes that are arranged inside the casing and at the outer periphery of the runner. The correct angular alignment of the guide vanes is mandatory for optimal performance of turbine as the angle of water jet striking the runner needs to hit the runner blade at correct angle for maximum transfer of angular momentum.

Pressure pulsations are the primary reason for unstable operation of any hydro machinery. Misaligned guide vanes (MGV) have been keenly incorporated in pump turbine system to improve flow stability and minimize pressure pulsations. A series of model tests were first carried out by KVAERNER using pre-opened wicket gates named as misaligned guide vanes in pump turbines in 1993. It was implemented in Tianhuangping pump storage plant [43] in China and was found helpful in eliminating machine vibration in reversible pump turbines. MGV has so far been exclusively tested and implemented in pump storage system to control the stability in the S-region and improve the unstable operation of pump turbines at no load conditions. [44] and [45] have studied and presented the results of the use of MGV to improve the stability of pump turbine correlating the numerical results with the experiments.

Likewise, [46] have mentioned that MGVs improve the S-characteristics of the pump turbine but demonstrated the increased pressure fluctuations in the draft tube causing unstable operation of the unit. Nonetheless, the use of MGVs in Francis hydro turbine system has not been reported so far. Qain et. al. have analyzed the influence of MGV on a 3D unsteady turbulent flow in the entire model of a Francis turbine by using two MGVs with 5 different opening angles, the results of which are elucidated in [22]. Use of MGV can be a feasible and effective measure to improve turbines stability and reduce pressure pulsations. In this study, two different angles of MGV were chosen and their effect on the flow in draft tube is analyzed numerically.

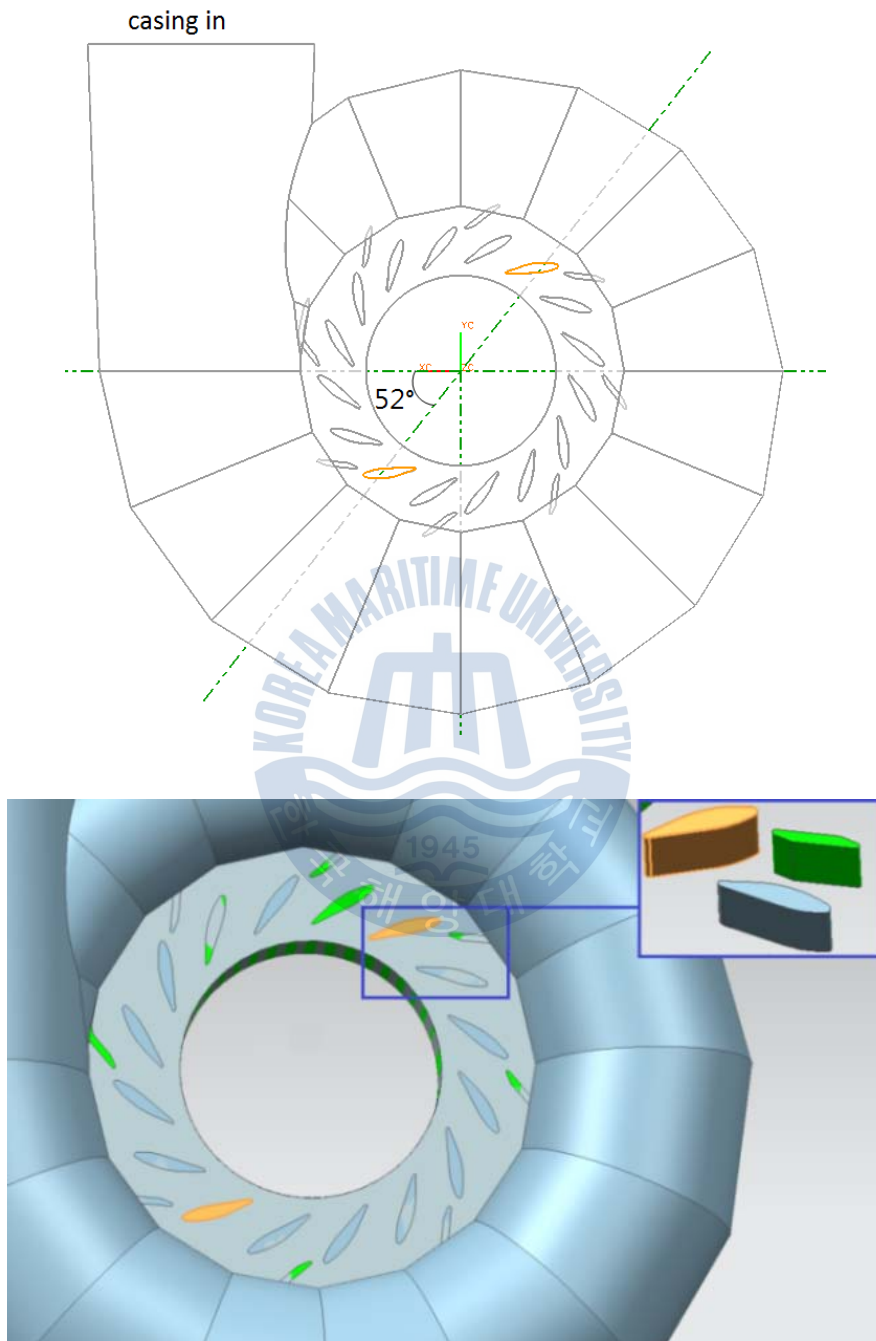


Fig. 5.6 Position of misaligned guide vanes

The guide vane angle of the turbine under study is 37.5° . The two different opening angle of 35° and 40° were chosen for the numerical analysis. As in Fig. 5.6, the circumferential position of the first MGV is kept above 45° from the vertical axis to minimize the influence of inlet boundary of casing and the location of the second MGVs is symmetrical to avoid the oscillation caused by resonant coupling. The time dependent numerical analysis was conducted followed by steady state simulation with the same timestep setting of 2° for 10 full rotation of the runner. SST turbulence treatment was used for steady state while RNG k- ϵ model of turbulence was used for transient analysis.

From the numerical results, the effect of MGV in controlling vortex in draft tube was not so substantial in both 35° and 40° MGVs. The steady state analysis suggests that the performance the turbine has been slightly increased with introduction of MGV at both the opening angles of 35° and 40° (Fig. 5.7). However, strong vortex existed for both opening angles of MGVs and the magnitude of vortex rope (Fig. 5.8) is also not diminished with respect to the one obtained from the base model, indicating that MGV did not influence the vortex shedding.

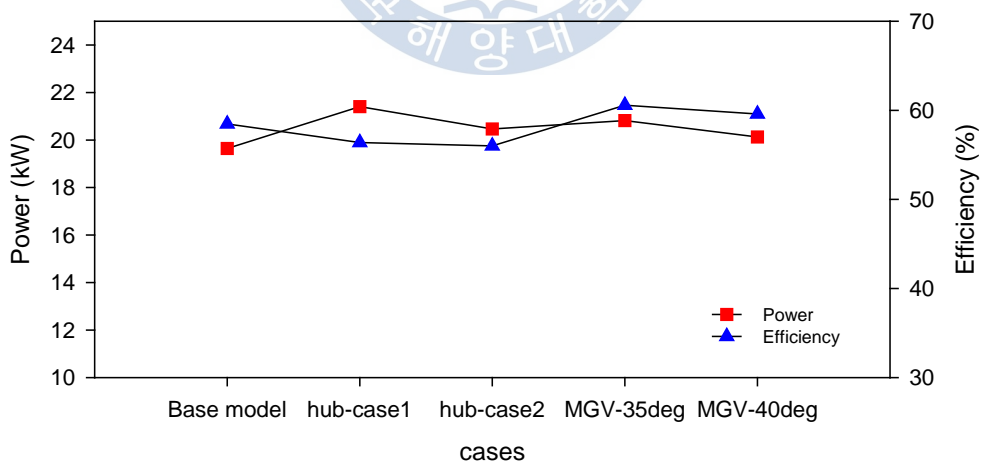


Fig. 5.7 Performance evaluation with modified hub and MGV

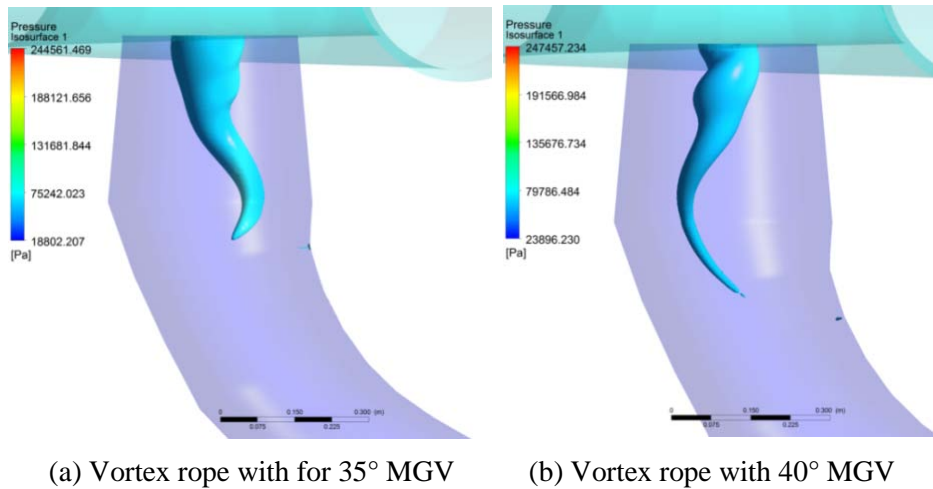


Fig. 5.8 Shape of vortex rope with MGV at 0.555s

The pressure distribution in the central vertical plane of the draft tube as in Fig. 5.9 for both the MGV angles were similar with low pressure zones pertaining to the existence of vortex rope. The shape and intensity of the vortex rope remained unchanged despite different MGV openings.

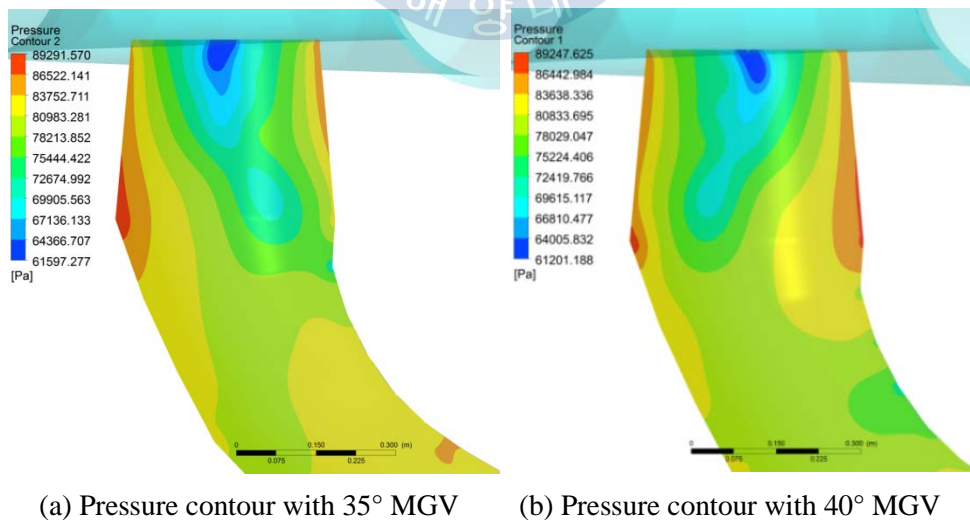
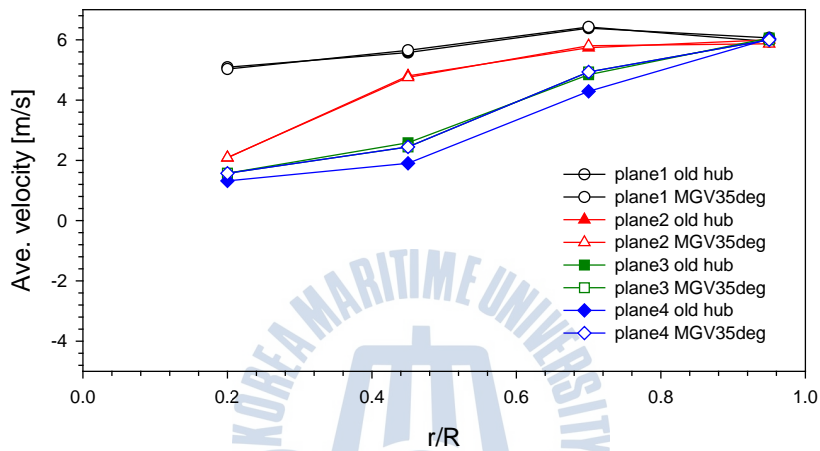
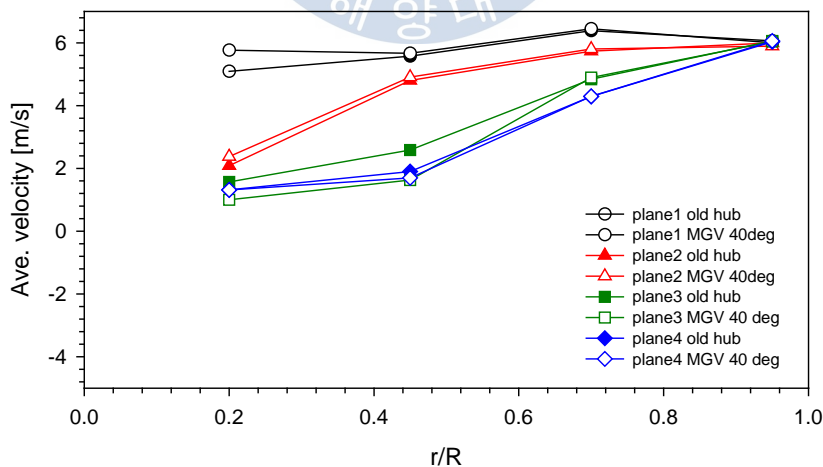


Fig. 5.9 Pressure distribution at central plane of draft tube with MGV

The average circumferential velocity taken at 4 different planes of the draft tube cone in Fig. 5.10 revealed almost no change in the swirl intensity with 35° MGV. Rather a very small amount of increment in swirl velocity could be observed at the core flow region of the draft tube with 40° MGV. The swirl intensities in the outer section towards the draft tube wall were similar in both the cases.



(a) Old hub v/s 35° MGV



(b) Old hub v/s 40° MGV

Fig. 5.10 Average circumferential velocity in draft tube with MGV

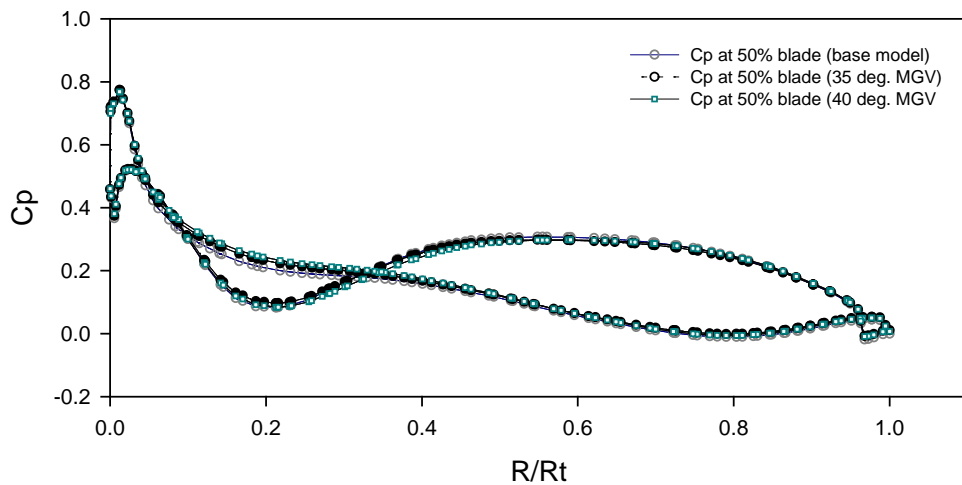


Fig. 5. 11 Comparison of C_p with base model and MGVs

These aside, the pressure distribution in the runner blades also had similar trend as with the one from the base model. In both the cases of MGVs, the C_p graphs as in Fig. 5.11 at 50% runner blade bore same pattern as that with base model indicating that the flow pattern in the runner is unchanged and so is the blade loading.

Several numerical and experimental studies advocate positive effect of MGVs in pump storage system in improving the unstable operation of pump-turbines and lessening the pressure pulsation but on the contrary, the same technique did not work satisfactorily in Francis turbine in controlling the vortex. MGVs did not considerably influence the flow in the runner and runner downstream, in the draft tube, to affect the flow instability occurring at part load operations. From the results obtained from transient analyses, the size of the vortex rope and its intensity both were larger with MGVs, in both opening angles. Hence, MGVs could not suffice to minimize swirl intensity and requires further research for practical applications.

5.3 Application of J-grooves in the draft tube

Vortex shedding in the draft tube is principally caused by the swirling flow at the runner outlet. The radial component in exiting flow causes the flow rotation at the core of the flow inducing a secondary flow. The whirling flow in the central region reverses and pressure field changes drastically in the divergent channel of the draft tube cone. A dead water zone with reverse flow is formed at the core due to the pressure drop in the adjacent flow passage. The more the unstable flow field, the steeper is the drop in pressure and swirl intensity will be higher. The pressure increases gradually in the axial direction due to the diffuser and the flow in the draft tube is forced towards the wall with main flow velocity higher than that in the core.

J-grooves are simple structure modification in draft tube cone of Francis hydro turbine that help minimize the vortex shedding. A number of shallow grooves are mounted parallel to the pressure gradient on the wall of conical diffuser that minimizes vortex breakdown downstream the runner by reducing the tangential velocity of swirling flow. J groove contribute to suppressing the anomalous flow phenomena commonly by controlling the angular momentum of the main fluid flow. Kurokawa et. al. [47] have discussed the benefit of J grooves in minimizing the swirl intensity not only in Francis hydro turbines, but also in mixed flow and axial flow pumps without compromising their maximum efficiency. Moreover, J-grooves too have demonstrated positive results in improving cavitation performance [48] and reduced axial thrust [49].

Active control method like air injection and passive control technique like fins installed at the inlet cone of the draft tube [50] are commonly accepted techniques to lessen the flow instability in the draft tube; however these apparatus have to be adjusted as per the operating point and reliability of these additional parts are bound to decrease eventually.

For the numerical analyses of the performance of turbine with J grooves, 2 aspects were considered- the number of J-grooves to be installed in the draft tube and depth of the grooves. The number of the J grooves is chosen as 13 and 16

pertaining to the number of runner vanes and guide vanes respectively and their depth were varied by 5 mm from 5mm to 15 mm. Steady state simulations with sufficient iteration were considered till satisfactory convergence for all the cases to evaluate the performance of the turbine at 72% load.

The number of J-grooves and their depth has a little influence on the turbine's performance. Compared to the power output performance of the turbine with base model, the efficiency of the turbine and its shaft power for all the cases have not changed much. With 5mm deep groove, the efficiency of the turbine was the same as with base model for both 13 grooves and 16 grooves (Fig. 5.12). However, the efficiency of the turbine dropped by 0.7% percentage when the depth of the groove was increased to 10mm. With declining trend in efficiency curve, the depth of groove beyond 10mm resulted in flow recirculation in cone region and backflow downward the outlet without any contribution to vortex control. Since the flow in draft tube was more influenced by the flow exiting the runner, the draft tube with 13 grooves 10 mm deep performed well in controlling the vortex pertaining to the number of runner blades.

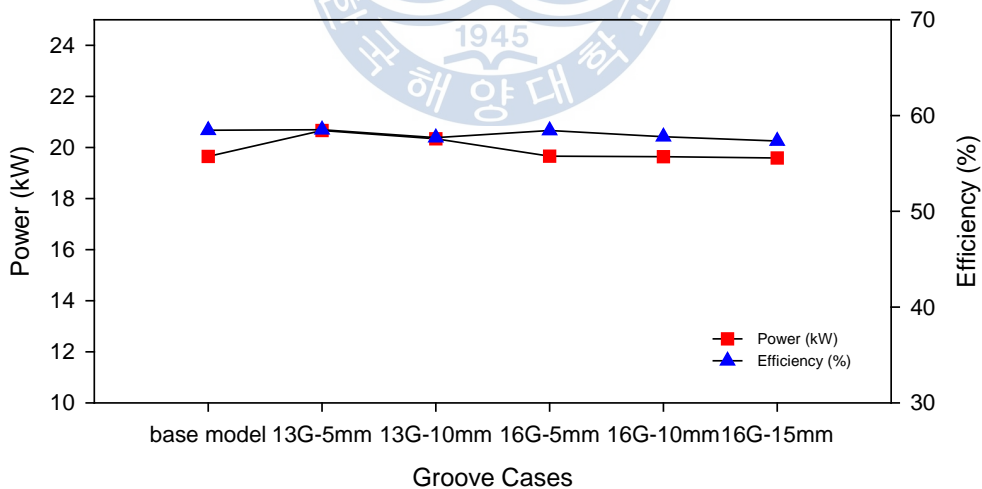


Fig. 5.12 Performance of turbine with different J-grooves

A comparative pressure map in Fig. 5.13 shows the pressure distribution in the central plane of the draft tube with the base model and 4 aforementioned cases with J-grooves. The pressure map of base model draft tube has a low pressure zone at the central flow field that is the outcome of the swirling flow and thus contributes to the genesis of vortex rope. With the use of J-groove, the central low pressure zone has been minimized indicating that the swirling flow at the dead water zone is relatively streamlined to the axial flow to minimize effect of swirl. However, a 13 groove diffuser showed a better pressure distribution map as compared to the one with 16 grooves.

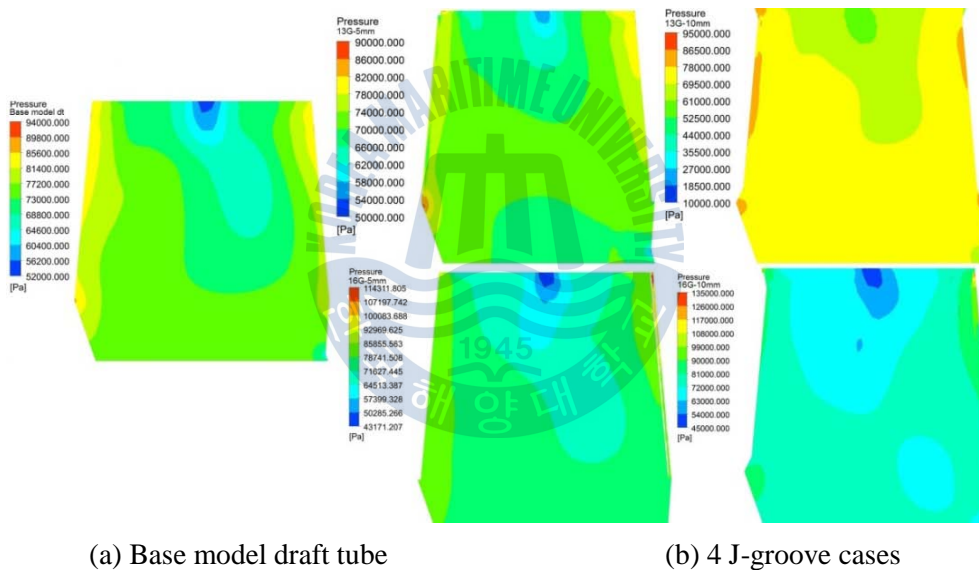
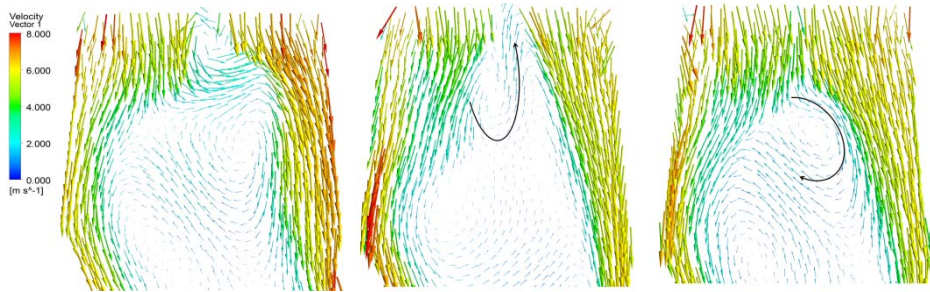
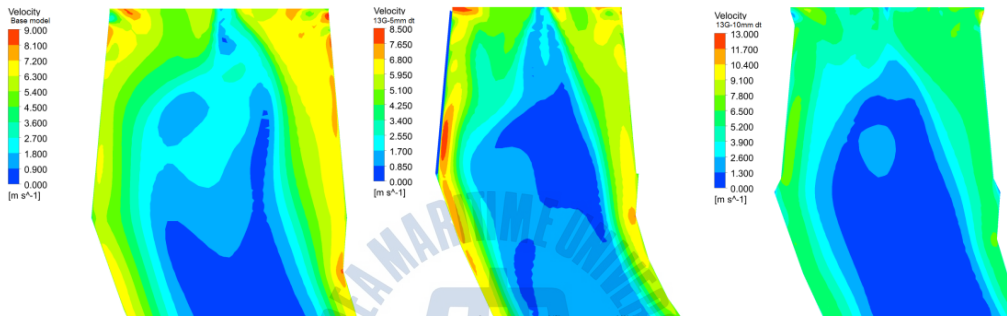


Fig. 5.13 Pressure map in central plane of draft tube



(a) Tangential velocity vector in mid vertical section of draft tube



(b) Velocity contour in mid vertical section of draft tube

(a) Base model draft tube (b) 13G-5mm draft tube (c) 13G-10mm draft tube

Fig. 5.14 Velocity distribution in base model and J-grooved draft tube

Referring to the tangential flow vector of the diffuser with 13 grooves, a distinct recirculation was visible with 5mm-deep groove while diffuser with 13groove-10mm depth stands out over other cases. The flow recirculation and corresponding low velocity zones could be correlated in Fig. 5.14.

Among the tested cases of grooved draft tube, the one with 13 grooves having 10 mm depth had comparatively better results with flow stability and minimized swirl intensity. The results with 13G-10mm draft tube was compared and analyzed quantitatively with the base model draft tube for the circumferential velocity, axial velocity, vorticity and turbulent kinetic energy (TKE). These parameters were quantified at 0.15m distance from the draft tube inlet, along the horizontal axes.

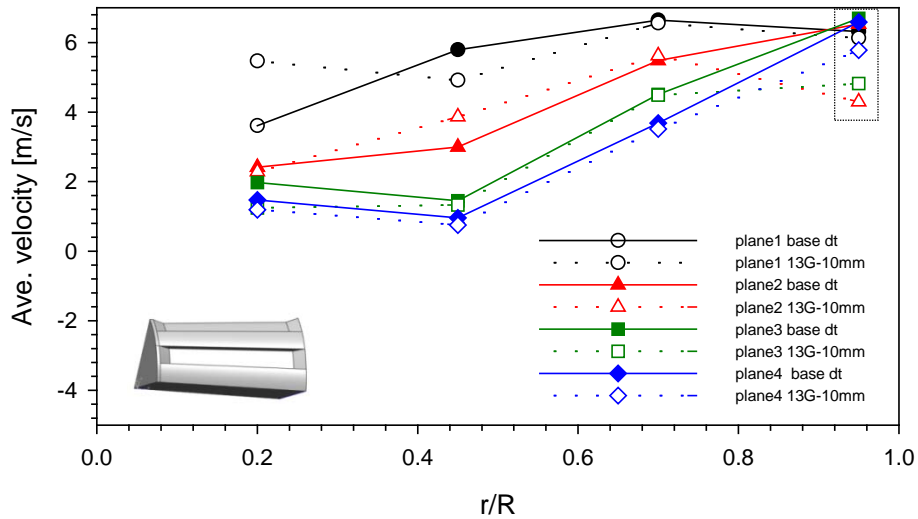
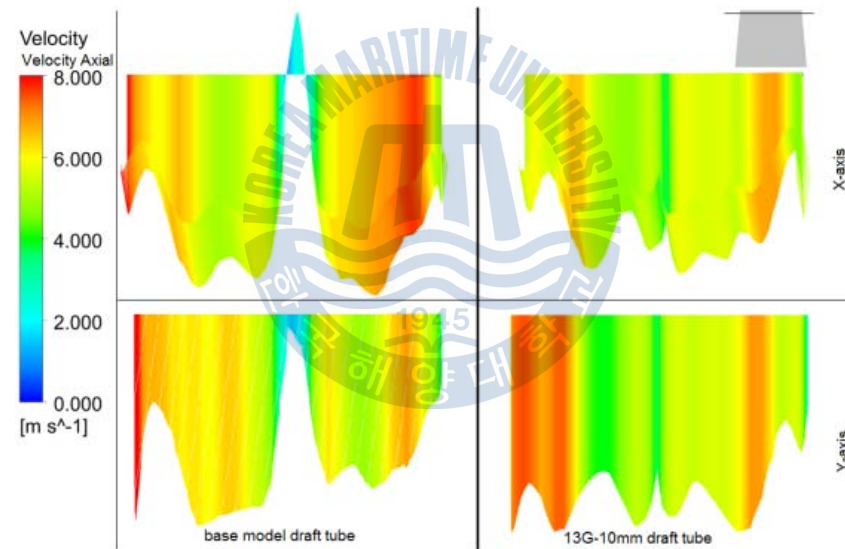
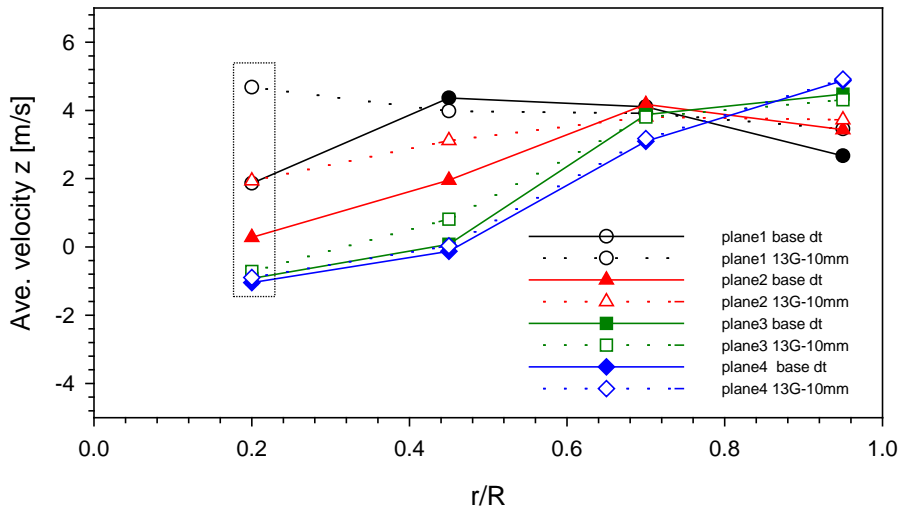


Fig. 5.15 Average circumferential velocity with J-groove 13G-10mm

The average circumferential velocity in J-grooved draft tube is compared with that in base model draft tube in Fig. 5.15. The magnitude of velocity decreased along the wall of the draft tube ($r/R > 0.8$) more prominently due to the presence of J-grooves. The swirling velocity has been decreased noticeably in all the 4 different layers of the draft tube cone along the vertical locations near the region of J-grooves. In plane#1, there was a small difference in circumferential velocity but in other 3 planes, the velocity has been decreased conspicuously indicating the minimized swirling flow.



(a) Base model draft tube

(b) J groove, 13G-10mm

Fig. 5.16 Average axial velocity with J-groove

Similarly, the axial velocity in the central flow region of the grooved draft tube has been improved significantly. The axial component of the flow velocity in the core and its vicinity for the first 3 layers have been increased (Fig. 5.16) resulting in

decreased swirl strength. As the radius ratio increased and approached the draft tube wall, small difference in axial flow was observed with J-grooves.

The distributions of vorticity and turbulence kinetic energy of the flow in the draft tube were examined for 13G-10mm and 16G-10mm with reference to those from base model draft tube. The graph reveals that the 13G-10mm, the vorticity at the centre of flow has been narrowed (Fig. 5.17) and had lowest magnitude of turbulence kinetic energy (Fig. 5.18) along both the axes.

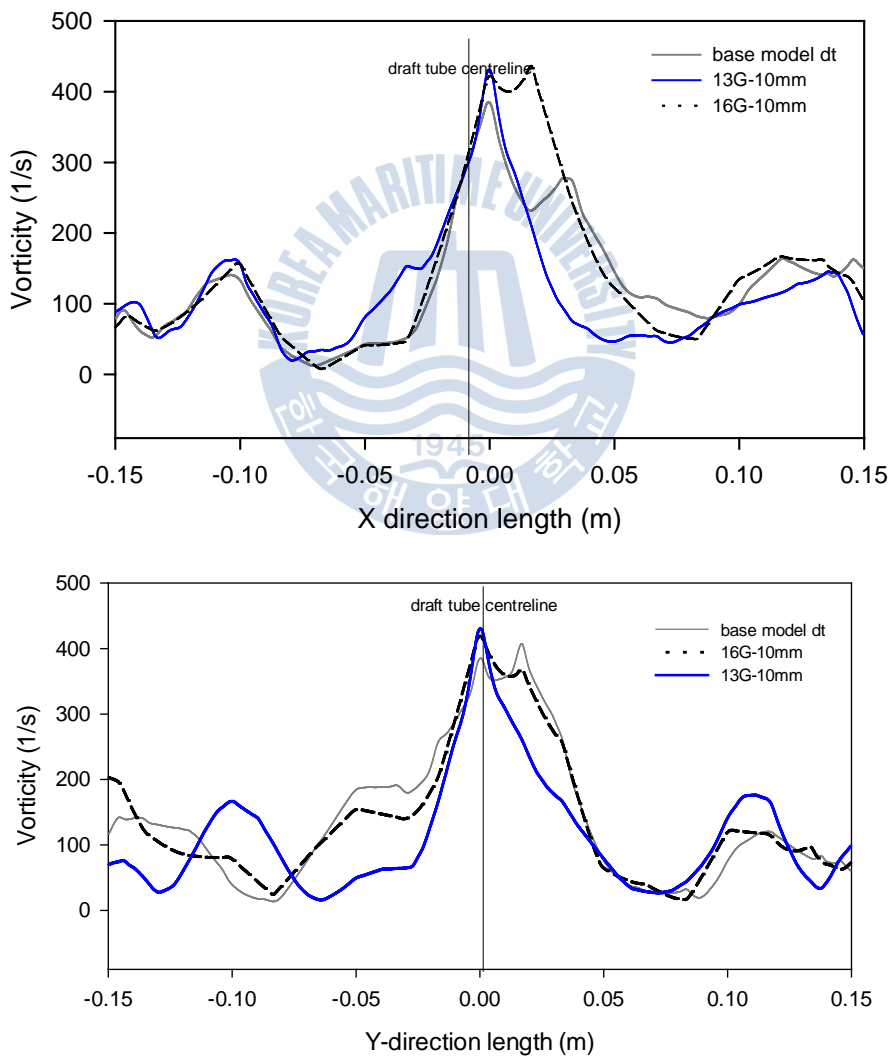


Fig. 5.17 Vorticity curves of base model draft tube with J-groove cases

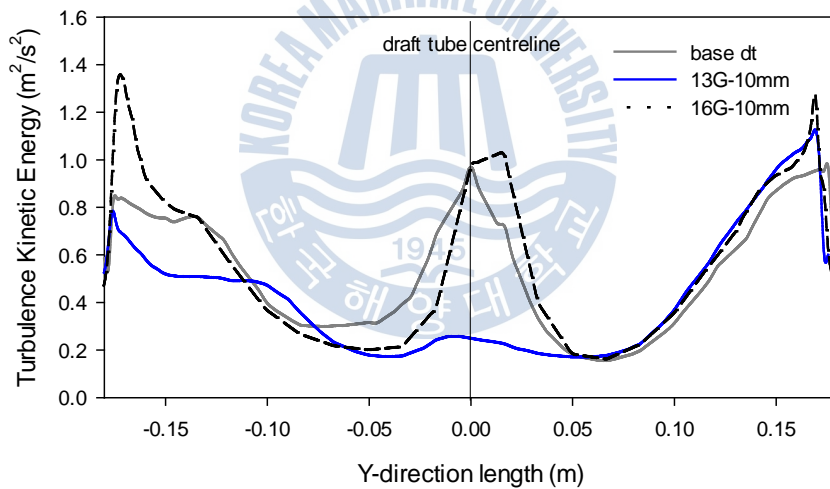
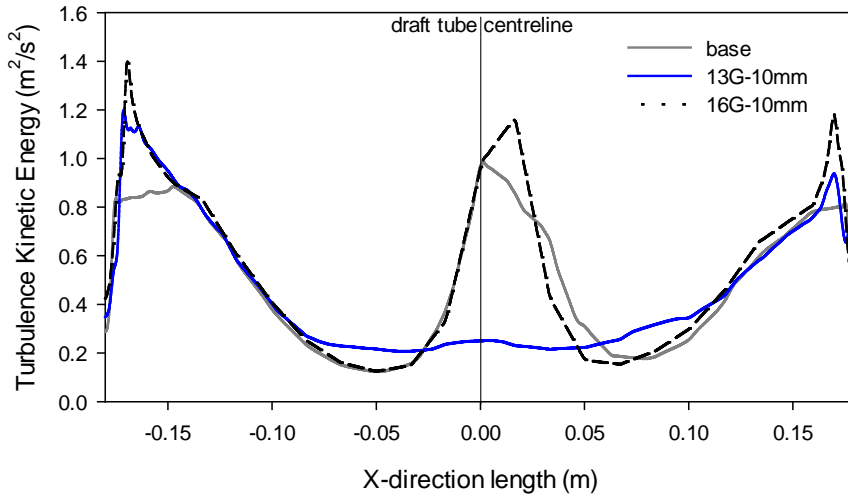


Fig. 5.18 Turbulence kinetic energy with J-groove, 2 cases

The intensity of turbulence and magnitude of vorticity both have been controlled with 13G-10mm. Compared to the base model draft tube, the vorticity was confined along the centerline narrowing the dead water region and confining it more along the central flow. The vortex rope so formed was straightened with negligible twist. As the rope rotated, the flow around its periphery were less disturbed which otherwise would be subjected to face turbulence due to changing shape of the vortex

rope. This was supported by the reduced turbulence kinetic level in draft tube core with the use of J grooves. Fig. 5.19 shows the reduced size of the vortex rope due to J-grooves in the draft tube.

With minimized vortex size and reduced turbulence, the pressure pulsation and vibration level brought about by the vortex shedding is also bound to decrease. The draft tube with 13 J-grooves, 10mm depth enhanced the flow in draft tube by minimizing the swirling flow and improving the axial flow along the core flow region.

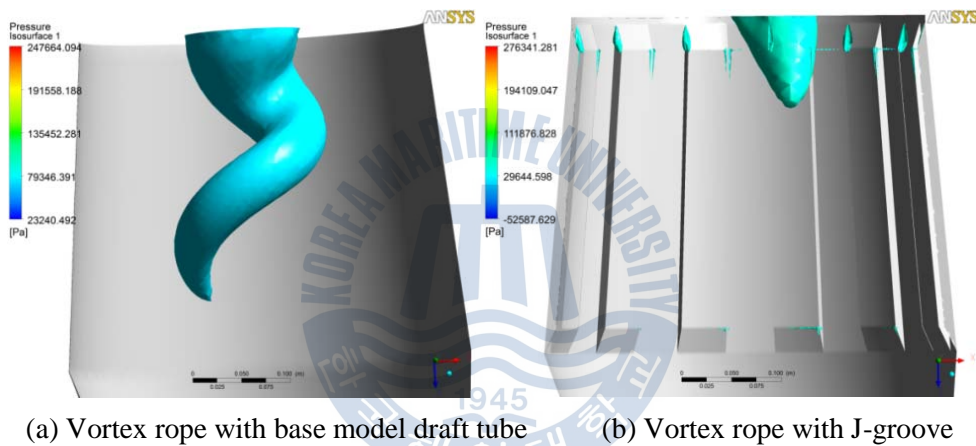


Fig. 5.19 Shape of vortex rope with J-groove

Chapter 6 Conclusion

In this study, a micro class Francis turbine of 70kW output power was designed and its flow dynamics was numerically analyzed using CFX to establish its best performing regimes.

To figure out the interaction between rotating and stationary parts of the turbine, a time dependent analysis of turbine at full load was carried out. Considering the presence of swirling flow at part load, genesis of vortex rope as draft tube surge was also studied. The results from the time dependent analyses were taken as a base for the design techniques to apply for controlling the vortex.

For vortex control techniques, 4 different methods were tried and tested in an attempt to control and/or minimize the vortex shedding in the draft tube.

- Misaligned guide vane (MGV) whose use is limited to pump-turbine was tried out and its influence in flow in the draft tube was investigated; only to deduce that MGV was not appropriate in suppressing the vortex and swirl intensities. However, MGV did elevate efficiency of the turbine by 2%.
- Modification of runner hub altered flow fashion downstream the runner. The qualitative analysis inferred that the swirl intensity and size of vortex was relatively minimized with new hubs. This provided an option for its design optimization for better control over vortex. About 2.5% of efficiency had to be compromised with this technique.
- The use of J-grooves has been taken positively in minimizing swirling flow in the draft tube by many authors. With J-grooves, the results were better and proved to be more effective in controlling the swirl intensity. J grooves did not alter the efficiency of the turbine so significantly but the depth of the J-groove did have distinct influence in the flow and swirl intensity at the draft tube.

Vortex shedding is a major operational problem in reaction turbines, especially in Francis hydro turbines. The techniques essayed in this research were applied to a micro class Francis turbine possessing a laudable efficiency of 88% and satisfactory

performance through its operating regimes. With small-size turbine, the level of vortex shedding is small and the results obtained with vortex control techniques also showed moderate effect in swirl control. However, should these techniques be applied for bigger Francis turbines that are designed for higher power output, the result in vortex control can be achieved and realized in bigger magnitude. Bigger turbines suffer vortex shedding of larger magnitude and with positive results from the control techniques discussed in this dissertation, they are like to render more distinct and better level of control over swirl and decrement in vortex intensity for bigger turbines. For large scale hydropower plants, even a small improvement in turbine's performance can contribute to maximized output power, lowered detrimental effects due to power/pressure fluctuation and prolonged operational period averting major operational challenges.

Generally, hydro turbines are tailor made to suit the site specific conditions and are designed, installed and evaluated as per their performance with respect to the site. Thus, the techniques discussed here can be extended for further design optimization and evaluation to suit best the flow feature of the specific turbine under consideration.

In this study, only one operational point at part load, 72% of the load, is considered to investigate the flow features and genesis of vortex rope. The nature (size, shape, direction of rotation, dominating frequencies) of the vortex rope can be checked for over-loads as well as other regimes of part-load operations.

For misaligned guide vanes, more options can be tried out by misaligning more than 2 guide vanes, at higher angles other than the ones discussed here. Additionally, controlling pressure oscillation by using MGVs can be determined by analyzing the peak to peak amplitudes at the given MGV openings.

With J-groove technique, it can be further analyzed quantitatively for the level of pressure pulsation, vibration and other flow phenomena it is bound to reduce. It is suggested that the techniques discussed be compared with the experimental data, to validate the numerical results.

Acknowledgement

I record my sincere appreciation to my supervisor Prof. Young-Ho LEE, Ph.D, for accepting me as research scholar and providing the opportunity to carry out this research work under his supervision in Flow Informatics Lab of Korea Maritime University (KMU). I have my heartfelt gratitude for his invaluable guidance and suggestions.

I am also highly indebted to Prof. Kweon-Ha PARK, Ph.D. (Chairperson, Review Panel) and Prof. Hyung-Ho JUNG, Ph.D. (Co-Chairperson) for their thumping encouragement and valuable suggestions during my research work.

My research work shall remain incomplete lest I thank my lab mates for assisting me during my study under their mentorship. I thank my seniors Mr. Chan-Gu KIM, Mr. Nak-Jung LEE and Mr. Jee-Hoon PARK for their valuable support, my peers Mr. Byung-Ha KIM, Mr. In-Cheol KIM, Mr. Joji Vulibeci Wata, Mr. Zhao Yuxin and Mr. Nirmal Acharya for their friendship and wonderful company.

I record my sincere appreciation to Prof. Bhola Thapa, Ph.D, Kathmandu University, Nepal (my Alma Mater) for his guidance and recommendations during my application processing in KMU.

I am immensely thankful to my beloved parents back in Nepal for being the wind under my wings. Roshan Bhinaju (Ph.D), Indira Didi, Suresh dai, Samundra Kaji and Ritvik babu hold a special place for many beautiful memories and making my stay in Busan no lesser than home.

Finally, I am equally thankful to all the staffs, friends and noble souls of KMU, the only island university of the world.

References

- [1] Turbine History. 08 Aug. 2012. <<http://science.jrank.org/pages/7030/Turbine-History.html>>
- [2] Thake, G., 2000. *The Micro-Hydro Pelton Turbine Manual*. Practical Action Publishing. UK.
- [3] Francis, J.B., 1909. *Lowell Hydraulic Experiments*. Van Nostrand, Princeton, New Jersey, 5th Edition.
- [4] Voith Hydro, 2009. *Francis Turbin*. Voith Hydro Holding GmbH & Co. KG, Germany.
- [5] Drtina, D., & Sallaberger, M., 1999. Hydraulic turbines- basic principles and state-of-the-art computational fluid dynamics applications. *Proceedings of the Intuition of Mechanical Engineers- Part C*, 213, pp.85-102.
- [6] Neopane, H., Dahlhaug, O.G., & Thapa, B., 2007. Alternative Design of a Francis Turbine for sand laden water. *International Conference on Small Hydropower- Hydro Sri Lanka*, Sri Lanka.
- [7] Brekke, H., 1996. Hydraulic design strategy for Francis turbines. *Hydropower and Dams*, Issue 3, pp.38-42.
- [8] *Rainpower's hydro heritage*, 2008. The International Journal on Hydropower and Dam.
- [9] *The X factor*, 2006. The International Journal on Hydropower and Dam.
- [10] Dumitru, N., Malciu, R., Dumitru, S., & Margine, A., 2011. Optimization in dynamic regime of a Francis hydro turbine wicket gate mechanism. *13th World Congress in Mechanism and Machine Science*, Mexico.
- [11] Hellstrom, J.G.I, Majavaara, B.D., & Lundstorm, T.S., 2007. Parallel CFD simulation of an original and redesigned hydraulic turbine draft tube. *Advanced Engineering Software*, 38(5), pp.338-344.
- [12] Khurana, S., Navtej & Singh, H., 2012. Effect of cavitation on hydraulic turbines- A review. *International Journal of Current Engineering and Technology*, 2(1), pp.172-177.
- [13] Kumar, P., & Saini, R.P., 2010. Study of cavitation in hydro turbines- A review. *Renewable and Sustainable Energy Reviews*. 14, pp.374-383.
- [14] Avellan, F., 2004. Introduction to Cavitation in Hydraulic Machinery, *The 6th International Conference on Hydraulic Machineries and Hydrodynamics*, Romania. pp.11-22.

- [15] Schiavello, B., & Frank C. V., 2009. Pump Cavitation- Various NPSH Criteria, NPSH Margins and Impeller Life Expectancy. *Proceedings of the 25th International Pump Users Symposium*, pp.113-144.
- [16] Kjølle, A., 2011. *Hydropower in Norway: Mechanical Equipment*. Norway.
- [17] Meland, H., 2010. *A new Design of a Francis Turbine in order to reduce Sediment Erosion*. Master's Degree Thesis, Norwegian University of Science and Technology, Norway.
- [18] Okyay, G., 2010. *Utilization of CFD tools in the design process of a Francis turbine*. Master's Degree Thesis, Middle East Technical University, Turkey.
- [19] Patel, K., Desai, J., Chauhan, V. & Charina, S., 2011. Development of Francis Turbine using Computational Fluid Dynamics. *The 11th Asian International Conference on Fluid Machinery and The 3rd Fluid Power Technology Exhibition*, Chennai.
- [20] Jost, D., & Lipej, A., 2009. Numerical Prediction of the Vortex Rope in the Draft Tube. *3rd IAHR International Meeting of the Workgroup on Cavitation and Dynamic Problems in Hydraulic Machinery and Systems*, Czech Republic. pp.75-85.
- [21] Benigni, H., & Jaberg, H., 2007. Stationary and Transient Numerical Simulation of a Bulb Turbine. *5th IASME/WSEAS International Conference on Fluid Machineries and Aerodynamics*, pp.135-140.
- [22] Qian, Z.D., Zheng, B., Huai, W.X., & Lee, Y.H., 2009. Analysis of pressure oscillations in a Francis Hydraulic turbine with Misaligned Guide Vanes. *ImechE, Vol. 224, Part A: I. Power and Energy*, pp.139-152.
- [23] Ruprecht, S., Heitele, M., & Helmrich, T. *Numerical simulation of a complete Francis Turbine including unsteady rotor/stator interactions*. Institute of Fluid Mechanics and Hydraulic Machinery, Germany.
- [24] Ying, H., Heming, C., Ji, H., & Xirong, L., 2011. Numerical Simulation of Unsteady Turbulent Flow through a Francis Turbine. *Journal of Natural Sciences*, 16(2), pp.179-184.
- [25] Li, J., Yu, J. and Wu, Y., 2010. 3D unsteady turbulent simulations for transients of the Francis Turbine. *25th IAHR Symposium of Hydraulic Machinery and Systems, IOP Conf. Series: Earth and Environmental Science*, 12 (2010).
- [26] Ruprecht, A., Helmrich, T., Aschenbrenner, T., & Scherer, T., 2002. Simulation of Vortex Rope in a Turbine Draft Tube. *Proceedings of the Hydraulic Machinery and Systems 21st IAHR Symposium*. Lausanne.
- [27] Jost, D., & Lipej, A., 2011. Numerical Prediction of Non- cavitating and cavitating

Vortex Rope in Francis Turbine Draft Tube. *Journal of Mechanical Engineering*, 57(6), pp. 445-456.

[28] Menter, F. R., 1994. Two-Equation Eddy-Viscosity Turbulence Models for Engineering Applications, *AIAA Journal*, Vol. 32 (8). pp. 1598-1605.

[29] Muntean, S., Baya, A., Resiga, S.R., & Anton, I., 2009. 3D Numerical flow analysis into a Francis turbine runner with medium specific speed at off-design operating conditions. *Series: Applied Mathematics and Mechanics*, Nr. 52, Vol. II.

[30] Chirkov, D., Avdyushenko, A., Panov, L., Bannikov, D., Cherny, S., Skorospelov, V., & Pylev, I., 2012. CFD simulation of pressure and discharge surge in Francis turbine at off-design conditions, *26th IAHR Symposium on Hydraulic Machinery and Systems*.

[31] Wang, Z., & Zhou, L., 2006. Simulations and Measurements of Pressure Oscillations Caused by Vortex Ropes. *Journal of Fluid Engineering*, 128, pp. 649-655.

[32] Nennemann, B.; Vu, T.C., & Farhat, M., 2006. CFD prediction of unsteady wicket gate-runner interaction in Francis turbines: A new standard hydraulic design procedure. *Proceedings of the 23rd Symposium on Hydraulic Machinery and Systems*.

[33] Wahl, T.L, 1990. *Draft Tube Surging Hydraulic Model Study*. Master's Degree Thesis, Colorado State University, Colorado.

[34] Wahl, T.L., 1994. Draft Tube Surging Times Two: The Twin Vortex Phenomenon. *Hydro Review*, XIII (1), pp.60-69.

[35] Houde, S., Illiescu, M.S., Fraser, R., Lemay, S., Ciocan, G.D., & Deschenes, C., 2011. Experimental and Numerical Analysis of the Cavitating part-load vortex dynamics of Low-head Hydraulic Turbines. *Proceedings of ASME-JSME-KSME Joint Fluids Engineering Conference*. Japan.

[36] Resiga, R. S., Ciocan, G.D., Anton, I. & Avellan, F., 2006. Analysis of the swirling flow downstream the Francis Turbine Runner. *Journal of Fluids Engineering*, 128, pp.177-189.

[37] Kubota, T., Han, F., & Avellan, F., 1996. Performance analysis of draft tube for GAMM Francis turbine. *Hydraulic Machinery and Cavitation*, I, Netherlands. pp.130-139.

[38] Cable, M., Oosthuizen, P.H., & Lightstone, M., 2009. An Evaluation of Turbulence Models for the Numerical Study of Forced and Natural Convective Flow in Atria. *2nd Canadian Solar Buildings Conference*, Canada.

- [39] Yakhot, V. Orszag, S.A., Thangam, S. Gatski, T.B. & Speziale, C.G., 1992. Development of turbulence models for shear flows by a double expansion technique. *Physics of Fluids A*, 4(7), pp. 1510-1520.
- [40] Resiga, R.S., Vu, T. C., Mutean, S., Ciocan, G. D., & Nenneman, B., 2006. Jet control of the draft tube vortex rope in Francis Turbines at Partial discharge, *23rd IAHR Symposium*, Japan, pp.1-14.
- [41] Papillion, B., Sabourin, M., Couston, M., & Deschenes, C., 2002. Methods for air admission in hydroturbines. *Proceedings of the XXIst IAHR Symposium on Hydraulic Machinery and Systems*, Lausanne.
- [42] Resiga, R.S., Muntean, S., Stein, P., & Avellan, F., 2008. Axisymmetric swirling flow simulation of the draft tube vortex in Francis Turbines at partial discharge. *XXIV IAHR Symposium on Hydraulic Machinery and Systems*, Brazil.
- [43] You, G. H., Kong, L. H., & Li, D. Y., 2006. Pump-turbine S-zone and its effect at Tianhuangping pumped storage power plant. *J. Hydroelectric Engineering*, 12, pp.136-140.
- [44] Sun, H., Xiao, R., Liu, W., & Wang, F., 2013. Analysis of S Characteristics and Pressure Pulsations in a Pump- Turbine with Misaligned Guide Vanes. *Journal of Fluid Engineering*, 135 (2013), pp.1-6.
- [46] Shao, W.Y., 2009. Improving stability by Misaligned Guide Vanes in Pump storage plant. *Power and Energy Engineering Conference*, Wuhan.
- [45] Sun, H, Xiao, R.F., Yung, W, & Lui, W.C., 2012. The optimal model of misaligned guide vanes for a particular pump- turbine. *26th IAHR Symposium on Hydraulic Machinery and Systems*, China.
- [47] Kurokawa, J., Imamura, H., & Choi, Y. D., 2010. Effect of J-groove on the Suppression of Swirl Flow in a Conical Diffuser, *Journal of Fluids Engineering*, 132(2010).
- [48] Choi, Y., Kurokawa, J., & Imamura, H., 2007. Suppression of cavitation instabilities in inducer by J-Groove. *ASME Journal of Fluids Engineering*, 129(2007), pp.15-22.
- [49] Abe, H., Matsumoto, K., Kurokawa, J., & Matsui, J. & Choi, Y, 2006. Analysis and Control of Axial Thrust in Centrifugal Pump by use of J-Groove. *Proceedings of 23rd IAHR Symposium*, Japan.
- [50] Nishi, M., Wang, X.M., Yoshida., K., & Takashashi, T., 1996. An experimental study on fins, their roles in control of the draft tube surging. *Hydraulic Machinery and Cavitation*, Kluwer Academic Publishers, pp.905-914.